CHANGE IN PROVENANCE AND SEDIMENT ROUTING HISTORY OF THE MIOCENE-PLEISTOCENE BENGAL FAN, INDIAN OCEAN USING DETRITAL ZIRCON (U-TH)/HE THERMOCHRONOLOGY

by

Timothy Spencer Dixon

A thesis submitted in partial fulfillment
of the requirements for the degree

of

Master of Science

in

Earth Sciences

MONTANA STATE UNIVERSITY
Bozeman, Montana

May 2023

©COPYRIGHT

by

Timothy Spencer Dixon

2023

All Rights Reserved

ACKNOWLEDGEMENTS

I would like to express my complete and absolute gratitude to my advisor, Dr. Devon A. Orme. Not only has she been a source of inspiration for young earth scientists through her constant enthusiasm and energetic style of teaching in and out of the classroom, but she has also proven to be supportive and understanding of life's hurdles in her students' lives outside of academia. I sincerely could not ask for a better advisor during this period of my academic and personal growth. I would also like to thank my graduate committee—Dr. Andrew Laskowski and Dr. Kurt Sundell—for their guidance, perspective, and advisement on all topics.

I would like to thank Ray Salazar for his influence in my life during this time. Our conversations have ranged from the absurd to the insightful, and it has been a pleasure to achieve, struggle, and persevere together in our respective programs of study. I would like to thank Chris Baird and Natalie Weis, who have enriched my school life and are incredible geologic inspirations; Mariah Romero, Nicole Stine and Ethan Oleson have a special place as well for perspectives from their levels of education and for their camaraderie.

Last and certainly not least, I must express my unfathomable love and appreciation for my mom and dad—Lisa Zottman and Timothy Dixon—for giving me everything since day one. Through education and career changes, life-altering events, and constant struggles with self, you have been the solid rocks on which my creativity, curiosity and understanding have been founded. I thank and love my siblings, Emily, Amanda, Olivia, and Michael, for being a part of and supporting this journey regardless of our wildly different career paths. Finally, I would like to express sincerest gratitude to the National Science Foundation and Montana State University for their financial support, of which this project would not be possible without.

TABLE OF CONTENTS

1. INTRODUCTION 1

Literature Cited 4

2. THERMO: TIBETAN-HIMALAYAN OROGEN THERMOCHRONOLOGY DATABASE 5

Contributions of Authors and Co-Authors 5
Manuscript Information Page 6
Abstract 8
Plain Language Summary 8
Introduction 8
Methods and Data presented 9
Database 9
Data availability 11
Example Applications 11
Kernel Interpolation of Regional Cooling Ages 12
Source-to-sink: Provenance of the Pliocene-Pleistocene Bengal Fan 13
Region-wide Lag-Time Interpretations 17
Provenance determination with Inverse Unmixing Modeling 17
Conclusions 19
Acknowledgements 20
Open Research 20
References 20

3. CHANGE IN PROVENANCE, SEDIMENT ROUTING AND DEPOSITIONAL HISTORY OF THE MIOCENE-PLEISTOCENE BENGAL FAN, INDIAN OCEAN USING DETRITAL ZIRCON (U-TH/HE) THERMOCHRONOLOGY 39

Contributions of Authors and Co-Authors 39
Manuscript Information Page 40
Abstract 41
Introduction 42
Geologic Setting 44
Orogen Assembly 44
Lithotectonic/Stratigraphic Units 46
Ganges-Brahmaputra Rivers 50
The Bengal Fan 50

TABLE OF CONTENTS CONTINUED

Evolution of the Ganges-Brahmaputra River System....51
Previous Low-Temperature Thermochronology....52
Tibetan Thermochronology....53
Himalayan Thermochronology....53
Bengal Fan Thermochronology....55
Methodology....55
Sample Collection and Preparation....55
Zircon (U-Th/He) Low-Temperature Thermochronology....56
Zircon Double-Dating....57
Similarity Models....59
Multi-Dimensional Scaling....59
Analytical Results....60
Zircon (U-Th)/He Results....60
Double Dating Results....65
Multi-Dimensional Scaling....67
Discussion....71
Miocene-Pleistocene Exhumation Variability....71
Tectonic-Climate Coupling: Exhumation Acceleration, Monsoon Intensification, and the Pliocene-Pleistocene Transition....72
Potential Spatial and Numerical Biases in Cooling Age Populations....75
Provenance Interpretations and Implications....78
Conclusions....84
Acknowledgements....86
Literature Cited....88

4. CONCLUSIONS....98

CUMULATIVE LITERATURE CITED....102

APPENDICES....128

APPENDIX A: Detailed Methodology and Analytical Parameters....129

APPENDIX B: Detailed Analytical Results....134

APPENDIX C: Model Constraints and Justification....143

APPENDIX D: Low-Temperature Thermochronology Compilation: ZHe data....145

LIST OF TABLES

Table Page

1. Single ZHe results 135

2. Zircon He-Pb results 141

LIST OF FIGURES

Figure Page

1. Overview of Ganges-Brahmaputra River system Drainage area, IODP 354 drilling locations, and geologic map of the Himalaya and Tibet 49

2. Kernel Density Estimates for Miocene-Pliocene-Pleistocene supersets 62

3. All single ZHe lag-time calculations 64

4. He-Pb Double-Dating 66

5. Multi-Dimensional Scaling plots 68

6. Heatmap plots for Bengal Fan samples 70

7. Overview Tectonic-Climatic Forcing through Miocene-Pleistocene time 77

8. All He-Pb lag-time calculations 81

A1. Conceptual model of the lag-time approach 131

A2. He-Pb double-dating method 133

A3. Additional heatmap plots 134

B1. Zircon (U-Th)/He data plots from all single ZHe Bengal Fan samples 140

ABSTRACT

The Ganges-Brahmaputra river system carries thousands of tons of sediment from the Himalaya each year to the submarine Bengal Fan within the Indian Ocean. Deposition of sediments to the fan has been ongoing since at least late-Oligocene time (Krishna et al., 2016), preserving a record of Himalayan tectonics and topographic evolution (Blum et al., 2018). IODP Expedition 354 (2015) collected 1.7 km of sediment core from the Bengal Fan to expand the record of Himalayan sediment routing (France-Lanord et al., 2016). Detrital zircon U-Pb data from core samples reflect five major tectonostratigraphic sequences from the Himalaya-Tibet Orogen (Blum et al., 2018). Age populations appear to vary temporally, suggesting change in erosion rates and sediment routing through time, especially apparent during the Pliocene-Pleistocene transition. This research uses detrital zircon (U-Th)/He thermochronology, double dating analyses, and sediment mixing model approaches to fingerprint changes in sediment routing and river deposition to the Bengal Fan. (U-Th)/He analyses are used to quantify rock uplift and exhumation experienced in the Himalayas, facilitating lag-time interpretations across Miocene-Pleistocene time.

To interpret the Bengal Basin sink record, a compilation of mid to low-temperature thermochronology datasets across the Himalaya-Tibet orogen is presented for characterization of modern-day thermochronologic age signals. This database highlights orogen wide trends in cooling dates that show younging apatite/zircon (U-Th)/He and fission tracks in the frontal Himalaya and syntaxes, and a younging trend in $^{40}Ar/^{39}Ar$ dates towards the orogen center. Zircon (U-Th)/He analyses of Bengal Fan sediments deposited 6.20 – 0.13 Ma reveal cooling dates from ~0.28 ± 0.03 – 540.15 ± 6.13 Ma. Age populations vary greatly between Miocene-Pleistocene time, with notable loss of >23 Ma populations between Miocene-Pliocene time and increasing 5.3 – 23 Ma populations across the Pliocene-Pleistocene transition with decreasing depositional lag-times. Comparison of age populations to previously recorded cooling dates from the orogen reveal shifts from Brahmaputra to Ganges sources between Miocene-Pliocene time before reaching a mixed drainage signal in the middle Pleistocene. Observed shifts in sediment provenance are attributed to coupled tectonic-climatic forces with regional acceleration of exhumation in the Himalaya, onset of northern hemisphere glaciation and increased denudation of the frontal-Himalaya during Miocene-Pleistocene time.

CHAPTER ONE

INTRODUCTION

The Himalaya is the world's tallest mountain range, with the highest peaks rising over 8 km above sea level. The exceptionally high elevation of the Himalaya is attributed to their geologically young beginnings ca. 59 Ma, when the Indian and Asian plates collided and continue to drive the uplift of the range to the present (see summary of Kapp and DeCelles, 2019 and references therein). Considered the archetype for active continent-continent collision, the Himalayan-Tibetan orogen is a nexus for intensive research on structural, geodynamic, geochemical, and geomorphologic processes in growing mountain belts. Ongoing collision and orogenic uplift since the early-Paleogene creates a complex feedback relationship between tectonics, enhanced precipitation, and erosion that presents itself in the dynamic topography of the region (Molnar et al., 1993; Clift et al., 2010; Jepson et al., 2021). This relationship has drastically changed through time due to environmental forcing, which includes processes such as climate change, sea level rise and fall, and tectonic/geodynamic influences on topographic growth.

Himalayan-Tibetan topography is not solitarily marked by jagged peaks and expansive valleys. The Ganges, Brahmaputra, and Yarlung rivers surround and drain the greater majority of the orogen, transporting and depositing thousands of tons of detrital material per year to the shelf margin and the Bengal Fan. This combination of river drainages, the Ganges-Brahmaputra River system (GBS), coupled with the Bengal Fan represents the world's largest source-to-sink (S2S) system, wherein the relationships between sediment production (source), fluvial routing, and accumulation/deposition (sink) are the subject of intense investigation (e.g., France-Lanord et al.,

2016; Blum et al., 2018; Huyghe et al., 2020). Because the Bengal Fan collects the majority of sediment shed from the Himalayan-Tibetan orogen, it also holds the most extensive detrital record of exhumation, denudation and sediment transport changes across the orogen since latest-Oligocene time (Krishna et al., 2016). In 2015, International Drilling Program (IODP) Expedition 354 drilled a 7-site transect 8°N across the Bengal Fan, collecting ~1.7 km of sediment core with extensive turbidite sand-silt deposits (France-Lanord et al., 2016). The cores have expanded the known record of sediment routing from the Himalaya, with initial work determining broad yet significant changes in Bengal Fan sediment provenance from environmental forcing during the Pliocene-Pleistocene transition (PPT) (Blum et al., 2018). Blum's study focused on U-Pb geochronology age spectra to determine these initial changes, establishing a temporal understanding of provenance shifts. However, questions remain regarding spatial variation of provenance signals, exhumation/sedimentation rates, and the potential impacts of climatic forcing on these factors across the PPT. In this work, I use zircon (U-Th)/He thermochronology and sediment mixing models to further expand and refine the Bengal Fan record of provenance and sediment routing change from Late Miocene to Late-Pleistocene time.

The following thesis is comprised of two chapters. Chapter 2 focuses on a manuscript describing a new, extensive, and publicly-available database of low-temperature thermochronology datasets from the Himalaya and Tibet, *THermO* (Dixon et al., *in review*). The 7,563 individual cooling ages compiled in *THermO* allow users to quickly search for and download information from multiple peer-reviewed sources implementing a variety of middle to low temperature thermochronometers (AFT, ZHe, etc.), and has been implemented into the study

presented herein. Chapter 3 describes the investigation into change in Bengal Fan provenance, sediment routing and deposition of Himalayan-Tibetan detritus. Specifically, I report a large (n = 114) zircon (U-Th)/He cooling age dataset, along with an additional He-Pb double date dataset (n = 49), to constrain provenance interpretations of Bengal Fan sediments. These thermochronometric ages are highly variable, ranging from the latest-Pleistocene to Cambro-Ordovician periods, and encompass a wide range of age populations unique to differing lithotectonic units across the orogen. I also conduct a series of age comparison and sediment mixing/unmixing modelling to test and strengthen initial age data interpretations of provenance, in order to fingerprint the historical shifts in sediment routing to the Bengal Fan. Extrapolating data from the above methods, I present my own conclusions in determining the impacts of climatic forcing on Bengal Fan provenance and sediment routing, with a specific emphasis on the interglacial Pliocene-Pleistocene transition.

Results suggest that the Brahmaputra River delivered the majority of sediment to the Bengal Fan during Late Miocene to Pliocene time, before a significant shift across the PPT resulted in a mainly Ganges River drained sediment source, opposite the results determined by Blum et al (2018) when comparing zircon U-Pb and zircon (U-Th)/He results. I suggest that this major shift in sediment routing and provenance was facilitated by a mixed process of tectonic and climatic forcing (Jepson et al., 2021), which produced large scale regional increases in exhumation (Himalayan syntaxes; e.g., Bracciali et al., 2016), of which certain age signals were effectively overridden by age signals derived from increased frontal-Himalayan denudation (glacial advance and monsoon intensification; e.g., Burbank et al., 2003).

Literature Cited

Blum, M., Rogers, K., Gleason, J., Najman, Y., Cruz, J., Fox, L., 2018. Allogenic and Autogenic Signals in the Stratigraphic Record of the Deep-Sea Bengal Fan. Sci. Rep. 8, 7973. https://doi.org/10.1038/s41598-018-25819-5

Clift, P.D., Giosan, L., Carter, A., Garzanti, E., Galy, V., Tabrez, A.R., Pringle, M., Campbell, I.H., France-Lanord, C., Blusztajn, J., Allen, C., Alizai, A., Lueckge, A., Danish, M., Rabbani, M.M., Tada, R., Zheng, H., 2010. Monsoon control over erosion patterns in the western Himalaya; possible feed-back into the tectonic evolution. Geol. Soc. Spec. Publ. 342, 185–218. https://doi.org/10.1144/SP342.12

France-Lanord, C., Spiess, V., Klaus, A., Schwenk, T., Adhikari, R.R., Adhikari, S.K., Bahk, J.-J., Baxter, A.T., Cruz, J.W., Das, S.K., Dekens, P., Duleba, W., Fox, L.R., Galy, A., Galy, V., Ge Junyi, Gleason, J.D., Gyawali, B.R., Huyghe, P., Jia Guodong, Lantzsch, H., Manoj, M.C., Martin, Y.M., Meynadier, L., Najman, Y.M.R., Nakajima, A., Ponton, C., Reilly, B.T., Rogers, K.G., Savian, J.F., Selkin, P.A., Weber, M.E., Williams, T., Yoshida, K., 2016. Expedition 354 summary. Proc. Int. Ocean Discov. Program Exped. Rep. 354, 35. https://doi.org/10.14379/iodp.proc.354.101.2016

Jepson, G., Carrapa, B., Gillespie, J., Feng, R., DeCelles, P.G., Kapp, P., Tabor, C.R., Zhu, J., 2021. Climate as the Great Equalizer of Continental-Scale Erosion. Geophys. Res. Lett. 48. https://doi.org/10.1029/2021GL095008

Kapp, P., DeCelles, P.G., 2019. Mesozoic–Cenozoic geological evolution of the Himalayan-Tibetan orogen and working tectonic hypotheses. Am. J. Sci. 319, 159–254. https://doi.org/10.2475/03.2019.01

Krishna, K.S., Ismaiel, M., Srinivas, K., Gopala Rao, D., Mishra, J., Saha, D., 2016. Sediment Pathways and Emergence of Himalayan Source Material in the Bay of Bengal. Curr. Sci. 110, 363. https://doi.org/10.18520/cs/v110/i3/363-372

Molnar, P., England, P., Martinod, J., 1993. Mantle dynamics, uplift of the Tibetan Plateau, and the Indian monsoon. Rev. Geophys. 31, 357–396. https://doi.org/10.1029/93RG02030

CHAPTER TWO

THERMO: TIBETAN-HIMALAYAN OROGEN THERMOCHRONOLOGY DATABASE

Contributions of Authors and Co-Authors

Manuscript in Chapter 2

Author: Spencer Dixon

Contributions: Designed study, performed analyses, interpreted results, created figures, designed webpage and database, wrote manuscript.

Co-Author: Devon A. Orme

Contributions: Conceived and designed study, discussed results and interpretations, assisted with webpage and database design, edited manuscript.

Co-Author: Andrew K. Laskowski

Contributions: Provided initial data compilation, assisted with webpage and database design, guided GIS implementation, edited manuscript.

Manuscript Information

Spencer Dixon, Devon A. Orme, Andrew K. Laskowski

Status of Manuscript:
____ Prepared for submission to a peer-reviewed journal
__X__ Officially submitted to a peer-reviewed journal
____ Accepted by a peer-reviewed journal
____ Published in a peer-reviewed journal

manuscript submitted to *Geochemistry, Geophysics, Geosystems: Data Article*

THermO: Tibetan-Himalayan Orogen Thermochronology Database

Spencer Dixon[1], Devon A. Orme[1], Andrew K. Laskowski[1]

[1]Department of Earth Sciences, Montana State University, Bozeman, Montana 59717, USA.

Corresponding author: Spencer Dixon (timothy.dixon2@student.montana.edu)

Key Points:

- Online database of medium to low-temperature thermochronologic data for the Himalayan-Tibetan orogen
- Highlights orogen-wide differences in cooling dates, young zircon/apatite trends near syntaxes and younging argon dates at orogen center
- Interactive site supports ongoing and future research on the region

Abstract

We present a database comprised of published medium to low-temperature thermochronologic data from bedrock and detrital samples of the Himalayan-Tibetan orogenic system. Cooling ages (Ma) and their errors are reported for the apatite and zircon (U-Th)/He, apatite and zircon fission track, and biotite and muscovite $^{40}Ar/^{39}Ar$ or K-Ar systems for a total of 7,563 ages; Respective uncertainty measurements are reported at the 1 or 2σ level depending on the original study. All data include latitude, longitude and elevation, the latter of which was determined through GIS geoprocessing, as many studies did not report this information. The database serves as a repository for new and existing thermochronology data, is accessible to the community through an interactive ArcGIS Online web system, and is continuously updated with newly aquired datasets through peer-reviewed author and user submissions. The utility of the database is demonstrated by example applications to both current and hypothetical studies across the orogen, including regional cooling age distribution comparisons, temporal changes in the source of deep-sea Bengal Fan sediments, wide temporal lag-time interpretation, and application of inverse-modeling techniques to reconstruct provenance.

Plain Language Summary

A new web-based database with an interactive interface is presented, containing compiled bedrock and detrital thermochronologic data of varying rock types and locales in the Himalayan-Tibetan orogen. This database centralizes 174 individual studies in an effort to aid future research efforts within the region that may seek to understand the timing and magnitude of local, regional, or continent wide tectonic and surface processes.

1 Introduction

The Himalayan-Tibetan orogen has been the subject of intense geologic interest and exploration for over a century as it is home to the world's tallest (superaerial) mountains, is the archetype for active continent-continent collision, and acts as a natural laboratory for linkages between synorogenic surface processes and inordinately high exhumation rates (Argand, 1924; Dewey, 1988; Yin & Harrison, 2000; Yin, 2010; Enklemann et al., 2011; Kapp and Decelles, 2019). Medium to low temperature thermochronology systems such as white mica $^{40}Ar/^{39}Ar$ (350-300°C) and apatite (U-Th)/He (75-60°C) are sensitive to middle to upper crustal processes. Thus, thermochronology is used to provide detailed and spatially variable interpretations of temporally dynamic tectonic processes within the orogen (van der Beek and Schildgen, 2022), and is especially useful in studies of rock uplift and exhumation (e.g., Enkelmann et al., 2011; Finnegan et al., 2008; Bernet and Spiegel, 2004; Garver et al., 1999). Thermochronology can also provide context and insights into the complex feedback systems between tectonics, precipitation and erosion (Clift et al., 2010; Molnar et al., 1993). As the amount of thermochronologic data available for the region has increased, so too has the difficulty in aquiring, processing and sifting through the hundreds of datasets and thousands of individual ages reported.

This database compiles and centralizes Himalayan-Tibetan middle to low-temperature thermochronologic data for current and future Earth scientists, formed in no small part from numerous efforts by previous research efforts to examine both wide and small-scale regional tectonic and thermal evolution of the orogen (See Table S1). The database follows other large-scale efforts to characterize a variety of attributes in specific geologic systems and regions, including the Central Andes geochemical GPS database (Mamani et al., 2010;

http://andes.gzg.geo.uni-goettingen.de) and the Tibetan Magmatism Database (Chapman and Kapp, 2017; jaychapman.org/tibet-magmatism-database.html)

2 Methods and Data presented

The compilation is comprised of medium to low temperature thermochronology data gathered from 174 individual studies published through November 2022, amounting to an initial 7,563 individual cooling ages (Table S1). Data from these studies were then categorized based on two attributes: 1) Collection location: Himalaya or Tibet, and 2) by thermochronometric system. Samples with no available coordinates or location data were assigned a geographic coordinate estimated from figures within the original text. Elevation data were not available for all samples, but provide critical context for integration into existing thermal models such as *age2exhume* (van der Beek and Schildgen, 2022), GLIDE (Fox et al., 2014), QTQt (Gallagher, 2012) or HeFTy (Ketcham, 2005). Therefore, we include elevation data for all samples via the "Multi Values to Points" Spatial Analyst tool in ArcGIS Pro. This tool allows the extrapolation of elevation data from a DEM to a select dataset based on coordinate values assigned to each point.

The database includes five thermochronometers that are grouped according to mineral system and temperature sensitivity range: apatite helium and fission track (AHe/AFT, 40-120°C), zircon helium and fission track (ZHe/ZFT, 120-220°C), and biotite or muscovite argon-argon (Ar-Ar/KAr, 300-400°C) age data. Sample ages represent cooling age (Ma), and are reported with respective uncertainty measurements at the 1 or 2σ level depending on the original study. The majority of samples report bedrock ages, with the minority reported as detrital material. ZHe was compiled from 47 studies amounting to 968 ages. ZFT was compiled from 38 studies amounting to 3,000 ages. AHe was compiled from 41 studies amounting to 713 ages. AFT data was compiled from 92 studies amounting to 1,805 ages. Finally, Ar-Ar/K-Ar was compiled from 58 studies amounting to 1077 ages. Ar-Ar/KAr age data compiled include both bulk and plateau age sets, including forced plateaus. Thus, we recommend that users interested in argon datasets investigate the data on a study-by-study basis. All data sources are provided in Supplementary Material I.

3 Database

Data are contained in a table-to-point web feature layer that is implemented into an ArcGIS Online host. Access to THermO is currently available at the following address: https://tinyurl.com/TeST-Thermo-Database. The application is optimized for viewing in most major internet browsers (Microsoft Edge, Google Chrome, Mozilla Firefox, Opera) on a standard desktop or laptop computer. The layout of the user interface contains an interactive map, data tables and search filter options for thermochronometric system, reference study, and age spectra (Figure 1).

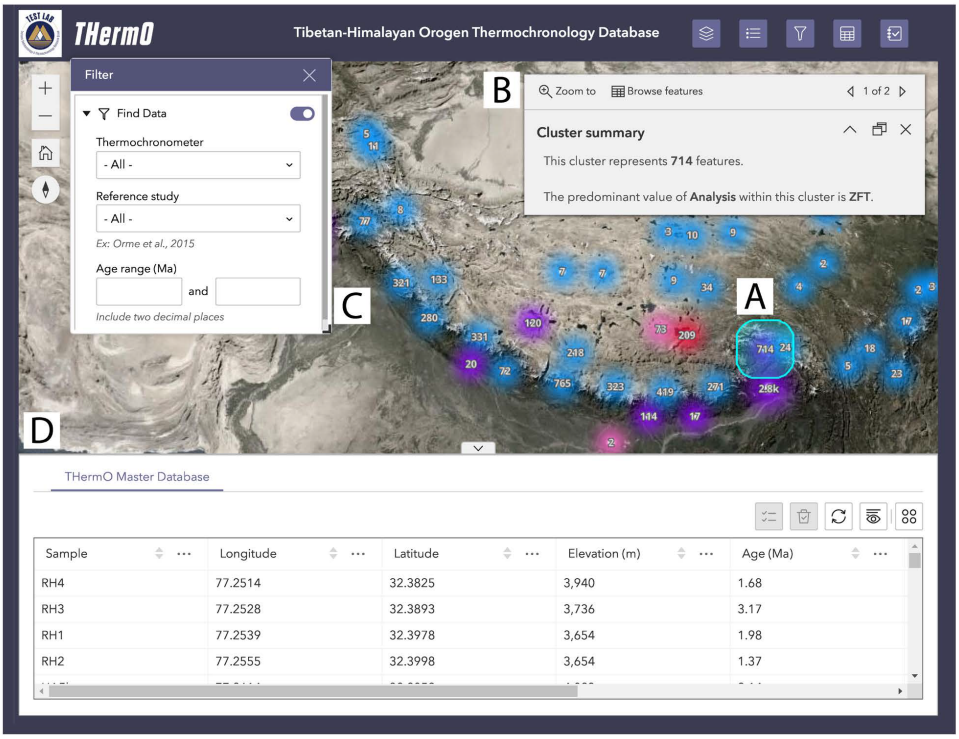


Figure 1: Main interface of THermO web application. (A) Data are clustered together by mineral system (blue = apatite, purple = zircon, red = biotite/muscovite, pink = multiple), and clusters are labelled with the number of samples present in an area. (B) Cluster summary window. Clicking "Browse Features" reveals individual sample information windows. (C) Built-in filter feature allows for specified searches of data. (D) Main data table containing all samples in the database, accessed by clicking the white arrow at the bottom of the application window. Once selected, data can be exported via the "Actions" button; smaller data sets can be specified manually or via the filter options.

The webpage is an ArcGIS Online web application created in Experience Builder, and the map presented utilizes the WGS 1984 Geographic Projection. Many features found in the default ArcGIS Online interface such as a topographic basemap and alternative imagery options are available for the user to toggle. The initial startup page brings up a window with introductory information about the webpage. Clicking off this window brings up the map view with initial clusters of data from all thermochronometric systems (Figure 1A). Zooming in on the map will break up large clusters into smaller clusters, until either 1) a single datapoint is isolated, or 2) a cluster of datapoints with matching coordinates is isolated. Clusters are colored based on their mineral system, with multiple thermochronometers in a single cluster colored light pink, and will automatically update upon further zooming.

Selecting a cluster will bring up a text box describing the dominant sample type, and allows for exploration of individual samples through a drop down menu on the "Browse Features" tab. Upon selecting a single datapoint, primary information is presented to the user including reference study, sample name, age (Ma), analysis type (AFT, ZHe, etc.), latitude, longitude and elevation (Figure 1B). Additionally, information for samples may also be available for lithotectonic units, physiographic zones, and any notes/interpretations that the original authors may have provided. Fields remain empty if no data is provided.

To search for specific datasets, the website includes a built in filter feature, allowing users to display data based on thermchronometric system, reference study, and age range (Figure 1C). Users can access the main data table directly by clicking the white arrow, initially at the bottom of the screen (Figure 1D). The main data table is affected by filter options simultaneously with the map display, and there is an option for the user to export a selection or all of the data as a CSV, JSON or GeoJSON file.

3 Data availability

To date, bedrock and detrital data are sourced from published, peer-reviewed research. References to data sources are found within sample metadata tables, and can be found by typing in the respective search filter "reference study". Samples are displayed on the map in their source-recorded locations. If a source location did not have specified coordinates, estimations from data source maps were used and are noted. Samples with no available location data can be found via filter searches, but are not displayed on the map. Locations are presented in decimal degrees (°N latitude, °E longitude) referenced to the WGS 84 coordinate system. Specific data can be filtered for by thermochronometric system, reference study, and age range.

To maintain a useful database in the future, we provide the opportunity for researchers to submit their datasets, once published. Data from user submitted sources are screened for peer-review status (Figure 2) and unpublished data is excluded. Data submissions are to be uploaded as .xls or .xlsx files, and must include the following minimum data requirements: Sample (name), Longitude, Latitude, Reference, Age (Ma), and uncertainty (1 or 2σ). It is *strongly* recommended that users also include: Elevation (m), lithotectonic unit [ex: Lesser Himalaya (LHS), Lhasa terrane], physiographic zone (ex: Dhauladar Range, Namche Barwa), and any notes/interpretations that may be provided with each sample.

4 Example Applications

The wide extent of information available through the THermO database allows researchers the opportunity to implement data in a variety of study types. Four example studies are provided here to demonstrate the usefulness of the web application. Each study uses a subset of the available data to investigate regional cooling age distributions, temporal lag-time interpretations, detrital grain provenance comparisons, and inverse-modeled provenance hypotheses.

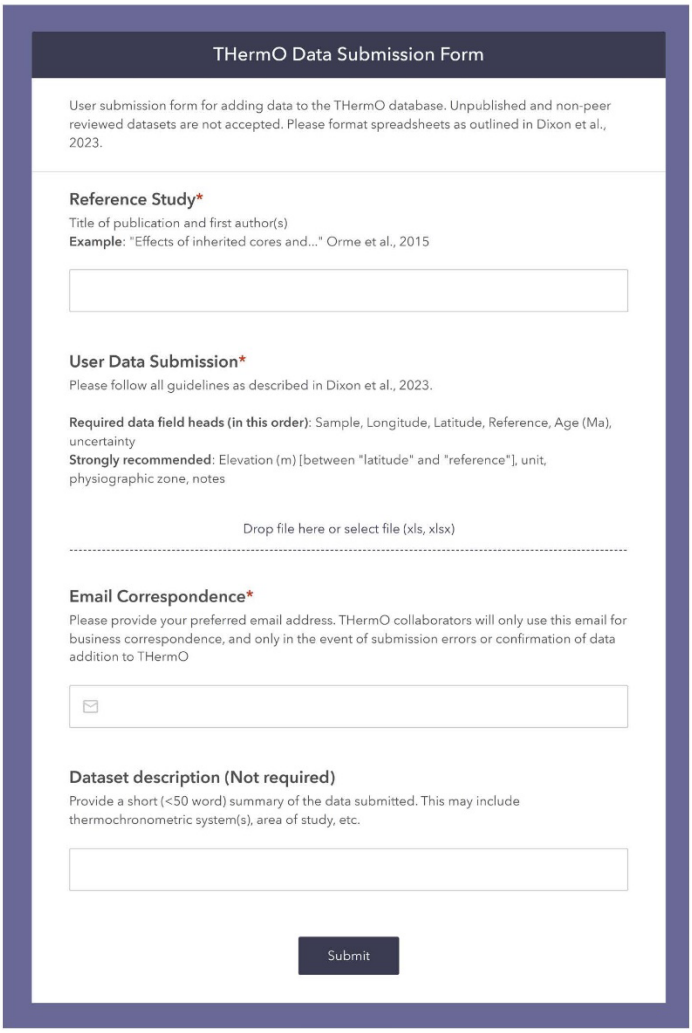


Figure 2: User/collaborator data submission form, accessible via the *THermO* webpage. Users must include reference study and respective spreadsheet for confirmation against source material, as indicated by red asterisks. Emails are required for correspondence regarding data additions.

Kernel Interpolation of Regional Cooling Ages

Geographic Information Sytems (GIS), such as ArcGIS, provide a plethora of tools for spatial analysis of variable data in a given region. One such tool is the Kernel Interpolation with Barriers tool (KIwB), which is part of the Geostatistical Analyst toolset provided in ArcGIS Pro.

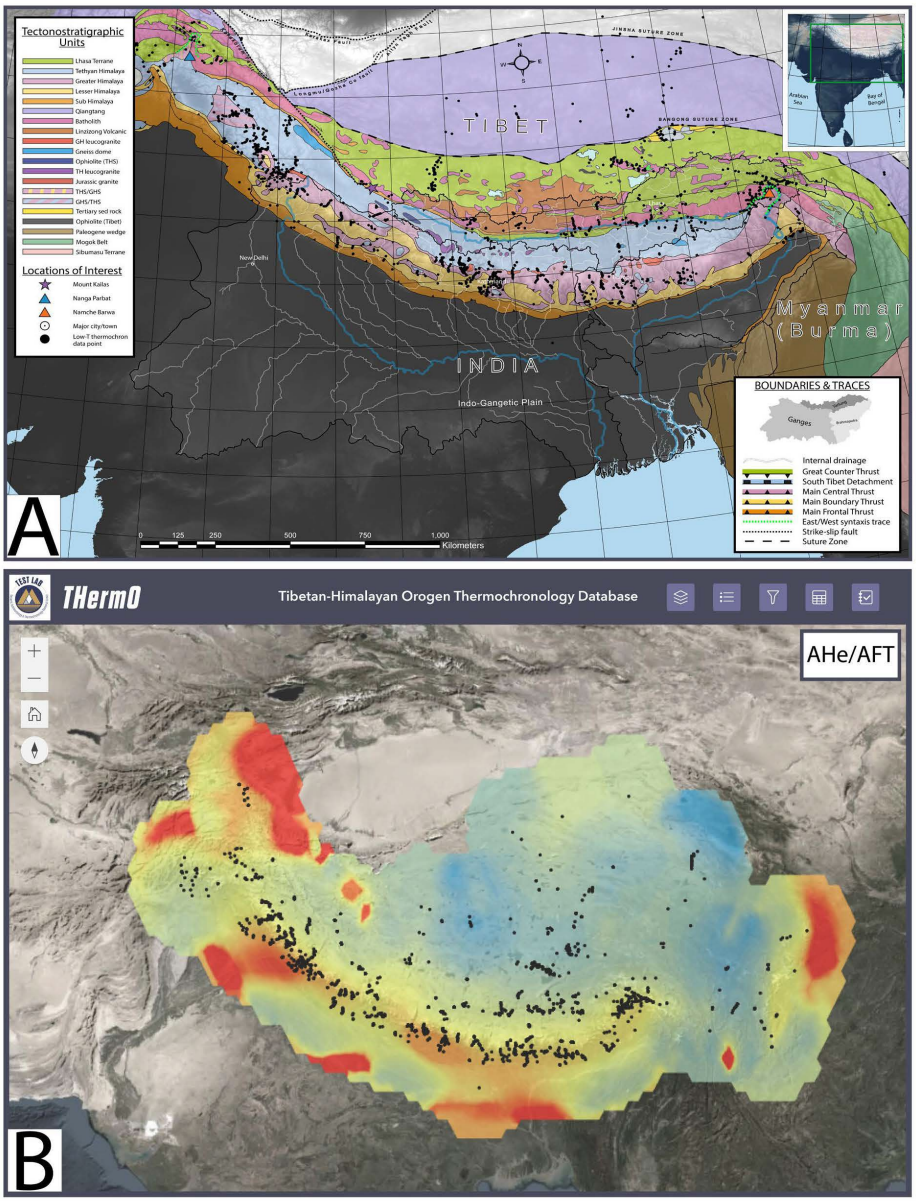
KIwB utilizes the shortest distance between points to determine gradients of data, in this case cooling age, across the region and thus predicts areas of young and old ages.

Interpolation of age data reveals potential large-scale, first order interpretations of cooling age trends across the entire Tibetan-Himalayan orogen (Figure 3C-E). Mixed AHe/AFT data show younging age trends north/northeast of the western Himalayan syntaxis (WHS) and Nanga Parbat, and within the frontal Himalaya nearest the Main Frontal and Main Boundary Thrusts (MFT and MBT, respectively). Mixed ZHe/ZFT data display similar younging trends while emphasizing recent and rapid exhumation of the eastern Himalayan syntaxis (EHS) as well. Biotite/muscovite $^{40}Ar/^{39}Ar$ data trends slightly diverge from the previous, revealing a younging trend into the orogen center. We can potentially interpret these cooling age trends to represent varying foci of rapid exhumation through time, moving out from the orogen center to the recently exhuming west and east syntaxes. Due to the higher closure temperatures recorded by argon-argon techniques, these trends may also represent older periods of fault slip/movement and orogenic cooling such as initial propagation of LHS duplexes (Long and Robinson, 2021).

Interpolations are calculated and values predicted based on an exponential equation utilizing user-determined bandwidth and radius values. This can create misleading results, as mapped areas with low to no clusters of data within a given radius are weighed unevenly against those with high data density. Whereas our interpolation displays younging thermochronology dates north/northeast of the WHS, previous studies demonstrate the foci of exhumation to be in the immediate area of Nanga Parbat (e.g. Zeitler et al., 1985; van der Beek et al., 2009). The data involved are also derived from areas of the Himalaya and Tibet with differing mechanisms of exhumation (van der Beek and Schildgen, 2022). Thus, single-factor interpolation techniques should be taken as a general guide to the regional age trends (old vs. young), rather than absolute "ground" truth. Nevertheless, the interpolation of large datasets is a potential application of this database, and we expect subsequent data contributions will serve to improve such interpolations.

Source-to-sink: Provenance of the Pliocene-Pleistocene Bengal Fan

Determination of sediment source regions often requires characterization and comparison of both unknown (sink) samples and "known" (source) regions by some common parameter. This compilation allows for orogen wide reconstruction of source regions. The Bengal Fan in the Indian Ocean, the world's largest submarine fan, acts as the outlet for both the Ganges and Brahmaputra River systems' (GBS) 2.6 million km^2 drainage area. The expansive coverage of the GBS drainage produces challenges for provenance interpretation for Bengal Fan sediments, as both rivers drain the majority of lithotectonic units in tandem—an exception being that the Yarlung River in southern Tibet, prior to connecting with the Siang-Brahmaputra river systems, drains the Mesozoic to Eocene Gangdese magmatic arc, which the Ganges river system does not (e.g. Wang et al., 2016; Ji et al., 2009; Zhu et al., 2009; Maluski et al., 1982; Schärer et al. 1984).


Tectonostratigraphic Units
Lhasa Terrane
Tethyan Himalaya
Greater Himalaya
Lesser Himalaya
Sub Himalaya
Qiangtang
Batholith
Linzizong Volcanic
GH leucogranite
Gneiss dome
Ophiolite (THS)
TH leucogranite
Jurassic granite
THS/GHS
GHS/THS
Tertiary sed rock
Ophiolite (Tibet)
Paleogene wedge
Mogok Belt
Sibumasu Terrane
Locations of Interest
Mount Kailas
Nanga Parbat
Namche Barwa
Major city/town
Low-T thermochron data point
TIBET
INDIA
Myanmar (Burma)
Indo-Gangetic Plain
New Delhi
Kathmandu
Lhasa
Yarlung Tsangpo
JINSHA SUTURE ZONE
BANGONG SUTURE ZONE
Arabian Sea
Bay of Bengal
BOUNDARIES & TRACES
Ganges
Brahmaputra
Internal drainage
Great Counter Thrust
South Tibet Detachment
Main Central Thrust
Main Boundary Thrust
Main Frontal Thrust
East/West syntaxis trace
Strike-slip fault
Suture Zone
0 125 250 500 750 1,000
Kilometers
A
THermO
Tibetan-Himalayan Orogen Thermochronology Database
AHe/AFT
B

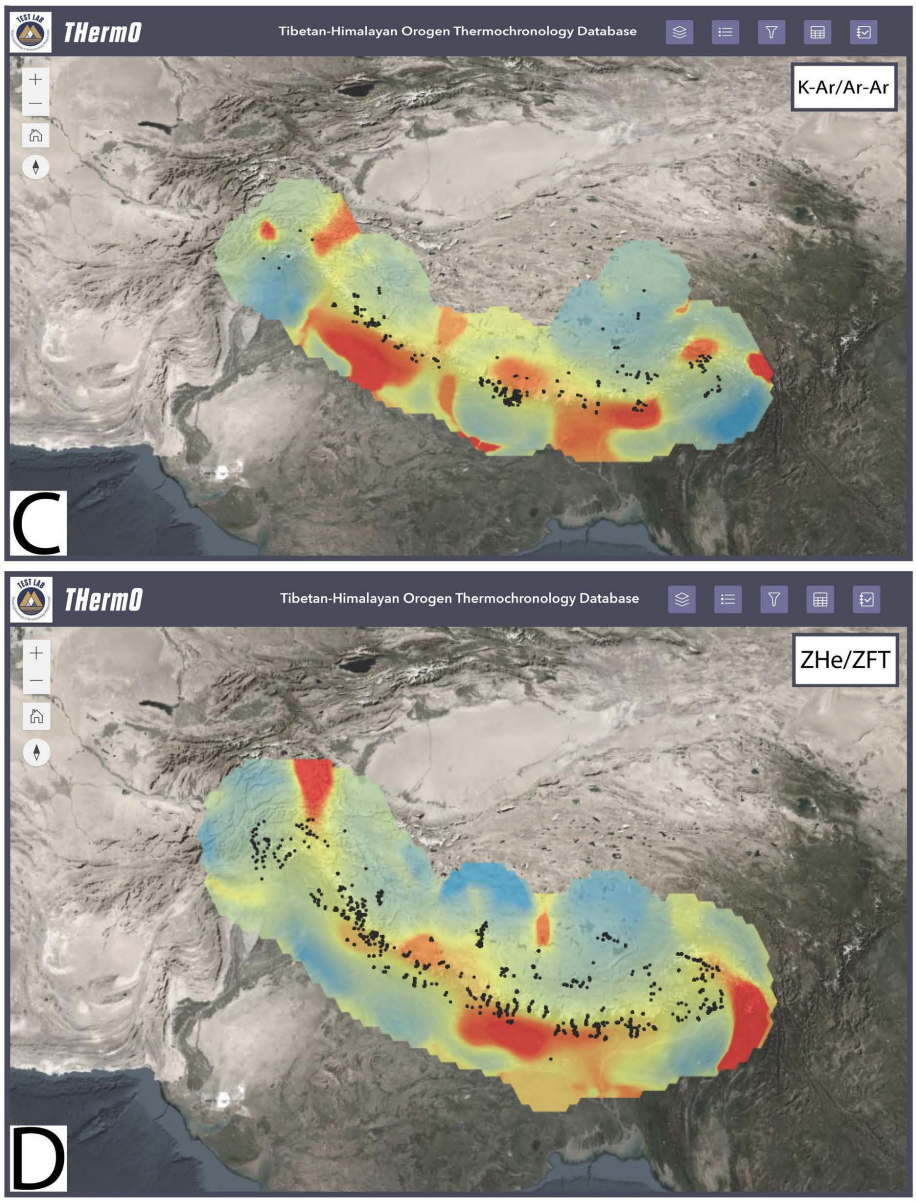


Figure 3: (A) Overview and geologic maps of the Tibetan-Himalayan orogen, synthesized and modified from previous publications (See Supplementary Material I for list of referenced publications). Compiled thermochronometer datapoints (black dots) may be

correlated with a given lithotectonic unit, and the sample unit may be identified from a given map location if not previously established. (B, C, D) Kernel interpolations of cooling age data across the Himalaya-Tibet orogen from apatite, mica argon-argon,, and zircon thermochronometers, respectively. Warm colors represent younger ages and cool colors represent older ages [Red = young (~5-<1 Ma), blue = old (>150 Ma)]. Apatite and zircon display similar age trends near the syntaxes and frontal portions of the orogen, whilst the mica argon-argon trends appear to show younging trends closer to the orogen center, suggesting previous orogen-center foci of exhumation.

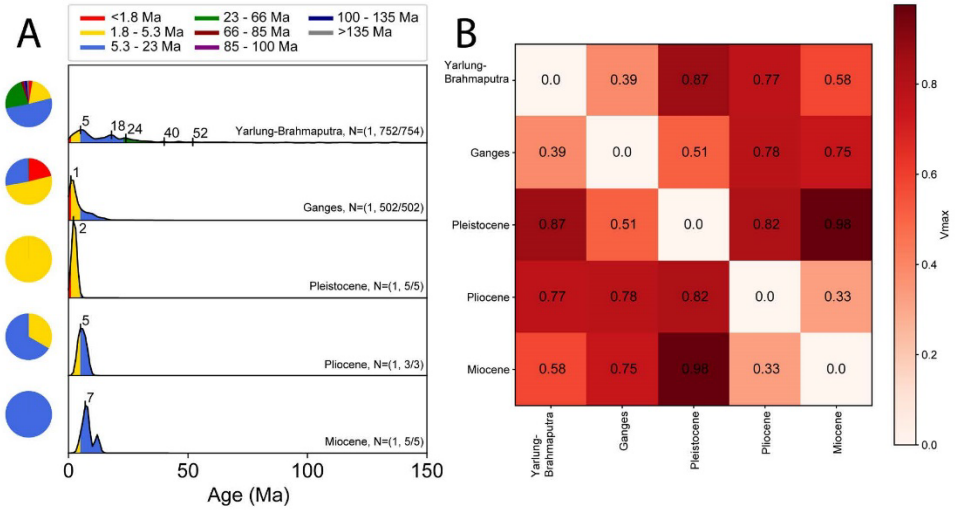


Figure 4: (A) KDE's of combined Bengal Fan AFT samples from Huyghe et al., 2020 and compiled Ganges and Yarlung-Brahmaputra cooling age distributions. Provenance shifts of Bengal Fan sediments are determined by more pronounced changes in age distributions, with an overall trend of younging AFT age spectra in detrital samples from Miocene to Pleistocene time. Age bins are colored based off the GSA Geologic Time Scale v. 5.0 (Walker et al., 2013; 2018), using the base Calabrian as the start of our Pleistocene samples to encompass latest Pliocene-earliest Pleistocene glaciation in the Northern Hemisphere. (B) Changes in age distribution through time quantified in MDS space. Lower (light color) Euclidean values (Vmax) represent greater similarity, and vice-versa.

To circumvent the spatial restrictions of U-Pb geochronology provenance methods (e.g., Blum et al., 2018), thermochronometric data such as AFT provides the regional variability required for differentiation of detrital grains derived from equivalent lithotectonic units, but differing river drainages. Kernel density estimates (KDE) of two major river drainages (Yarlung-Brahmaputra and Ganges) and 3 compiled Bengal Fan samples from Huyghe et al. (2020) of Miocene (8.72-5.59 Ma, n=5), Pliocene (4.04-2.28 Ma, n=3), and Pleistocene (0.49-0.26 Ma, n=5) depositional ages were compared for similarity in AFT age spectra present (Figure 4).

Initial results of qualitative analysis of KDE's and quantitative multi-dimensional scaling (MDS) show the decrease in Miocene ages (23 - >5.3 Ma) and an increase in Pliocene ages (≤5.3 Ma), reflecting the rapid exhumation and short lag-times of the system (Huyghe et al., 2020). In addition, comparison of the dates to our source compilation documents the gradual shift in age spectra from a more Brahmaputra source signal to predominantly Ganges source signal that lacks Miocene cooling ages prevalent across southern Tibet. This contradicts U-Pb age spectra for Pleistocene sediments that show a mixed Brahmaputra and Ganges signal, with a <300 Ma age signal fingerprinting Gangdese (Brahmaputra) drainage sources increasing and remaining consistent post-Pliocene time (Blum et al., 2018). The mixed signals from these two studies could be resolved from a coupled tectonic-climatic forcing perspective. The Pliocene-Pleistocene transition (PPT) marks a time when rapid exhumation of the eastern Himalayan syntaxis occurred in tandem with the onset of widespread Northern Hemisphere glaciation and intensification of the South Asian Monsoon (SAM) (Najman et al., 2019; Bartoli et al., 2005; Lindhorst et al., 2019; Huntington et al., 2006; Sobel et al., 2003). We may attribute the increasingly Ganges cooling age signal in the Pleistocene to rapid denudation of the frontal Himalaya from the SAM, amplifying Ganges sediment flux and effectively diluting the Brahmaputra signal we would expect from southern Tibet and accelerated syntaxial exhumation (Jepson et al., 2021; Najman et al., 2019; Enklemann et al., 2011). Initial results are almost certainly affected by the low-n recovery of currently available Bengal Fan AFT samples, which prompts a call for future thermochronology studies of this submarine record. If one were to compare U-Pb age spectra from the same combined sample group to the AFT results, it may be possible to refine these provenance interpretations of detrital materials, especially at higher n values.

Region-wide Lag-Time Interpretations

The sheer volume of data within the THermO database allows for very wide temporal interpretations of lag-time variations across the region. The *age2exhume* software, a new MatLab based application (van der Beek and Schildgen, 2022), is able to take large cooling age datasets with multiple thermochronometers and model lag-time variations through time for a large region, such as the Himalaya. Section 3.2 of van der Beek and Schildgen 2022 describes an example dataset from the Himalaya comprised of 1785 thermochronologic ages, derived from a multitude of studies that have been included in THermO's database as well. Results from this test revealed a band of rapid exhumation in the high Himalaya, slower rates to the north and south, and increasing exhumation rates with time suggested by AHe and AFT data (van der Beek and Schildgen, 2022).

Provenance determination with Inverse Unmixing Modeling

A unique application of the data compiled in THermO is the opportunity to predict source regions of detrital grains from cooling age data. DZ*nmf* is a software that implements non-negative matrix factorization (NMF) to "unmix" an unknown sink sample into a number of optimized source regions (Saylor et al., 2019). A subset of AFT ages from four samples (River 3, River 4, River 5, River 7) collected from the Yarlung River drainage northwest of Mount Everest (derived from Carrapa et al., 2017) is investigated for provenance using DZ*nmf*. Modeling determined an optimal 3 source signal that encompasses all age populations present within the sink samples (Figure 5). "Known" source signals were characterized by compiling both AFT and

AHe samples found within the Yarlung River drainage from the west to the easternmost sink sample (River 3), and divided by lithotectonic unit (Lhasa, Gangdese Batholith, and Tethyan Himalaya). Because AFT and AHe share a portion of their partial retention zones (PRZ) with one another, we chose to implement AHe age data into the source characterization due to low n values of AFT datasets while maintaining reasonable age ranges.

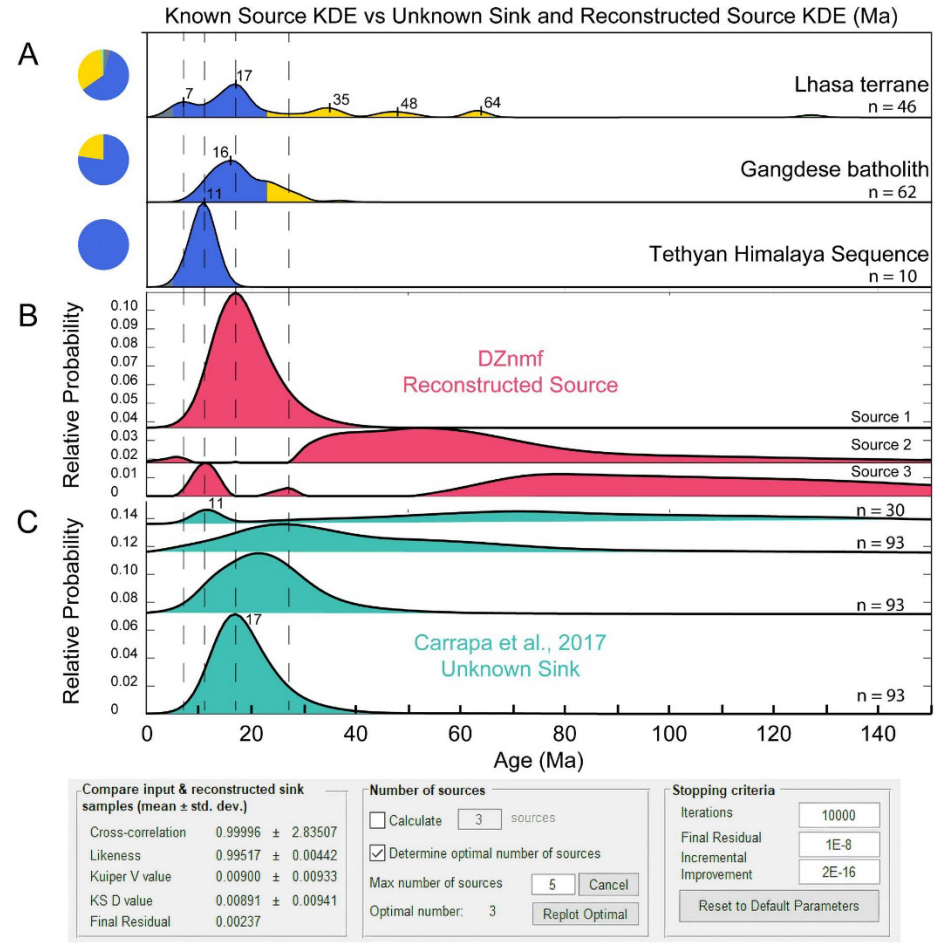


Figure 5: (A) Compiled AFT/AHe data for three lithtectonic units within the Yarlung River drainage. An initial test was conducted for the program to determine the optimal number of sources required to create the mixed sample age distributions. (B) Upon determination of an optimized 3 source signals, the model was rerun to create the factorized sources. (C) Comparison of unknown sink samples derived from Carrapa et al., (2017) (Top to bottom: River 3, 4, 5, 7) and reconstructed sources to known potential sources in the Yarlung River drainage. Statistical calculations of likeness and dissimilarity (Cross-correlation/Likeness

and Kuiper V/KS-D values) are automated by the program to determine wellness of fit between modeled sources and input data (Saylor et al., 2019).

Results of source reconstructions compared to "known" source signals revealed strikingly similar age peaks and groupings at ~11 Ma and ~17 Ma, as well as a broad source signal ~25–70 Ma. The NMF was unable to resolve > 70 Ma age populations against known KDEs, implying either an additional, undetected source within the Yarlung drainage, or an artifact of the lack of recorded AFT/AHe data to fully characterize a source within the drainage. The latter serves as an excellent observation for continued research in the Yarlung River drainage and, by proxy, continuous updates to the THermO database.

Interpretation of the first two reconstructed sources is straightforward. Source 1 reflects known Gangdese granitoid AFT cooling age populations, evident by the unimodal ~17 Ma population (e.g. Ge et al., 2017; 2018). Similarly, Source 2 displays population consistency with the known Lhasa terrane samples, reflected in the ~5–7 Ma age peak and moreso in Cretaceous age ranges (e.g. Kapp & Decelles, 2019; Wang et al., 2016; Lu et al., 2015). Source 3 interpretations initially prove challenging due to the reconstructed ≥70 Ma populations not present in known KDEs. We attribute the variability of Source 3 KDEs to a mixed-signal of old Lhasa signals, Gangdese batholith, and younger Tethyan Himalaya Sequence populations which can be sourced from cross-terrane, south-north draining tributaries within the greater Yarlung River drainage. Tributaries include both modern-day drainage patterns and high input potential from west-directed paleoflow ca. 27 Ma and younger (Taylor et al., 2021).

5 Conclusions

Middle and low-temperature thermochronology data from bedrock and detrital samples in the Himalayan-Tibetan orogen are compiled in the web-based database THermO. The online interface allows for simple exploaration of available data through search filters and downloadable spreadsheets, and is publicly available to current and future members of the Earth science community. The database is expected to see widespread use in generating new research via manual compilation of cooling ages for comparison with novel data or via machine learning modeling, and testing varying hypotheses, as thermochronology data is a powerful tool in provenance, tectonic and thermal history studies. Previous datasets from the Yarlung River drainage system and Bengal Fan were compiled to demonstrate potential applications of the database. Comparisons of Bengal Fan samples to Yarlung-Brahmaputra and Ganges KDE datasets revealed evidence of shifting sediment proveance and routing across Miocene-Pleistocene time. Inverse modeling of AFT/AHe data with *DZnmf* against compiled Yarlung AFT sink signals determined 3 distinct source signals for further investigation and characterization into major Tibetan sources. Finally, examples were given of region-wide applications of the database for the *age2exhume* lag-time calculation model described in van der Beek and Schildgen 2022, along with kernel interpolations of widespread cooling-age trends across the orogen. We demonstrate the potential of large-scale datasets in spatial characterization of regional exhumation variability through these methods, and welcome any new additions to the database to maintain relevance and importance into the future.

Acknowledgments

The authors declare no financial conflicts of interests or affiliations with respect to the results of this paper. The database can be accessed at https://tinyurl.com/TeST-Thermo-Database. The authors would like to thank the National Science Foundation (NSF-GEO-NERC #2026870) for providing funding for this research, and all authors of the original studies recorded for their contributions to the web application presented herein.

Open Research

All data needed to evaluate conclusions are present in the paper and/or in the THermO Supplementary Material I folder, available in the figshare data repository. Full thermochronometer datasets are available for export via the THermO database webpage as well: https://tinyurl.com/TeST-Thermo-Database.

References

Adams, B., Dietsch, C., Owen, L.A., Caffee, M.W., Spotila, J., Haneberg, W.C., 2009. Exhumation and incision history of the Lahul Himalaya, northern India, based on (U-Th)/He thermochronometry and terrestrial cosmogenic nuclide methods. Geomorphology 107, 285–299. https://doi.org/10.1016/j.geomorph.2008.12.017

Adams, B.A., Hodges, K.V., Whipple, K.X., Ehlers, T.A., van Soest, M.C., Wartho, J., 2015. Constraints on the tectonic and landscape evolution of the Bhutan Himalaya from thermochronometry: Late Cenozoic Evolution of Bhutan. Tectonics 34, 1329–1347. https://doi.org/10.1002/2015TC003853

Adlakha, V., Lang, K.A., Patel, R.C., Lal, N., Huntington, K.W., 2013a. Rapid long term erosion in the rain shadow of the Shillong Plateau, eastern Himalaya. Tectonophysics 582, 76–83. https://doi.org/10.1016/j.tecto.2012.09.022

Adlakha, V., Patel, R.C., Kumar, A., Lal, N., Sharma, R., Villa, I.M., Kumar, S., 2018. Tectonic control over exhumation in the Arunachal Himalaya; new constraints from apatite fission track analysis. Spec. Publ. - Geol. Soc. Lond. 481, 65–79. https://doi.org/10.1144/SP481.1

Adlakha, V., Patel, R.C., Lal, N., 2013b. Exhumation and its mechanisms: A review of exhumation studies in the Himalaya. J. Geol. Soc. India 81, 481–502. https://doi.org/10.1007/s12594-013-0064-0

Aoya, M., Wallis, S.R., Terada, K., Lee, J., Kawakami, T., Wang, Y., Heizler, M., 2005. North-south extension in the Tibetan crust triggered by granite emplacement. Geology 33, 853. https://doi.org/10.1130/G21806.1

Argand, E., 1977. Tectonics of Asia, Tectonics of Asia. Hafner Press.

Arita, K., Ganzawa, Y., Ono, Y., Endo, K., Iwata, S., 1997. Thrust tectonics and uplift process of the Nepal Himalaya revealed from fission-track ages. Chigaku Zasshi J. Geogr. 106, 156–167.

Bartoli, G., Sarnthein, M., Weinelt, M., Erlenkeuser, H., Garbe-Schönberg, D., Lea, D.W., 2005. Final closure of Panama and the onset of northern hemisphere glaciation. Earth Planet. Sci. Lett. 237, 33–44. https://doi.org/10.1016/j.epsl.2005.06.020

Bernet, M., Spiegel, C., 2004. Introduction: Detrital thermochronology, in: Detrital Thermochronology - Provenance Analysis, Exhumation, and Landscape Evolution of Mountain Belts. Geological Society of America. https://doi.org/10.1130/0-8137-2378-7.1

Bian, S., Gong, J., Zuza, A.V., Yang, R., Chen, L., Ji, J., Yu, X., Tian, Y., Yu, Z., Cheng, X., Lin, X., Chen, H., 2022. Along-Strike Variation in the Initiation Timing of the North-Trending Rifts in Southern Tibet as Revealed From the Yadong-Gulu Rift. Tectonics 41. https://doi.org/10.1029/2021TC007091

Bian, S., Gong, J., Zuza, A.V., Yang, R., Tian, Y., Ji, J., Chen, H., Xu, Q., Chen, L., Lin, X., Cheng, X., Tu, J., Yu, X., 2020. Late Pliocene onset of the Cona rift, eastern Himalaya, confirms eastward propagation of extension in Himalayan-Tibetan orogen. Earth Planet. Sci. Lett. 544, 116383. https://doi.org/10.1016/j.epsl.2020.116383

Blum, M., Rogers, K., Gleason, J., Najman, Y., Cruz, J., Fox, L., 2018. Allogenic and Autogenic Signals in the Stratigraphic Record of the Deep-Sea Bengal Fan. Sci. Rep. 8, 7973. https://doi.org/10.1038/s41598-018-25819-5

Blythe, A.E., Burbank, D.W., Carter, A., Schmidt, K., Putkonen, J., 2007. Plio-Quaternary exhumation history of the central Nepalese Himalaya: 1. Apatite and zircon fission track and apatite [U-Th]/He analyses: CENTRAL NEPAL PLIO-QUATERNARY EXHUMATION. Tectonics 26, n/a-n/a. https://doi.org/10.1029/2006TC001990

Bojar, A.-V., Fritz, H., Nicolescu, S., Bregar, M., Gupta, R.P., 2005. Timing and mechanisms of Central Himalayan exhumation: discriminating between tectonic and erosion processes. Terra Nova 17, 427–433. https://doi.org/10.1111/j.1365-3121.2005.00629.x

Bollinger, L., Avouac, J.P., Beyssac, O., Catlos, E.J., Harrison, T.M., Grove, M., Goffé, B., Sapkota, S., 2004. Thermal structure and exhumation history of the Lesser Himalaya in central Nepal: THERMAL STRUCTURE OF THE LESSER HIMALAYA. Tectonics 23, n/a-n/a. https://doi.org/10.1029/2003TC001564

Burbank, D.W., Blythe, A.E., Putkonen, J., Pratt-Sitaula, B., Gabet, E., Oskin, M., Barros, A., Ojha, T.P., 2003. Decoupling of erosion and precipitation in the Himalayas. Nature 426, 652–655. https://doi.org/10.1038/nature02187

Burg, J.-P., Nievergelt, P., Oberli, F., Seward, D., Davy, P., Maurin, J.-C., Diao Zhizhong, Meier, M., Gaetani, M., Windley, B., 1998. The Namche Barwa syntaxis; evidence for exhumation related to compressional crustal folding. J. Asian Earth Sci. 16, 239–252.

Burg, J.P., Nievergelt, P., Oberli, F., Seward, D., Ristedt, H., Matter, A., Pfiffner, O.A., 1998. Erosion of crustal folds in the Himalayan syntaxes. Terra Nostra Bonn 98–1, 5.

Burke, W.B., Laskowski, A.K., Orme, D.A., Sundell, K.E., Taylor, M.H., Guo, X., Ding, L., 2021. Record of Crustal Thickening and Synconvergent Extension from the Dajiamang Tso Rift, Southern Tibet. Geosciences 11, 209. https://doi.org/10.3390/geosciences11050209

Carrapa, B., Faiz bin Hassim, M., Kapp, P.A., DeCelles, P.G., Gehrels, G., 2017. Tectonic and erosional history of southern Tibet recorded by detrital chronological signatures along the Yarlung River drainage. Geol. Soc. Am. Bull. 129, 570–581. https://doi.org/10.1130/B31587.1

Carrapa, B., Orme, D.A., DeCelles, P.G., Kapp, P., Cosca, M.A., Waldrip, R., 2014. Miocene burial and exhumation of the India-Asia collision zone in southern Tibet: Response to slab dynamics and erosion. Geology 42, 443–446. https://doi.org/10.1130/G35350.1

Carrapa, B., Robert, X., DeCelles, P.G., Orme, D.A., Thomson, S.N., Schoenbohm, L.M., 2016. Asymmetric exhumation of the Mount Everest region: Implications for the tectono-topographic evolution of the Himalaya. Geology 44, 611–614. https://doi.org/10.1130/G37756.1

Catlos, E.J., Harrison, T.M., Kohn, M.J., Grove, M., Ryerson, F.J., Manning, C.E., Upreti, B.N., 2001. Geochronologic and thermobarometric constraints on the evolution of the Main Central Thrust, central Nepal Himalaya. J. Geophys. Res. Solid Earth 106, 16177–16204. https://doi.org/10.1029/2000JB900375

Célérier, J., Harrison, T.M., Beyssac, O., Herman, F., Dunlap, W.J., Webb, A.A.G., 2009. The Kumaun and Garwhal Lesser Himalaya, India: Part 2. Thermal and deformation histories. Geol. Soc. Am. Bull. 121, 1281–1297. https://doi.org/10.1130/B26343.1

Chapman, J.B., Kapp, P., 2017. Tibetan Magmatism Database. Geochem. Geophys. Geosystems 18, 4229–4234. https://doi.org/10.1002/2017GC007217

Chirouze, F., Bernet, M., Huyghe, P., Erens, V., Dupont-Nivet, G., Senebier, F., 2012. Detrital thermochronology and sediment petrology of the middle Siwaliks along the Muksar Khola section in eastern Nepal. J. Asian Earth Sci. 44, 94–106. https://doi.org/10.1016/j.jseaes.2011.01.009

Clark, R.J., 2005. Structural constraints on the exhumation of the Tso Morari Dome, NW Himalaya (Master's). Struct. Constraints Exhum. Tso Morari Dome NW Himalaya. University of Wisconsin at Madison.

Clift, P.D., Giosan, L., Carter, A., Garzanti, E., Galy, V., Tabrez, A.R., Pringle, M., Campbell, I.H., France-Lanord, C., Blusztajn, J., Allen, C., Alizai, A., Lueckge, A., Danish, M., Rabbani, M.M., Tada, R., Zheng, H., 2010. Monsoon control over erosion patterns in the western Himalaya; possible feed-back into the tectonic evolution. Geol. Soc. Spec. Publ. 342, 185–218. https://doi.org/10.1144/SP342.12

Coleman, M.E., Hodges, K.V., 1998. Contrasting Oligocene and Miocene thermal histories from the hanging wall and footwall of the South Tibetan detachment in the central Himalaya from ^{40}Ar/^{39}Ar thermochronology, Marsyandi Valley, central Nepal. Tectonics 17, 726–740. https://doi.org/10.1029/98TC02777

Colleps, C.L., McKenzie, N.R., Stockli, D.F., Hughes, N.C., Singh, B.P., Webb, A.A.G., Myrow, P.M., Planavsky, N.J., Horton, B.K., 2018. Zircon (U-Th)/He Thermochronometric Constraints on Himalayan Thrust Belt Exhumation, Bedrock Weathering, and Cenozoic Seawater Chemistry. Geochem. Geophys. Geosystems 19, 257–271. https://doi.org/10.1002/2017GC007191

Copeland, P., Harrison, T.M., Hodges, K.V., Maruejol, P., Le Fort, P., Pecher, A., 1991. An early Pliocene thermal disturbance of the Main Central Thrust, central Nepal; implications for Himalayan tectonics. J. Geophys. Res. 96, 8475–8500. https://doi.org/10.1029/91JB00178

Copeland, P., Harrison, T.M., Pan, Y., Kidd, W.S.F., Roden, M., Zhang, Y., 1995. Thermal evolution of the Gangdese batholith, southern Tibet: A history of episodic unroofing. Tectonics 14, 223–236. https://doi.org/10.1029/94TC01676

Copeland, P., Harrison, T.M., Parrish, R.R., Burchfiel, B.C., Hodges, K.V., Kidd, W.S.F., Anonymous, 1987. Constraints on the age of normal faulting, north face of Mt. Everest; implications for Oligo-Miocene uplift. Eos Trans. Am. Geophys. Union 68, 1444.

Copeland, P., Mark Harrison, T., Le Fort, P., 1990. Age and cooling history of the Manaslu granite: implications for Himalayan tectonics. J. Volcanol. Geotherm. Res. 44, 33–50. https://doi.org/10.1016/0377-0273(90)90010-D

Coutand, I., Whipp, D.M., Grujic, D., Bernet, M., Fellin, M.G., Bookhagen, B., Landry, K.R., Ghalley, S.K., Duncan, C., 2014. Geometry and kinematics of the Main Himalayan Thrust and Neogene crustal exhumation in the Bhutanese Himalaya derived from inversion of multithermochronologic data: NEOGENE EXHUMATION OF BHUTAN HIMALAYAS. J. Geophys. Res. Solid Earth 119, 1446–1481. https://doi.org/10.1002/2013JB010891

Cross, E.A., III, 2014. The structure, stratigraphy, and evolution of the Lesser Himalaya of central Nepal (Master's). Struct. Stratigr. Evol. Lesser Himalaya Cent. Nepal. University of Arizona.

Crouzet, C., Dunkl, I., Paudel, L., Árkai, P., Rainer, T.M., Balogh, K., Appel, E., 2007. Temperature and age constraints on the metamorphism of the Tethyan Himalaya in Central Nepal: A multidisciplinary approach. J. Asian Earth Sci. 30, 113–130. https://doi.org/10.1016/j.jseaes.2006.07.014

Dai, J., Fox, M., Han, X., Tremblay, M.M., Xu, S., Shuster, D.L., Liu, B., Zhang, J., Wang, C., 2021. Two Stages of Accelerated Exhumation in the Middle Reach of the Yarlung River, Southern Tibet Since the Mid-Miocene. Tectonics 40. https://doi.org/10.1029/2020TC006618

Dai, J., Fox, M., Shuster, D.L., Hourigan, J., Han, X., Li, Y., Wang, C., 2020. Burial and exhumation of the Hoh Xil Basin, northern Tibetan Plateau: Constraints from detrital (U-Th)/He ages. Basin Res. 32, 894–915. https://doi.org/10.1111/bre.12405

Dai, J., Wang, C., Hourigan, J., Santosh, M., 2013. Insights into the early Tibetan Plateau from (U–Th)/He thermochronology. J. Geol. Soc. 170, 917–927. https://doi.org/10.1144/jgs2012-076

DeCelles, P.G., Carrapa, B., Gehrels, G.E., Chakraborty, T., Ghosh, P., 2016. Along-strike continuity of structure, stratigraphy, and kinematic history in the Himalayan thrust belt: The view from Northeastern India: EASTERN HIMALAYAN THRUST BELT. Tectonics 35, 2995–3027. https://doi.org/10.1002/2016TC004298

DeCelles, P.G., Carrapa, B., Ojha, T.P., Gehrels, G.E., Collins, D., 2020. Structural and thermal evolution of the Himalayan thrust belt in midwestern Nepal. Spec. Pap. - Geol. Soc. Am. 547, 79. https://doi.org/10.1130/2020.2547(01)

DeCelles, P.G., Robinson, D.M., Quade, J., Ojha, T.P., Garzione, C.N., Copeland, P., Upreti, B.N., 2001. Stratigraphy, structure, and tectonic evolution of the Himalayan fold-thrust belt in western Nepal. Tectonics 20, 487–509. https://doi.org/10.1029/2000TC001226

Deeken, A., Thiede, R.C., Sobel, E.R., Hourigan, J.K., Strecker, M.R., 2011. Exhumational variability within the Himalaya of northwest India. Earth Planet. Sci. Lett. 305, 103–114. https://doi.org/10.1016/j.epsl.2011.02.045

Dewey, J.F., Shackleton, R.M., Chengfa, C., Yiyin, S., Chengfa, C., Shackleton, R.M., Dewey, J.F., Jixiang, Y., 1988. The tectonic evolution of the Tibetan Plateau. Philos. Trans. R. Soc. Lond. Ser. Math. Phys. Sci. 327, 379–413. https://doi.org/10.1098/rsta.1988.0135

Dezes, P.J., Vannay, J.C., Steck, A., Bussy, F., Cosca, M., 1999. Synorogenic extension; quantitative constraints on the age and displacement of the Zanskar shear zone (Northwest Himalaya). Geol. Soc. Am. Bull. 111, 364–374. https://doi.org/10.1130/0016-7606(1999)111<0364:SEQCOT>2.3.CO;2

Ding, L., Dalai, Z., Yin, A., Kapp, P., Harrison, T.M., 2001. Cenozoic structural and metamorphic evolution of the eastern Himalayan syntaxis (Namche Barwa). Earth Planet. Sci. Lett. 192, 423–438. https://doi.org/10.1016/S0012-821X(01)00463-0

Dunkl, I., Antolin, B., Wemmer, K., Rantitsch, G., Kienast, M., Montomoli, C., Ding, L., Carosi, R., Appel, E., El Bay, R., Xu, Q., von Eynatten, H., Gloaguen, R., Ratschbacher, L., 2011. Metamorphic evolution of the Tethyan Himalayan flysch in SE Tibet. Geol. Soc. Spec. Publ. 353, 45–69. https://doi.org/10.1144/SP353.4

Edwards, R.M., 1995. (super 40) Ar/ (super 39) Ar geochronology of the Main Central Thrust (MCT) region; evidence for late Miocene to Pliocene disturbances along the MCT, Marsyangdi River valley, west-central Nepal Himalaya. J. Nepal Geol. Soc. 10, 41–46.

Enkelmann, E., Ehlers, T.A., Zeitler, P.K., Hallet, B., 2011. Denudation of the Namche Barwa antiform, eastern Himalaya. Earth Planet. Sci. Lett. 307, 323–333. https://doi.org/10.1016/j.epsl.2011.05.004

Eugster, P., Thiede, R.C., Scherler, D., Stübner, K., Sobel, E.R., Strecker, M.R., 2018. Segmentation of the Main Himalayan Thrust Revealed by Low-Temperature Thermochronometry in the Western Indian Himalaya. Tectonics 37, 2710–2726. https://doi.org/10.1029/2017TC004752

Fan, S., Murphy, M.A., Whipp, D.M., Saylor, J.E., Copeland, P., Hoxey, A.K., Taylor, M.H., Stockli, D.F., 2022. Megathrust Heterogeneity, Crustal Accretion, and a Topographic Embayment in the Western Nepal Himalaya: Insights From the Inversion of Thermochronological Data. Tectonics 41. https://doi.org/10.1029/2021TC007071

Finnegan, N.J., Hallet, B., Montgomery, D.R., Zeitler, P.K., Stone, J.O., Anders, A.M., Yuping, L., 2008. Coupling of rock uplift and river incision in the Namche Barwa-Gyala Peri massif, Tibet. Geol. Soc. Am. Bull. 120, 142–155. https://doi.org/10.1130/B26224.1

Foster, D.A., Gleadow, A.J.W., Mortimer, G., 1994. Rapid Pliocene exhumation in the Karakoram (Pakistan), revealed by fission-track thermochronology of the K2 gneiss. Geol. Boulder 22, 19–22. https://doi.org/10.1130/0091-7613(1994)022<0019:RPEITK>2.3.CO;2

Fox, M., Herman, F., Willett, S.D., May, D.A., 2014. A linear inversion method to infer exhumation rates in space and time from thermochronometric data. Earth Surf. Dyn. 2, 47–65. https://doi.org/10.5194/esurf-2-47-2014

Gallagher, K., 2012. Transdimensional inverse thermal history modeling for quantitative thermochronology: TRANSDIMENSIONAL INVERSE THERMAL HISTORY. J. Geophys. Res. Solid Earth 117, n/a-n/a. https://doi.org/10.1029/2011JB008825

Garver, J.I., Brandon, M.T., Roden-Tice, M., Kamp, P.J.J., 1999. Exhumation history of orogenic highlands determined by detrital fission-track thermochronology. Geol. Soc. Lond. Spec. Publ. 154, 283–304. https://doi.org/10.1144/GSL.SP.1999.154.01.13

Gautam, P., Koshimizu, S., 1991. Zircon & apatite fission track dating of the Ampipal alkaline massif, the Nepal Lesser Himalaya. J. Nepal Geol. Soc. 7, 1–8.

Gavillot, Y., Meigs, A.J., Sousa, F.J., Stockli, D., Yule, D., Malik, M., 2018. Late Cenozoic Foreland-to-Hinterland Low-Temperature Exhumation History of the Kashmir Himalaya. Tectonics 37, 3041–3068. https://doi.org/10.1029/2017TC004668

Ge, Y., Li, Y., Wang, X., Qian, X., Zhang, J., Zhou, A., Liu-Zeng, J., 2018. Oligocene-Miocene burial and exhumation of the southernmost Gangdese mountains from sedimentary and thermochronological evidence. Tectonophysics 723, 68–80. https://doi.org/10.1016/j.tecto.2017.12.003

Ge, Y.-K., Dai, J.-G., Wang, C.-S., Li, Y.-L., Xu, G.-Q., Danisik, M., 2017. Cenozoic thermo-tectonic evolution of the Gangdese batholith constrained by low-temperature thermochronology. Gondwana Res. 41, 451–462. https://doi.org/10.1016/j.gr.2016.05.006

Ghoshal, S., McQuarrie, N., Robinson, D.M., Adhikari, D.P., Morgan, L.E., Ehlers, T.A., 2020. Constraining Central Himalayan (Nepal) Fault Geometry Through Integrated Thermochronology and Thermokinematic Modeling. Tectonics 39. https://doi.org/10.1029/2020TC006399

Godin, L., Parrish, R.R., Brown, R.L., Hodges, K.V., 2001. Crustal thickening leading to exhumation of the Himalayan Metamorphic core of central Nepal: Insight from U-Pb Geochronology and ^{40}Ar/ ^{39}Ar Thermochronology. Tectonics 20, 729–747. https://doi.org/10.1029/2000TC001204

Gong Junfeng, Ji Jianqing, Han Baofu, Chen, J., Sun Dongxia, Li, B., Zhou, J., Tu Jiyao, Dalai, Z., 2012. Early subduction-exhumation and late channel flow of the Greater Himalayan Sequence; implications from the Yadong section in the eastern Himalaya. Int. Geol. Rev. 54, 1184–1202. https://doi.org/10.1080/00206814.2011.626604

Gourbet, L., Mahéo, G., Shuster, D.L., Tripathy-Lang, A., Leloup, P.H., Paquette, J.-L., 2016. River network evolution as a major control for orogenic exhumation: Case study from the western Tibetan plateau. Earth Planet. Sci. Lett. 456, 168–181. https://doi.org/10.1016/j.epsl.2016.09.037

Govin, G., van der Beek, P., Najman, Y., Millar, I., Gemignani, L., Huyghe, P., Dupont-Nivet, G., Bernet, M., Mark, C., Wijbrans, J., 2020. Early onset and late acceleration of rapid exhumation in the Namche Barwa syntaxis, eastern Himalaya. Geology 48, 1139–1143. https://doi.org/10.1130/G47720.1

Grujic, D., Ashley, K.T., Coble, M.A., Coutand, I., Kellett, D.A., Larson, K.P., Whipp, D.M., Gao, M., Whynot, N., 2020. Deformational Temperatures Across the Lesser Himalayan Sequence in Eastern Bhutan and Their Implications for the Deformation History of the Main Central Thrust. Tectonics 39. https://doi.org/10.1029/2019TC005914

Grujic, D., Coutand, I., Bookhagen, B., Bonnet, S., Blythe, A., Duncan, C., 2006. Climatic forcing of erosion, landscape, and tectonics in the Bhutan Himalayas. Geol. Boulder 34, 801–804. https://doi.org/10.1130/G22648.1

Guillot, S., Pecher, A., Le Fort, P., Anonymous, 1994. Comparison of the emplacement of some High-Himalayan leucogranites (Mugu-Mustang, Manaslu and Kula-Kangri). J. Nepal Geol. Soc. 10, Special issue, 61.

Haider, V.L., Dunkl, I., von Eynatten, H., Ding, L., Frei, D., Zhang, L., 2013. Cretaceous to Cenozoic evolution of the northern Lhasa Terrane and the early Paleogene development of peneplains at Nam Co, Tibetan Plateau. J. Asian Earth Sci. 70–71, 79–98. https://doi.org/10.1016/j.jseaes.2013.03.005

Haproff, P.J., Odlum, M.L., Zuza, A.V., Yin, A., Stockli, D.F., 2020. Structural and thermochronologic constraints on the Cenozoic tectonic development of the northern Indo-Burma Ranges. Tectonics 39, Article e2020TC006231. https://doi.org/10.1029/2020TC006231

Hein, C.J., Galy, V., Galy, A., France-Lanord, C., Kudrass, H., Schwenk, T., 2017. Post-glacial climate forcing of surface processes in the Ganges–Brahmaputra river basin and implications for carbon sequestration. Earth Planet. Sci. Lett. 478, 89–101. https://doi.org/10.1016/j.epsl.2017.08.013

Herman, F., Copeland, P., Avouac, J.-P., Bollinger, L., Mahéo, G., Le Fort, P., Rai, S., Foster, D., Pêcher, A., Stüwe, K., Henry, P., 2010. Exhumation, crustal deformation, and thermal structure of the Nepal Himalaya derived from the inversion of thermochronological and thermobarometric data and modeling of the topography. J. Geophys. Res. 115, B06407. https://doi.org/10.1029/2008JB006126

Hetzel, R., Dunkl, I., Haider, V., Strobl, M., von Eynatten, H., Ding, L., Frei, D., 2011. Peneplain formation in southern Tibet predates the India-Asia collision and plateau uplift. Geol. Boulder 39, 983–986. https://doi.org/10.1130/G32069.1

Hodges, K.V., Bowring, S.A., Davidek, K.L., Hawkins, D., Krol, M., 1998. Evidence for rapid displacement on Himalayan normal faults and the importance of tectonic denudation in the evolution of mountain ranges. Geol. Boulder 26, 483–486. https://doi.org/10.1130/0091-7613(1998)026<0483:EFRDOH>2.3.CO;2

Hodges, K.V., Hames, W.E., Olszewski, W., Burchfiel, B.C., Royden, L.H., Chen, Z., 1994. Thermobarometric and (super 40) Ar/ (super 39) Ar geochronologic constraints on Eohimalayan metamorphism in the Dinggye area, southern Tibet. Contrib. Mineral. Petrol. 117, 151–163.

Huntington, K.W., Blythe, A.E., Hodges, K.V., 2006. Climate change and Late Pliocene acceleration of erosion in the Himalaya. Earth Planet. Sci. Lett. 252, 107–118. https://doi.org/10.1016/j.epsl.2006.09.031

Huyghe, P., Bernet, M., Galy, A., Naylor, M., Cruz, J., Gyawali, B.R., Gemignani, L., Mugnier, J.-L., 2020. Rapid exhumation since at least 13 Ma in the Himalaya recorded by detrital apatite fission-track dating of Bengal fan (IODP Expedition 354) and modern Himalayan river sediments. Earth Planet. Sci. Lett. 534, 116078. https://doi.org/10.1016/j.epsl.2020.116078

Jain, A.K., Kumar, D., Singh, S., Kumar, A., Lal, N., 2000. Timing, quantification and tectonic modelling of Pliocene-Quaternary movements in the NW Himalaya; evidence from fission track dating. Earth Planet. Sci. Lett. 179, 437–451. https://doi.org/10.1016/S0012-821X(00)00133-3

Jepson, G., Carrapa, B., Gillespie, J., Feng, R., DeCelles, P.G., Kapp, P., Tabor, C.R., Zhu, J., 2021. Climate as the Great Equalizer of Continental-Scale Erosion. Geophys. Res. Lett. 48. https://doi.org/10.1029/2021GL095008

Ji, W.-Q., Wu, F.-Y., Chung, S.-L., Li, J.-X., Liu, C.-Z., 2009. Zircon U–Pb geochronology and Hf isotopic constraints on petrogenesis of the Gangdese batholith, southern Tibet. Chem. Geol. 262, 229–245. https://doi.org/10.1016/j.chemgeo.2009.01.020

Jia Dong, Li, Y., Yan, B., Li, Z., Wang Maomao, Chen Zhuxin, Zhang, Y., Chen, H., Xia Qunke, Xu Yixian, 2020. The Cenozoic thrusting sequence of the Longmen Shan fold-and-thrust belt, eastern margin of the Tibetan Plateau; insights from low-temperature thermochronology. J. Asian Earth Sci. 198, Article 104381. https://doi.org/10.1016/j.jseaes.2020.104381

Jolivet, M., Brunel, M., Seward, D., Xu, Z., Yang, J., Roger, F., Tapponnier, P., Malavieille, J., Arnaud, N., Wu, C., 2001. Mesozoic and Cenozoic tectonics of the northern edge of the Tibetan plateau: fission-track constraints. Tectonophysics 343, 111–134. https://doi.org/10.1016/S0040-1951(01)00196-2

Kang, W., Xu Xiwei, Yu, G., Tan Xibin, Kang, L., Luo Jiahong, Zhang, W., 2019. Differential late-Cenozoic uplift across the Dongjiu-Milin fault zone in the eastern Himalayan Syntaxis revealed by low-temperature thermochronology. J. Asian Earth Sci. 179, 189–199. https://doi.org/10.1016/j.jseaes.2019.04.022

Kapp, J.L.D., 2005. Nyainqentanglha Shan: A window into the tectonic, thermal, and geochemical evolution of the Lhasa block, southern Tibet. J. Geophys. Res. 110, B08413. https://doi.org/10.1029/2004JB003330

Kapp, P., DeCelles, P.G., 2019. Mesozoic–Cenozoic geological evolution of the Himalayan-Tibetan orogen and working tectonic hypotheses. Am. J. Sci. 319, 159–254. https://doi.org/10.2475/03.2019.01

Kellett, D.A., Grujic, D., Coutand, I., Cottle, J., Mukul, M., 2013. The South Tibetan detachment system facilitates ultra rapid cooling of granulite-facies rocks in Sikkim Himalaya: S. TIBETAN DETACHMENT, SIKKIM HIMALAYA. Tectonics 32, 252–270. https://doi.org/10.1002/tect.20014

Ketcham, R.A., 2005. Forward and Inverse Modeling of Low-Temperature Thermochronometry Data. Rev. Mineral. Geochem. 58, 275–314. https://doi.org/10.2138/rmg.2005.58.11

Khanal, S., 2014. Structural and kinematic evolution of the Himalayan thrust belt, central Nepal (Ph.D.). ProQuest Diss. Theses. The University of Alabama, Ann Arbor.

Kirby, E., Reiners, P.W., Krol, M.A., Whipple, K.X., Hodges, K.V., Farley, K.A., Tang, W., Chen, Z., 2002. Late Cenozoic evolution of the eastern margin of the Tibetan Plateau: Inferences from ^{40}Ar/^{39}Ar and (U-Th)/He thermochronology: LATE CENOZOIC EVOLUTION OF EASTERN TIBET. Tectonics 21, 1-1-1–20. https://doi.org/10.1029/2000TC001246

Kirstein, L.A., Foeken, J.P.T., van der Beek, P., Stuart, F.M., Phillips, R.J., 2009. Cenozoic unroofing history of the Ladakh Batholith, western Himalaya, constrained by thermochronology and numerical modelling. J. Geol. Soc. 166, 667–678. https://doi.org/10.1144/0016-76492008-107

Kirstein, L.A., Sinclair, H., Stuart, F.M., Dobson, K., 2006. Rapid early Miocene exhumation of the Ladakh batholith, western Himalaya. Geology 34, 1049. https://doi.org/10.1130/G22857A.1

Kumar, A., Lal, N., Jain, A.K., Sorkhabi, R.B., 1995. Late Cenozoic-Quaternary thermo-tectonic history of Higher Himalayan Crystalline (HHC) in Kishtwar-Padar-Zanskar region, NW Himalaya; evidence from fission track ages. J. Geol. Soc. India 45, 375–391.

Lai, Q., Ding, L., Wang, H., Yue, Y., Cai, F., 2007. Constraining the stepwise migration of the eastern Tibetan Plateau margin by apatite fission track thermochronology. Sci. China Ser. Earth Sci. 50, 172–183. https://doi.org/10.1007/s11430-007-2048-7

Lal, N., Mehta, Y.P., Kumar, D., Kumar, A., Jain, A.K., Manickavasagam, R.M., 1999. Cooling and exhumation history of the Mandi Granite and adjoining tectonic units, Himachal Pradesh, and estimation of closure temperature from external surface of zircon. Gondwana Res. Group Mem. 6, 207–216.

Lama Sherpa, T., DeCelles, P.G., Carrapa, B., Anonymous, 2019. Exhumation history of the Bhumichula Plateau; a relict low relief surface in the Himalayan thrust belt of Nepal? Abstr. Programs - Geol. Soc. Am. 51, Abstract no. 283-10.

Landry, K.R., Coutand, I., Whipp, D.M., Grujic, D., Hourigan, J.K., 2016. Late Neogene tectonically driven crustal exhumation of the Sikkim Himalaya: Insights from inversion of multithermochronologic data: Neogene Tectonics of the Sikkim Himalaya. Tectonics 35, 833–859. https://doi.org/10.1002/2015TC004102

Lang, K.A., Huntington, K.W., Burmester, R., Housen, B., 2016. Rapid exhumation of the eastern Himalayan syntaxis since the late Miocene. Geol. Soc. Am. Bull. 128, 1403–1422. https://doi.org/10.1130/B31419.1

Laskowski, A.K., Kapp, P., Cai, F., 2018. Gangdese culmination model: Oligocene–Miocene duplexing along the India-Asia suture zone, Lazi region, southern Tibet. GSA Bull. 130, 1355–1376. https://doi.org/10.1130/B31834.1

Laskowski, A.K., Kapp, P., Ding, L., Campbell, C., Liu, X., 2017. Tectonic evolution of the Yarlung suture zone, Lopu Range region, southern Tibet: India-Asia Suture Tectonics, Lopu Range. Tectonics 36, 108–136. https://doi.org/10.1002/2016TC004334

Leary, R.J., DeCelles, P.G., Quade, J., Gehrels, G.E., Waanders, G., 2016. The Liuqu Conglomerate, southern Tibet: Early Miocene basin development related to deformation within the Great Counter Thrust system. Lithosphere 8, 427–450. https://doi.org/10.1130/L542.1

Lee, J., Hacker, B.R., Dinklage, W.S., Wang, Y., Gans, P., Calvert, A., Wan, J., Chen, W., Blythe, A.E., McClelland, W., 2000. Evolution of the Kangmar Dome, southern Tibet: Structural, petrologic, and thermochronologic constraints. Tectonics 19, 872–895. https://doi.org/10.1029/1999TC001147

Li, G., Kohn, B., Sandiford, M., Xu, Z., 2017. India-Asia convergence: Insights from burial and exhumation of the Xigaze fore-arc basin, south Tibet. J. Geophys. Res. Solid Earth 122, 3430–3449. https://doi.org/10.1002/2017JB014080

Li, G., Kohn, B., Sandiford, M., Xu, Z., Tian, Y., Seiler, C., 2016. Synorogenic morphotectonic evolution of the Gangdese batholith, South Tibet: Insights from low-temperature thermochronology: EXHUMATION OF GANGDESE BATHOLITH. Geochem. Geophys. Geosystems 17, 101–112. https://doi.org/10.1002/2015GC006047

Li, G., Kohn, B.P., Sandiford, M., Ma Zeliang, Xu Zhiqin, 2018. Post-collisional exhumation of the Indus-Yarlung suture zone and northern Tethyan Himalaya, Saga, SW Tibet. Gondwana Res. 64, 1–10. https://doi.org/10.1016/j.gr.2018.06.006

Li, G., Tian, Y., Kohn, B.P., Sandiford, M., Xu Zhiqin, Cai Zhihui, 2015. Cenozoic low temperature cooling history of the northern Tethyan Himalaya in Zedang, SE Tibet and its implications. Tectonophysics 643, 80–93. https://doi.org/10.1016/j.tecto.2014.12.014

Li, H.-A., Dai, J.-G., Xu, S.-Y., Liu, B.-R., Han, X., Wang, Y.-N., Wang, C.-S., 2019. The formation and expansion of the eastern Proto-Tibetan Plateau: Insights from low-temperature thermochronology. J. Asian Earth Sci. 183, 103975. https://doi.org/10.1016/j.jseaes.2019.103975

Lindhorst, S., Betzler, C., Kroon, D., 2019. Wind variability over the northern Indian Ocean during the past 4 million years – Insights from coarse aeolian dust (IODP exp. 359, site U1467, Maldives). Palaeogeogr. Palaeoclimatol. Palaeoecol. 536, 109371. https://doi.org/10.1016/j.palaeo.2019.109371

Long, S.P., McQuarrie, N., Tobgay, T., Coutand, I., Cooper, F.J., Reiners, P.W., Wartho, J.-A., Hodges, K., Anonymous, 2012. Variable shortening rates in the Bhutan thrust belt; implications for strain partitioning in the eastern Himalayan-Tibetan orogenic system. Am. Geophys. Union Fall Meet. 2012, Abstract T51F-2661.

Long, S.P., McQuarrie, N., Tobgay, T., Reiners, P.W., Anonymous, 2010. Preliminary timing constraints on Lesser Himalayan duplex development from zircon (U-Th)/He thermochronometry, eastern Bhutan. Abstr. Programs - Geol. Soc. Am. 42, 665.

Long, S.P., Robinson, D.M., 2021. Construction of the Lesser Himalayan–Subhimalayan thrust belt: The primary driver of thickening, exhumation, and high elevations in the Himalayan orogen since the middle Miocene. Geology 49, 1283–1288. https://doi.org/10.1130/G48967.1

Lu, L., Zhao, Z., Wu Zhenhan, Cheng, Q., Ye Peisheng, 2015. Fission track thermochronology evidence for the Cretaceous and Paleogene tectonic event of Nyainrong Microcontinent, Tibet. Acta Geol. Sin. Engl. Ed. 89, 133–144. https://doi.org/10.1111/1755-6724.12400

Macfarlane, A.M., 1993. Chronology of tectonic events in the crystalline core of the Himalaya, Langtang National Park, central Nepal. Tectonics 12, 1004–1025. https://doi.org/10.1029/93TC00916

Macfarlane, A.M., Hodges, K.V., Lux, D., 1992. A structural analysis of the Main Central Thrust zone, Langtang National Park, central Nepal Himalaya. Geol. Soc. Am. Bull. 104, 1389–1402. https://doi.org/10.1130/0016-7606(1992)104<1389:ASAOTM>2.3.CO;2

Maluski, H., Matte, P., Brunel, M., Xiao Xusheng, 1988. Argon 39 - argon 40 dating of metamorphic and plutonic events in the North and High Himalaya belts (southern Tibet, China). Tectonics 7, 299–326. https://doi.org/10.1029/TC007i002p00299

Maluski, H., Proust, F., Xiao, X.C., 1982. 39Ar/40 Ar dating of the trans-Himalayan calc-alkaline magmatism of southern Tibet. Nature 298, 152–154. https://doi.org/10.1038/298152a0

Mamani, M., Worner, G., Sempere, T., 2010. Geochemical variations in igneous rocks of the Central Andean orocline (13 S to 18 S): Tracing crustal thickening and magma generation through time and space. Geol. Soc. Am. Bull. 122, 162–182. https://doi.org/10.1130/B26538.1

McCallister, A.T., Taylor, M.H., Murphy, M.A., Styron, R.H., Stockli, D.F., 2014. Thermochronologic constraints on the late Cenozoic exhumation history of the Gurla Mandhata metamorphic core complex, Southwestern Tibet: GURLA MANDHATA, SW TIBET. Tectonics 33, 27–52. https://doi.org/10.1002/2013TC003302

McDermott, J.A., Hodges, K.V., Whipple, K.X., Soest, M.C. van, HurtadoJr., and J.M., 2015. Evidence for Pleistocene Low-Angle Normal Faulting in the Annapurna-Dhaulagiri Region, Nepal. J. Geol. 123, 133–151.

McQuarrie, N., Eizenhöfer, P.R., Long, S.P., Tobgay, T., Ehlers, T.A., Blythe, A.E., Morgan, L.E., Gilmore, M.E., Dering, G.M., 2019. The Influence of Foreland Structures on Hinterland Cooling: Evaluating the Drivers of Exhumation in the Eastern Bhutan Himalaya. Tectonics 38, 3282–3310. https://doi.org/10.1029/2018TC005340

McQuarrie, N., Tobgay, T., Long, S.P., Reiners, P.W., Cosca, M.A., 2014. Variable exhumation rates and variable displacement rates: Documenting recent slowing of Himalayan shortening in western Bhutan. Earth Planet. Sci. Lett. 386, 161–174. https://doi.org/10.1016/j.epsl.2013.10.045

Metcalfe, R.P., Treloar, P.J., Searle, M.P., 1993. Pressure, temperature and time constraints on metamorphism across the Main Central Thrust zone and high Himalayan slab in the Garhwal Himalaya. Geol. Soc. Spec. Publ. 74, 485–509.

Molnar, P., England, P., Martinod, J., 1993. Mantle dynamics, uplift of the Tibetan Plateau, and the Indian monsoon. Rev. Geophys. 31, 357–396. https://doi.org/10.1029/93RG02030

Morell, K.D., Sandiford, M., Kohn, B., Codilean, A., Fülöp, R.-H., Ahmad, T., 2017. Current strain accumulation in the hinterland of the northwest Himalaya constrained by landscape analyses, basin-wide denudation rates, and low temperature thermochronology. Tectonophysics 721, 70–89. https://doi.org/10.1016/j.tecto.2017.09.007

Nadin, E.S., Martin, A.J., 2012. Apatite thermochronometry within a knickzone near the Higher Himalaya front, central Nepal: No resolvable fault motion in the past one million years: APATITE THERMOCHRONOMETRY, CENTRAL NEPAL. Tectonics 31, n/a-n/a. https://doi.org/10.1029/2011TC003000

Najman, Y., Mark, C., Barfod, D.N., Carter, A., Parrish, R., Chew, D., Gemignani, L., 2019. Spatial and temporal trends in exhumation of the Eastern Himalaya and syntaxis as determined from a multitechnique detrital thermochronological study of the Bengal Fan. GSA Bull. 131, 1607–1622. https://doi.org/10.1130/B35031.1

Nakajima, T., Kawakami, T., Iwano, H., Danhara, T., Sakai, H., 2022. Denudation Process of Crystalline Nappes in a Continental Collision Zone Constrained by Inversion of Fission-Track Data and Thermokinematic Forward Modeling: An Example From Eastern Nepalese Himalaya. J. Geophys. Res. Solid Earth 127. https://doi.org/10.1029/2021JB023630

Orme, D.A., 2019. Burial and exhumation history of the Xigaze forearc basin, Yarlung suture zone, Tibet. Geosci. Front. 10, 895–908. https://doi.org/10.1016/j.gsf.2017.11.011

Orme, D.A., Carrapa, B., Kapp, P., 2015a. Sedimentology, provenance and geochronology of the upper Cretaceous-lower Eocene western Xigaze forearc basin, southern Tibet. Basin Res. 27, 387–411. https://doi.org/10.1111/bre.12080

Orme, D.A., Reiners, P.W., Hourigan, J.K., Carrapa, B., 2015b. Effects of inherited cores and magmatic overgrowths on zircon (U-Th)/He ages and age-eU trends from Greater Himalayan sequence rocks, Mount Everest region, Tibet: EFFECTS OF ZONATION ON AGE-EU TRENDS. Geochem. Geophys. Geosystems 16, 2499–2507. https://doi.org/10.1002/2015GC005818

Ouimet, W., Whipple, K., Royden, L., Reiners, P., Hodges, K., Pringle, M., 2010. Regional incision of the eastern margin of the Tibetan Plateau. Lithosphere 2, 50–63. https://doi.org/10.1130/L57.1

Patel, R.C., Adlakha, V., Singh, P., Kumar, Y., Lal, N., 2011. Geology, structural and exhumation history of the Higher Himalayan Crystallines in Kumaon Himalaya, India. J. Geol. Soc. India 77, 47–72. https://doi.org/10.1007/s12594-011-0008-5

Patel, R.C., Carter, A., 2009. Exhumation history of the Higher Himalayan Crystalline along Dhauliganga-Goriganga river valleys, NW India: New constraints from fission track analysis: EXHUMATION HISTORY OF KUMAON HIMALAYA. Tectonics 28, n/a-n/a. https://doi.org/10.1029/2008TC002373

Patel, R.C., Kumar, Y., Lal, N., Kumar, A., Arita, K., Yin, A., Singh, S., Okada, H., 2007. Thermotectonic history of the Chiplakot crystalline belt in the Lesser Himalaya, Kumaon, India; constraints from apatite fission-track thermochronology. J. Asian Earth Sci. 29, 430–439. https://doi.org/10.1016/j.jseaes.2006.04.008

Patel, R.C., Singh, P., Lal, N., 2015. Thrusting and back-thrusting as post-emplacement kinematics of the Almora klippe: Insights from Low-temperature thermochronology. Tectonophysics 653, 41–51. https://doi.org/10.1016/j.tecto.2015.03.025

Pebam, J., Adlakha, V., Jain, A.K., Patel, R.C., Lal, N., Singh, S., Kumar, R., Devrani, R., 2021. Apatite and zircon fission-track thermochronology constraining the interplay between tectonics, topography and exhumation, Arunachal Himalaya. J. Earth Syst. Sci. 130, 178. https://doi.org/10.1007/s12040-021-01667-2

Puniya, M.K., Patel, R.C., Pant, P.D., 2019. Structural and thermochronological studies of the Almora klippe, Kumaun, NW India: implications for crustal thickening and exhumation of the NW Himalaya. Geol. Soc. Lond. Spec. Publ. 481, 81–110. https://doi.org/10.1144/SP481-2017-74

Rai, S.P., Noble, J., Singh, D., Rawat, Y.S., Kumar, B., 2021. Spatiotemporal variability in stable isotopes of the Ganga River and factors affecting their distributions. CATENA 204, 105360. https://doi.org/10.1016/j.catena.2021.105360

Reid, A.J., Fowler, A.P., Phillips, D., Wilson, C.J.L., 2005. Thermochronology of the Yidun Arc, central eastern Tibetan Plateau: constraints from 40Ar/39Ar K-feldspar and apatite fission track data. J. Asian Earth Sci. 25, 915–935. https://doi.org/10.1016/j.jseaes.2004.09.002

Robert, X., van der Beek, P., Braun, J., Perry, C., Dubille, M., Mugnier, J.-L., 2009. Assessing Quaternary reactivation of the Main Central thrust zone (central Nepal Himalaya); new thermochronologic data and numerical modeling. Geol. Boulder 37, 731–734. https://doi.org/10.1130/G25736A.1

Robert, X., van der Beek, P., Braun, J., Perry, C., Mugnier, J.-L., 2011. Control of detachment geometry on lateral variations in exhumation rates in the Himalaya: Insights from low-temperature thermochronology and numerical modeling. J. Geophys. Res. 116, B05202. https://doi.org/10.1029/2010JB007893

Robinson, D.M., DeCelles, P.G., Copeland, P., 2006. Tectonic evolution of the Himalayan thrust belt in western Nepal; implications for channel flow models. Geol. Soc. Am. Bull. 118, 865–885, 1 sheet. https://doi.org/10.1130/B25911.1

Rohrmann, A., Kapp, P., Carrapa, B., Reiners, P.W., Guynn, J., Ding, L., Heizler, M., 2011. Thermochronologic evidence for plateau formation in central Tibet by 45 Ma. Geol. Boulder 40, 187–190. https://doi.org/10.1130/G32530.1

Sakai H., Imayama T., Yoshida K., Asahi K., 2017. Tectonics of the Himalayas. J. Geol. Soc. Jpn. 123, 403–421. https://doi.org/10.5575/geosoc.2017.0026

Sakai, H., Iwano, H., Danhara, T., Hirata, T., Takigami, Y., 2013. Emplacement of hot Lesser Himalayan nappes from 15 to 10 Ma in the Jumla-Surkhet region, western Nepal, and their thermal imprint on the underlying Early Miocene fluvial Dumri Formation: Emplacement of hot Himalayan nappes. Isl. Arc 22, 361–381. https://doi.org/10.1111/iar.12030

Sakai, H., Sawada, M., Takigami, Y., Orihashi, Y., Danhara, T., Iwano, H., Kuwahara, Y., Dong Qi, Cai Huawei, Li, J., Gautam, P., Watanabe, T., Nishi, H., Yasunari, T., 2005. Geology of the summit limestone of Mount Qomolangma (Everest) and cooling history of the Yellow Band under the Qomolangma Detachment. Isl. Arc 14, 297–310.

Salameh, E., Frappart, F., Papa, F., Güntner, A., Venugopal, V., Getirana, A., Prigent, C., Aires, F., Labat, D., Laignel, B., 2017. Fifteen Years (1993–2007) of Surface Freshwater Storage Variability in the Ganges-Brahmaputra River Basin Using Multi-Satellite Observations. Water 9, 245. https://doi.org/10.3390/w9040245

Salvi, D., Mathew, G., Kohn, B., Pande, K., Borgohain, B., 2020. Thermochronological insights into the thermotectonic evolution of Mishmi hills across the Dibang Valley, NE Himalayan Syntaxis. J. Asian Earth Sci. 190. https://doi.org/10.1016/j.jseaes.2019.104158

Sanchez, V.I., Murphy, M.A., Robinson, A.C., Lapen, T.J., Heizler, M.T., Ivanov, A.V. (Ivanov, Aleksei V.)., Deverchere, J., Ernst, R., Gladkochub, D.P., 2013. Tectonic evolution of the India-Asia suture zone since middle Eocene time, Lopukangri area, south-central Tibet. J. Asian Earth Sci. 62, 205–220. https://doi.org/10.1016/j.jseaes.2012.09.004

Saylor, J.E., Sundell, K.E., Sharman, G.R., 2019. Characterizing sediment sources by non-negative matrix factorization of detrital geochronological data. Earth Planet. Sci. Lett. 512, 46–58. https://doi.org/10.1016/j.epsl.2019.01.044

Schärer, U., Xu, R.-H., Allègre, C.J., 1984. UPb geochronology of Gangdese (Transhimalaya) plutonism in the Lhasa-Xigaze region, Tibet. Earth Planet. Sci. Lett. 69, 311–320. https://doi.org/10.1016/0012-821X(84)90190-0

Schlup M., Carter A., Cosca M., Steck A., 2003. Exhumation history of eastern Ladakh revealed by 40Ar/39Ar and fission-track ages: the Indus River–Tso Morari transect, NW Himalaya. J. Geol. Soc. 160, 385–399. https://doi.org/10.1144/0016-764902-084

Schultz, M.H., Hodges, K.V., Ehlers, T.A., van Soest, M., Wartho, J.-A., 2017. Thermochronologic constraints on the slip history of the South Tibetan detachment system in the Everest region, southern Tibet. Earth Planet. Sci. Lett. 459, 105–117. https://doi.org/10.1016/j.epsl.2016.11.022

Searle, M.P., Noble, S.R., Hurford, A.J., Rex, D.C., 1999. Age of crustal melting, emplacement and exhumation history of the Shivling Leucogranite, Garhwal Himalaya. Geol. Mag. 136, 513–525. https://doi.org/10.1017/S0016756899002885

Seward, D., Burg, J.P., Sorkhabi, R., Heydari, E., 2008. Growth of the Namche Barwa Syntaxis and associated evolution of the Tsangpo Gorge; constraints from structural and thermochronological data. Tectonophysics 451, 282–289. https://doi.org/10.1016/j.tecto.2007.11.057

Shen, T., Wang, G., Leloup, P.H., van der Beek, P., Bernet, M., Cao, K., Wang, A., Liu, C., Zhang, K., 2016. Controls on Cenozoic exhumation of the Tethyan Himalaya from fission-track thermochronology and detrital zircon U-Pb geochronology in the Gyirong basin area, southern Tibet: The Tethyan Himalaya Cenozoic Exhumation. Tectonics 35, 1713–1734. https://doi.org/10.1002/2016TC004149

Shen, T., Wang, G., van der Beek, P., Bernet, M., Chen, Y., Zhang, P., Wang, A., Cao, K., 2022. Impacts of late Miocene normal faulting on Yarlung Tsangpo River evolution, southeastern Tibet. GSA Bull. https://doi.org/10.1130/B36210.1

Singh, P., Patel, R.C., 2017. Post-emplacement kinematics and exhumation history of the Almora klippe of the Kumaun–Garhwal Himalaya, NW India: revealed by fission track thermochronology. Int. J. Earth Sci. 106, 2189–2202. https://doi.org/10.1007/s00531-016-1422-0

Singh, P., Patel, R.C., Lal, N., 2012. Plio-Plistocene in-sequence thrust propagation along the Main Central Thrust zone (Kumaon–Garhwal Himalaya, India): New thermochronological data. Tectonophysics 574–575, 193–203. https://doi.org/10.1016/j.tecto.2012.08.015

Sobel, E.R., Hilley, G.E., Strecker, M.R., 2003. Formation of internally drained contractional basins by aridity-limited bedrock incision: FORMATION OF INTERNALLY DRAINED BASINS. J. Geophys. Res. Solid Earth 108. https://doi.org/10.1029/2002JB001883

Sorkhabi, R.B., Stump, E., Foland, K.A., Jain, A.K., Burg, J.-P., 1996. Fission-track and (super 40) Ar/ (super 39) Ar evidence for episodic denudation of the Gangotri granites in the Garhwal Higher Himalaya, India. Tectonophysics 260, 187–199.

Streule, M.J., Carter, A., Searle, M.P., Cottle, J.M., 2012. Constraints on brittle field exhumation of the Everest-Makalu section of the Greater Himalayan Sequence: Implications for models of crustal flow: EVEREST-MAKALU FISSION TRACK DATA. Tectonics 31, n/a-n/a. https://doi.org/10.1029/2011TC003062

Stübner, K., Grujic, D., Dunkl, I., Thiede, R., Eugster, P., 2018. Pliocene episodic exhumation and the significance of the Munsiari thrust in the northwestern Himalaya. Earth Planet. Sci. Lett. 481, 273–283. https://doi.org/10.1016/j.epsl.2017.10.036

Stübner, K., Ratschbacher, L., Rutte, D., Stanek, K., Minaev, V., Wiesinger, M., Gloaguen, R., Project TIPAGE members, 2013. The giant Shakhdara migmatitic gneiss dome, Pamir, India-Asia collision zone: 1. Geometry and kinematics: SHAKHDARA DOME: GEOMETRY AND KINEMATICS. Tectonics n/a-n/a. https://doi.org/10.1002/tect.20057

Stuewe, K., Grasemann, B., 2001. The influence of Himalayan topography on low-T geochronology. J. Asian Earth Sci. 19, 65.

Styron, R.H., Taylor, M.H., Sundell, K.E., Stockli, D.F., Oalmann, J.A.G., Möller, A., McCallister, A.T., Liu, D., Ding, L., 2013. Miocene initiation and acceleration of extension in the South Lunggar rift, western Tibet: Evolution of an active detachment system from structural mapping and (U-Th)/He thermochronology: SOUTH LUNGGAR RIFT, SW TIBET. Tectonics n/a-n/a. https://doi.org/10.1002/tect.20053

Sundell, K.E., Taylor, M.H., Styron, R.H., Stockli, D.F., Kapp, P., Hager, C., Liu, D., Ding, L., 2013. Evidence for constriction and Pliocene acceleration of east-west extension in the North Lunggar rift region of west central Tibet: NORTH LUNGGAR RIFT, WEST CENTRAL TIBET. Tectonics 32, 1454–1479. https://doi.org/10.1002/tect.20086

Taylor, M., Forte, A., Laskowski, A., Ding, L., 2021. Active Uplift of Southern Tibet Revealed. GSA Today 31, 4–10. https://doi.org/10.1130/GSATG487A.1

Thiede, R., Robert, X., Stübner, K., Dey, S., Faruhn, J., 2017. Sustained out-of-sequence shortening along a tectonically active segment of the Main Boundary thrust: The Dhauladhar Range in the northwestern Himalaya. Lithosphere 9, 715–725. https://doi.org/10.1130/L630.1

Thiede, R.C., Arrowsmith, J.R., Bookhagen, B., McWilliams, M., Sobel, E.R., Strecker, M.R., Anonymous, 2006. Timing of dome formation and extension in the Tethyan Himalaya, Leo Pargil, NW India. Terra Nostra Bonn 2006–3, 98.

Thiede, R.C., Arrowsmith, J.R., Bookhagen, B., McWilliams, M.O., Sobel, E.R., Strecker, M.R., 2005. From tectonically to erosionally controlled development of the Himalayan Orogen. Geol. Boulder 33, 689–692. https://doi.org/10.1130/G21483AR.1

Thiede, R.C., Bookhagen, B., Arrowsmith, J.R., Sobel, E.R., Strecker, M.R., 2004. Climatic control on rapid exhumation along the Southern Himalayan Front. Earth Planet. Sci. Lett. 222, 791–806. https://doi.org/10.1016/j.epsl.2004.03.015

Thiede, R.C., Ehlers, T.A., 2013. Large spatial and temporal variations in Himalayan denudation. Earth Planet. Sci. Lett. 371–372, 278–293. https://doi.org/10.1016/j.epsl.2013.03.004

Thiede, R.C., Ehlers, T.A., Bookhagen, B., Strecker, M.R., 2009. Erosional variability along the northwest Himalaya. J. Geophys. Res. 114, F01015. https://doi.org/10.1029/2008JF001010

Tremblay, M.M., Fox, M., Schmidt, J.L., Tripathy-Lang, A., Wielicki, M.M., Harrison, T.M., Zeitler, P.K., Shuster, D.L., 2015. Erosion in southern Tibet shut down at ~10 Ma due to enhanced rock uplift within the Himalaya. Proc. Natl. Acad. Sci. 112, 12030–12035. https://doi.org/10.1073/pnas.1515652112

Tshering, P., 2007. Detrital muscovite thermochronology in two drainage basins in western Bhutan (Master's). Detrital Muscovite Thermochronology Two Drain. Basins West. Bhutan. Massachusetts Institute of Technology.

van der Beek, P., Litty, C., Baudin, M., Mercier, J., Robert, X., Hardwick, E., 2016. Contrasting tectonically driven exhumation and incision patterns, western versus central Nepal Himalaya. Geology 44, 327–330. https://doi.org/10.1130/G37579.1

van der Beek, P., Robert, X., Mugnier, J.-L., Bernet, M., Huyghe, P., Labrin, E., 2006. Late Miocene - Recent exhumation of the central Himalaya and recycling in the foreland basin assessed by apatite fission-track thermochronology of Siwalik sediments, Nepal: Recent exhumation of the central Himalaya. Basin Res. 18, 413–434. https://doi.org/10.1111/j.1365-2117.2006.00305.x

van der Beek, P., Schildgen, T.F., 2022. Short Communication: age2exhume – A Matlab script to calculate steady-state vertical exhumation rates from thermochronologic ages in regional datasets and application to the Himalaya (preprint). Geochronological data analysis/statistics/modelling. https://doi.org/10.5194/egusphere-2022-888

van der Beek, P., Van Melle, J., Guillot, S., Pêcher, A., Reiners, P.W., Nicolescu, S., Latif, M., 2009. Eocene Tibetan plateau remnants preserved in the northwest Himalaya. Nat. Geosci. 2, 364–368. https://doi.org/10.1038/ngeo503

Vannay, J.-C., Grasemann, B., Rahn, M., Frank, W., Carter, A., Baudraz, V., Cosca, M., 2004. Miocene to Holocene exhumation of metamorphic crustal wedges in the NW Himalaya: Evidence for tectonic extrusion coupled to fluvial erosion: TECTONICS AND EROSION IN THE NW HIMALAYA. Tectonics 23, n/a-n/a. https://doi.org/10.1029/2002TC001429

Vannay, J.C., Hodges, K.V., 1996. Tectonometamorphic evolution of the Himalayan metamorphic core between the Annapurna and Dhaulagiri, central Nepal. J. Metamorph. Geol. 14, 635–656.

Walker, J.D., Geissman, J.W., Bowring, S.A., Babcock, L.E., 2013. The Geological Society of America Geologic Time Scale. Geol. Soc. Am. Bull. 125, 259–272. https://doi.org/10.1130/B30712.1

Walker, J.D., Martin, M.W., Bowring, S.A., Searle, M.P., Waters, D.J., Hodges, K.V., 1999. Metamorphism, melting, and extension; age constraints from the High Himalayan slab of Southeast Zanskar and Northwest Lahaul. J. Geol. 107, 473–495.

Wang, A., Garver, J.I., Wang, G., Smith, J.A., Zhang, K., 2010. Episodic exhumation of the Greater Himalayan Sequence since the Miocene constrained by fission track thermochronology in Nyalam, central Himalaya. Tectonophysics 495, 315–323. https://doi.org/10.1016/j.tecto.2010.09.037

Wang, A., Min, K., Wang Guocan, Cao, K., Shen Tianyi, Jiang Pengfei, Wei Jiangwei, 2019. Slow exhumation of the Greater Himalaya in the Yadong region, the transition between the central and eastern Himalaya, during the late Neogene. J. Geol. Soc. Lond. 176, 1207–1217. https://doi.org/10.1144/jgs2018-186

Wang, C., Ding, L., Zhang, L.-Y., Kapp, P., Pullen, A., Yue, Y.-H., 2016. Petrogenesis of Middle–Late Triassic volcanic rocks from the Gangdese belt, southern Lhasa terrane: Implications for early subduction of Neo-Tethyan oceanic lithosphere. Lithos 262, 320–333. https://doi.org/10.1016/j.lithos.2016.07.021

Wang, Y., Zhang, X., Sun, L., Wan Jinglin, Arita, K., Yin, A., Singh, S., Okada, H., 2007. Cooling history and tectonic exhumation stages of the south-central Tibetan Plateau (China); constrained by (super 40) Ar/ (super 39) Ar and apatite fission-track thermochronology. J. Asian Earth Sci. 29, 266–282. https://doi.org/10.1016/j.jseaes.2005.11.001

Wang, Y., Zheng Jianjing, Zheng Youwei, Liu, X., Sun, G., 2015. Early Cenozoic Altyn Mountains uplift recorded by detrital zircon fission track age in northwestern Qaidam Basin. Jilin Daxue Xuebao Diqiu Kexue Ban J. Jilin Univ. Earth Sci. Ed. 45, 1447–1459. https://doi.org/10.13278/j.cnki.jjuese.201505116

Wang, Z., Li, T., Zhang, J., Liu, Y., Ma, Z., 2008. The uplifting process of the Bogda Mountain during the Cenozoic and its tectonic implication. Sci. China Ser. Earth Sci. 51, 579–593. https://doi.org/10.1007/s11430-008-0038-z

Warren, C.J., Singh, A.K., Roberts, N.M.W., Regis, D., Halton, A.M., Singh, R.B., 2014. Timing and conditions of peak metamorphism and cooling across the Zimithang Thrust, Arunachal Pradesh, India. Lithos 200–201, 94–110. https://doi.org/10.1016/j.lithos.2014.04.005

Wiesmayr, G., Grasemann, B., 2002. Eohimalayan fold and thrust belt; implications for the geodynamic evolution of the NW-Himalaya (India). Tectonics 21, 18. https://doi.org/10.1029/2002TC001363

Wobus, C.W., Hodges, K.V., Whipple, K.X., 2003. Has focused denudation sustained active thrusting at the Himalayan topographic front? Geology 31, 861. https://doi.org/10.1130/G19730.1

Wolff, R., Hetzel, R., Dunkl, I., Xu, Q., Bröcker, M., Anczkiewicz, A.A., 2019. High-Angle Normal Faulting at the Tangra Yumco Graben (Southern Tibet) since ~15 Ma. J. Geol. 127, 15–36. https://doi.org/10.1086/700406

Wolff, R., Hetzel, R., Hölzer, K., Dunkl, I., Xu, Q., Anczkiewicz, A.A., Li, Z., 2022a. Rift propagation in south Tibet controlled by underthrusting of India: A case study at the Tangra Yumco graben (south Tibet). J. Geol. Soc. jgs2022-090. https://doi.org/10.1144/jgs2022-090

Wolff, R., Hölzer, K., Hetzel, R., Xu, Q., Dunkl, I., Anczkiewicz, A.A., Li, Z., 2022b. Spatially focused erosion in the High Himalaya and the geometry of the Main Himalayan Thrust in Central Nepal (85°E) from thermo-kinematic modeling of thermochronological data in the Gyirong region (southern China). Tectonophysics 834, 229378. https://doi.org/10.1016/j.tecto.2022.229378

Wu, C., Yin, A., Zuza, A.V., Zhang, J., Liu, W., Ding, L., 2016. Pre-Cenozoic geologic history of the central and northern Tibetan Plateau and the role of Wilson cycles in constructing the Tethyan orogenic system. Lithosphere 8, 254–292. https://doi.org/10.1130/L494.1

Xu, Y., Zhang, K., Wang Guocan, Jiang Shangsong, Chen Fenning, Xiang Shuyuan, Dupont-Nivet, G., Hoorn, C., Clift, P., An, Y., 2012. Extended stratigraphy, palynology and depositional environments record the initiation of the Himalayan Gyirong Basin (Neogene China). J. Asian Earth Sci. 44, 77–93. https://doi.org/10.1016/j.jseaes.2011.04.007

Xu Zhiqin, Wang, Q., Pecher, A., Liang Fenghua, Qi Xuexiang, Cai Zhihui, Li Huaqi, Zeng Lingsen, Cao, H., 2013. Orogen-parallel ductile extension and extrusion of the Greater Himalaya in the late Oligocene and Miocene. Tectonics 32, 191–215. https://doi.org/10.1002/tect.20021

Yang, R., Herman, F., Liu, T., Biswas, R.H., Fellin, M.G., Tian, Y., Gong, J., Jiao, R., Maden, C., Chen, H., 2021. Enhanced Quaternary exhumation in the Namche Barwa syntaxis, eastern Himalaya. Geology 49, 958–962. https://doi.org/10.1130/G48595.1

Yin, A., 2010. Cenozoic tectonic evolution of Asia: A preliminary synthesis. Tectonophysics 488, 293–325. https://doi.org/10.1016/j.tecto.2009.06.002

Yin, A., 2006. Cenozoic tectonic evolution of the Himalayan orogen as constrained by along-strike variation of structural geometry, exhumation history, and foreland sedimentation. Earth-Sci. Rev. 76, 1–131. https://doi.org/10.1016/j.earscirev.2005.05.004

Yin, A., Dubey, C.S., Kelty, T.K., Webb, A.A.G., Harrison, T.M., Chou, C.Y., Celerier, J., 2010. Geologic correlation of the Himalayan orogen and Indian craton: Part 2. Structural geology, geochronology, and tectonic evolution of the Eastern Himalaya. Geol. Soc. Am. Bull. 122, 360–395. https://doi.org/10.1130/B26461.1

Yin, A., Harrison, T.M., 2000. Geologic Evolution of the Himalayan-Tibetan Orogen. Annu. Rev. Earth Planet. Sci. 28, 211–280. https://doi.org/10.1146/annurev.earth.28.1.211

Yuan, W., Deng, J., Zheng, Q., Dong, J., Bao, Z., Eizenhoefer, P.R., Xu, X., Huang, Z., 2009. Apatite fission track constraints on the Neogene tectono-thermal history of Nimu area, southern Gangdese terrane, Tibet Plateau. Isl. Arc 18, 488–495. https://doi.org/10.1111/j.1440-1738.2009.00669.x

Yuan, W., Dong, J., Shicheng, W., Carter, A., 2006. Apatite fission track evidence for Neogene uplift in the eastern Kunlun Mountains, northern Qinghai–Tibet Plateau, China. J. Asian Earth Sci. 27, 847–856. https://doi.org/10.1016/j.jseaes.2005.09.002

Zeitler, P.K., 1985. Cooling history of the NW Himalaya, Pakistan. Tectonics 4, 127–151. https://doi.org/10.1029/TC004i001p00127

Zeitler, P.K., Meltzer, A.S., Brown, L., Kidd, W.S.F., Lim, C., Enkelmann, E., 2014. Tectonics and topographic evolution of Namche Barwa and the easternmost Lhasa block, Tibet, in: Toward an Improved Understanding of Uplift Mechanisms and the Elevation History of the Tibetan Plateau. Geological Society of America. https://doi.org/10.1130/2014.2507(02)

Zhang, P., Mei, L., Jiang, S.-Y., Xu, S., Donelick, R.A., Li, R., Zhang, H., 2021. Erosion and sedimentation in SE Tibet and Myanmar during the evolution of the Burmese continental margin from the Late Cretaceous to Early Neogene. Gondwana Res. 95, 149–175. https://doi.org/10.1016/j.gr.2021.04.005

Zhang, P., Najman, Y., Mei, L., Millar, I., Sobel, E.R., Carter, A., Barfod, D., Dhuime, B., Garzanti, E., Govin, G., Vezzoli, G., Hu, X., 2019. Palaeodrainage evolution of the large rivers of East Asia, and Himalayan-Tibet tectonics. Earth-Sci. Rev. 192, 601–630. https://doi.org/10.1016/j.earscirev.2019.02.003

Zhao, Z., Lu, L., Wu Zhenhan, Hu Daogong, 2017. Cenozoic uplift process in Gangdese Belt, Xizang; evidence from thermal history modeling of apatite fission track. Dizhi Tongbao Geol. Bull. China 36, 1553–1561.

Zhu, D.-C., Zhao, Z.-D., Pan, G.-T., Lee, H.-Y., Kang, Z.-Q., Liao, Z.-L., Wang, L.-Q., Li, G.-M., Dong, G.-C., Liu, B., 2009. Early cretaceous subduction-related adakite-like rocks of the Gangdese Belt, southern

Tibet: Products of slab melting and subsequent melt–peridotite interaction? J. Asian Earth Sci. 34, 298–309. https://doi.org/10.1016/j.jseaes.2008.05.003

CHAPTER THREE

CHANGES IN PROVENANCE AND SEDIMENT ROUTING HISTORY OF THE MIOCENE-PLEISTOCENE BENGAL FAN, INDIAN OCEAN USING DETRITAL ZIRCON (U-TH/HE) THERMOCHRONOLOGY

Contributions of Authors and Co-Authors

Manuscript in Chapter 3

Author: Spencer Dixon

Contributions: Performed analyses, determined modeling constraints, interpreted results, created figures, wrote manuscript.

Co-Author: Devon A. Orme

Contributions: Designed study, discussed results and interpretations, edited manuscript.

Co-Author: Kurt Sundell

Contributions: Provided insights and advisement on modeling techniques, discussed results and interpretations, edited manuscript.

Co-Author: Mike Blum

Contributions: Provided U-Pb data for Bengal Fan samples, discussed results and interpretations, edited manuscript.

Co-Author: William Guenthner

Contributions: Provided (U-Th)/He data for Bengal Fan samples, discussed methodologies.

Manuscript Information

Spencer Dixon, Devon A. Orme, Andrew K. Laskowski

Status of Manuscript:
_X_ Prepared for submission to a peer-reviewed journal
____ Officially submitted to a peer-reviewed journal
____ Accepted by a peer-reviewed journal
____ Published in a peer-reviewed journal

Abstract

The Bengal Fan in the Indian Ocean contains a temporally extensive (latest Oligocene – present) detrital record of Himalayan-Tibetan orogenic processes. IODP Expedition 354 conducted in 2015 obtained core sediment samples with the purpose of investigating and expanding this record (France-Lanord et al., 2016). A previous study on Bengal Fan provenance yielding U-Pb age populations from 25 core samples reveal temporal variations in differing depositional age ranges from the mid-Miocene to mid-Pleistocene, suggesting significant changes in sediment routing and drainage patterns from the Himalaya (Blum et al., 2018). We use single zircon (U-Th)/He (ZHe), zircon U-Pb and (U-Th)/He double dating, and sediment mixing models to expand and refine the depositional record of the Bengal Fan from late-Miocene to late-Pleistocene time by introducing additional spatial constraints on provenance interpretations. Herein we report a dataset comprised of 112 individual ZHe ages and 49 ZHe-Pb ages from 15 new core samples of IODP 354, deposited between 6.20 and 0.13 Ma. ZHe ages for the entire dataset range from ~0.28 ± 0.03 Ma – 540.2 ± 6.1 Ma, with 93% of single grains <50 Ma, and 60% <10 Ma. ZHe samples reveal a significant change in cooling age populations across the Pliocene-Pleistocene transition (PPT), with decreasing <5.3 Ma populations and increasing >23 Ma populations, suggesting a shift from Tibetan source regions (Yarlung-Brahmaputra river system) to Greater and Lesser Himalayan sources (Ganges river system). We attribute the variations in cooling age populations to simultaneous tectonic regime change and climatic forcing at key time periods, such as initiation of rapid exhumation in the eastern Himalaya syntaxis (EHS), PPT interglacial periodicity, and intensification of the South Asian Monsoon (SAM).

Introduction

For nearly a century, the Himalayan-Tibetan orogen has been the site of intense research and geologic exploration into continental-scale tectonics, geophysics, geochemistry, geomorphology and thermal histories (e.g. Argand, 1924; Dewey et al., 1988; Yin and Harrison, 2000; Kapp and Decelles, 2019). The Himalayan-Tibetan orogen represents a temporally extensive series of craton and terrane accretions from the Late-Triassic to early Cenozoic when continent-continent collision of the Asian and Indian plates initiated, driving uplift and exhumation of the mountain range into the roof of the world as we know it today (see summary by Kapp and Decelles, 2019). Since the first writings of Argand (1924,1977), the extent of data recovered from both bedrock and detrital records of the orogen has vastly expanded our understanding of the underlying mechanisms behind the topographic expression of the Himalaya. Despite a century of exploration, many mysteries remain regarding the rates at which the mountain range has grown, eroded and evolved both temporally and spatially. In recent years, source-to-sink (S2S) sediment provenance studies of the orogen have focused attention on detrital geochronology and thermochronology age signals from large-scale depositional basins within and surrounding the orogen to determine these rates of change (e.g., Clift et al., 2011; Chirouze et al., 2015; Blum et al., 2018). Even so, vital spatial and temporal constraints on these calculated rate changes are still widely enigmatic.

The Bengal Fan in the Indian Ocean is the world's largest submarine fan, collecting nearly 80% of sediment from the Himalayan-Tibetan orogen (France-Lanord et al., 2016). Since the fan's inception as a distinct entity in the Oligocene, the sediments delivered to the Bengal Fan have varied due to constant avulsions and drainage pattern changes of the Ganges and

Brahmaputra rivers. Large-scale variation in sediment routing has been attributed to a multi-mechanism system of complex feedback between tectonic and climatic processes (Clift et al., 2008; Jepson et al., 2021). Intensification of the South Asian Monsoon (SAM), acute erosion of the frontal Himalaya, and increasingly rapid exhumation of the Eastern Himalayan Syntaxis (EHS) have contributed greatly to disturbance and redistribution of sediment transportation since at least Middle-Miocene time (Huntington et al., 2006; Garzanti et al., 2010; Deeken et al., 2011; Zeitler et al., 2014; Bracciali et al., 2015; Lang et al., 2016; Blum et al., 2018).

In 2015, IODP Expedition 354 drilled a 7-site transect across the Bengal Fan at 8°N, collecting over 1.7 km of sediment core (Figure 1A) (France-Lanord et al., 2016). Sediments from these cores have been analyzed for detrital zircon, apatite, and rutile U-Pb geochronology with the intent of determining the provenance of Fan sediments from the orogen and tracking exhumation rate changes through time (Blum et al., 2018; Najman et al., 2019). Results of these studies demonstrated the capabilities of U-Pb analyses in establishing temporally constrained provenance interpretations of Bengal Fan sediments to major lithotectonic units that comprise the Himalayan-Tibetan orogen (e.g., Blum et al., 2018; Najman et al., 2019). However, U-Pb alone is unable to determine key spatial constraints in provenance interpretations when source regions have the same crystallization ages (e.g., Reiners et al., 2005), effectively limiting interpretations to more simplistic one-dimensional models. The lithotectonic units of the Himalaya extend for thousands of kilometers east to west, with highly variable rates of exhumation and lag-time calculations between the orogen core and syntaxes (Dixon et al., *in review*). Over the last two decades, advances in detrital (U-Th)/He thermochronology methods have facilitated a newfound interest in Himalayan thermal histories, allowing for unprecedented levels of detail regarding

both ancient and near-modern day records of orogen-wide sediment production, transport and deposition(e.g., Bernet et al., 2006; Chirouze et al., 2013; Bracciali et al., 2016; Lang et al., 2016; Govin et al., 2020; Schildgen and van der Beek, 2022). This thesis work implements detrital zircon (U-Th)/He thermochronology and sediment unmixing models to provide spatio-temporal constraints on sediment provenance while simultaneously expanding and refining the detrital record of the Bengal Fan. We report a dataset of both single zircon (U-Th)/He (n = 112) along with U-Pb and (U-Th)/He double dated crystals (n = 49) derived from 20 new Bengal Fan sediment samples across the seven cores recovered during IODP Expedition 354. Coupling this data with previously published thermochronologic data and novel sediment unmixing models, we investigate the provenance, sediment routing and depositional history of the Late-Miocene to Late-Pleistocene Bengal Fan. Observed cooling age data compared to compiled bedrock cooling ages across the orogen reveal a pronounced change in age populations present within Bengal Fan sediments across the Pliocene-Pleistocene Transition (PPT), suggesting orogen-wide sediment routing variations associated with tectonic regime changes and, potentially, climatic forcing during glacial-interglacial periods.

Geologic Setting

Orogen Assembly

The Himalaya-Tibet orogen is comprised of a series of successive terrane accretions starting from Triassic time to ~59 Ma (Kapp and Decelles, 2019). Following the collision of the Tarim and Tian-Shan cratons ~350 Ma and the opening of the Tethys Ocean and formation of Pangea ~230 Ma (Qin et al., 2016), Tethyan oceanic crust began to subduct northward below the southern Asian continental margin. The continued northward subduction precipitated accretion

of the Kunlun and Hoh-Xil (>220 Ma), Qiangtang (~200 Ma), and Lhasa terranes (~120 Ma) cotemporally with the closure of the Paleo and Meso-Tethys oceans (Kapp and Decelles, 2019 and references therein). The four terranes are geographically and geologically separated by the Kunlun, Jinsha, and Bangong sutures, respectively (Figure 1B). Pulses of magmatism in Northern Lhasa (~170 Ma) and the Gangdese magmatic arc (200 – 225 Ma, 90 – 110 Ma, 45 – 60 Ma) further constructed the southernmost terrane. Periods of magmatic lulls within the arc are coeval with ophiolite generation within the Xigaze forearc along the southern Lhasa terrane (e.g., Huang et al., 2015).

Post-terrane accretion, tectono-thermal activity continued in the Lhasa terrane with the subsequent subduction of Neo-Tethys oceanic crust until ~59 Ma. At that time, the Indian and Asian plates collided and initiated Himalayan-Tibetan orogenesis (Garzanti et al., 1987; Decelles et al., 2014; Orme et al., 2015; Hu et al., 2016). The continent-continent collision is geographically marked by the Yarlung Suture Zone (YSZ), comprised of a series of discontinuous ophiolite complexes and serpentine-matrix mélange between the Lhasa terrane and Tethyan Himalayan rocks (e.g., Metcalf et al., 2017). Post India-Asia collision, topographic uplift of the Himalaya developed since the Miocene (<23 Ma) and has drastically affected regional and worldwide climate patterns (Raymo and Ruddiman, 1992), most notably with the changes in the intensity of the South Asian Monsoon (SAM) in the middle Miocene (e.g., Clift et al., 2008) and Pliocene (Srinivasan and Sinha, 2000). The topography of the area thus represents a complex relationship between intense precipitation, tectonics, and erosion from the early-Paleogene to present day (Molnar et al., 1993; Burbank et al., 2003; Clift et al., 2010; Jepson et al., 2021).

Lithotectonic/Stratigraphic Units

Within the bounds of the Himalaya-Tibet orogen and modern-day drainages of the Ganges and Yarlung-Brahmaputra River systems, six major tectonostratigraphic regions separated by crustal-scale faults are recognized (Figure 1B). From north to south, they are:

***Lhasa terrane*:** Comprised of Paleozoic-Cenozoic clastic and carbonate rocks that are mixed with Cambrian-age granites (Kohn et al., 2009; Gehrels et al., 2011), the Lhasa terrane generally consists of 500-3200 Ma age peaks, most prominently at 500-560 Ma (Gehrels et al., 2011). Intrusions by Early Cretaceous-Paleogene granitoids of the Gangdese magmatic arc are present in the southern and northern Lhasa terrane, respectively (e.g., Chapman and Kapp, 2017).

Gangdese Batholith (GB): Norian-Paleogene igneous granitoids intruded the Lhasa terrane during and after the accretion of terranes and India-Asia collision. U-Pb ages from the Gangdese arc are <250 Ma with spatially variable peaks ranging from 200-220 Ma, 90-110 Ma, 50-60 Ma, and 10-20 Ma (Zhu et al., 2008, 2018 and references therein; Chapman and Kapp, 2017; Laskowski et al., 2019).

***Tethyan Himalaya Sequence (THS)*:** The THS is comprised of Neoproterozoic-Paleogene marine sedimentary rocks that are intruded by Neogene leucogranites (Gehrels et al., 2006a, 2006b, 2011; Guo and Wilson, 2012). THS detrital zircon U-Pb age populations generally are recorded as >400 Ma, with dominant modes near 500 Ma, 1000 Ma, and 2500 Ma (Gehrels et al., 2011; Orme et al., 2021), and some detrital THS samples recording broad distributions from 180–1250 Ma (Laskowski et al., 2018). Detrital material in the unit also appears dominated by Pan-African age populations (500-600 Ma). Volcaniclastic and Paleocene modes have been recorded between 115-145 Ma and 58-65 Ma, respectively (Cai et al., 2011; DeCelles et al., 2014; Hu et al., 2015; Orme et al., 2021).

***Greater Himalayan Sequence (GHS)*:** These Neoproterozoic-Cambrian highly-deformed metamorphic and plutonic rocks form a multitude of nappes and klippes in the central-southern Himalaya with THS rocks as structural outliers (Parrish and Hodges, 1996; Gehrels et al., 2006a) . Neogene plutonic rocks (granites) intrude here as well, generally near or along the footwall of the South Tibetan Detachment (Guo and Wilson, 2012). Comprised of three major "formations", Formation I, II, and III formed of biotite schists/paragneisses, marble/calc-silicate gneisses, and Ordovician granite-derived orthogneisses, respectively (Gehrels et al., 2011). U-Pb ge data from this region show modes at 800-1200 Ma, 1.6-1.9 Ga, and 2.4-2.7 Ga (see Figure 6, Gehrels et al., 2011). Plutonic intrusions and associated xenoliths consistently record 500-570 Ma age modes (Cawood et al., 2007; Gehrels et al., 2011).

***Lesser Himalaya Sequence (LHS)*:** The LHS is comprised of both lower (1) and upper (2) stratagraphic units; (1) Paleo-Mesoproterozoic igneous rocks with GHS and THS structural outliers (DeCelles et al., 2000, 2001; Kohn et al., 2009; Gehrels et al., 2011). (2) Neoproterozoic and younger strata with Carboniferous-Cretaceous Gondwana-sequences, formed on a passive-margin (Gansser, 1964; Gehrels et al., 2011). LHS antiformal duplexing resulted in large windows trending east to west (e.g. Teesta and Kishtwar windows) (Bhattacharyya et al., 2015; Gavillot et al., 2018; Long and Robinson, 2021) and LHS strata have produced zircon U-Pb age ranges between ~1.6-2.8 Ga, with age modes between 1.8-2.0 Ga (Gehrels et al., 2011).

***Sub-Himalaya (SH)*:** A series of Paleogene-Neogene (Miocene-Pleistocene) foreland basin sediments (Gansser, 1964, 1983; Le Fort, 1975; DeCelles et al., 2016). The Muree and Siwalik Formations compose the majority of the unit, with a combined stratigraphic thickness of up to ~9.6 km (Gavillot et al., 2018). Detrital zircon age data from the Siwalik group indicate

Oligocene to middle-Miocene deposition and zircon U-Pb age data report a major peak age group ca. 507 Ma (Cina et al., 2009; Lang and Huntington, 2014; DeCelles et al., 2016).

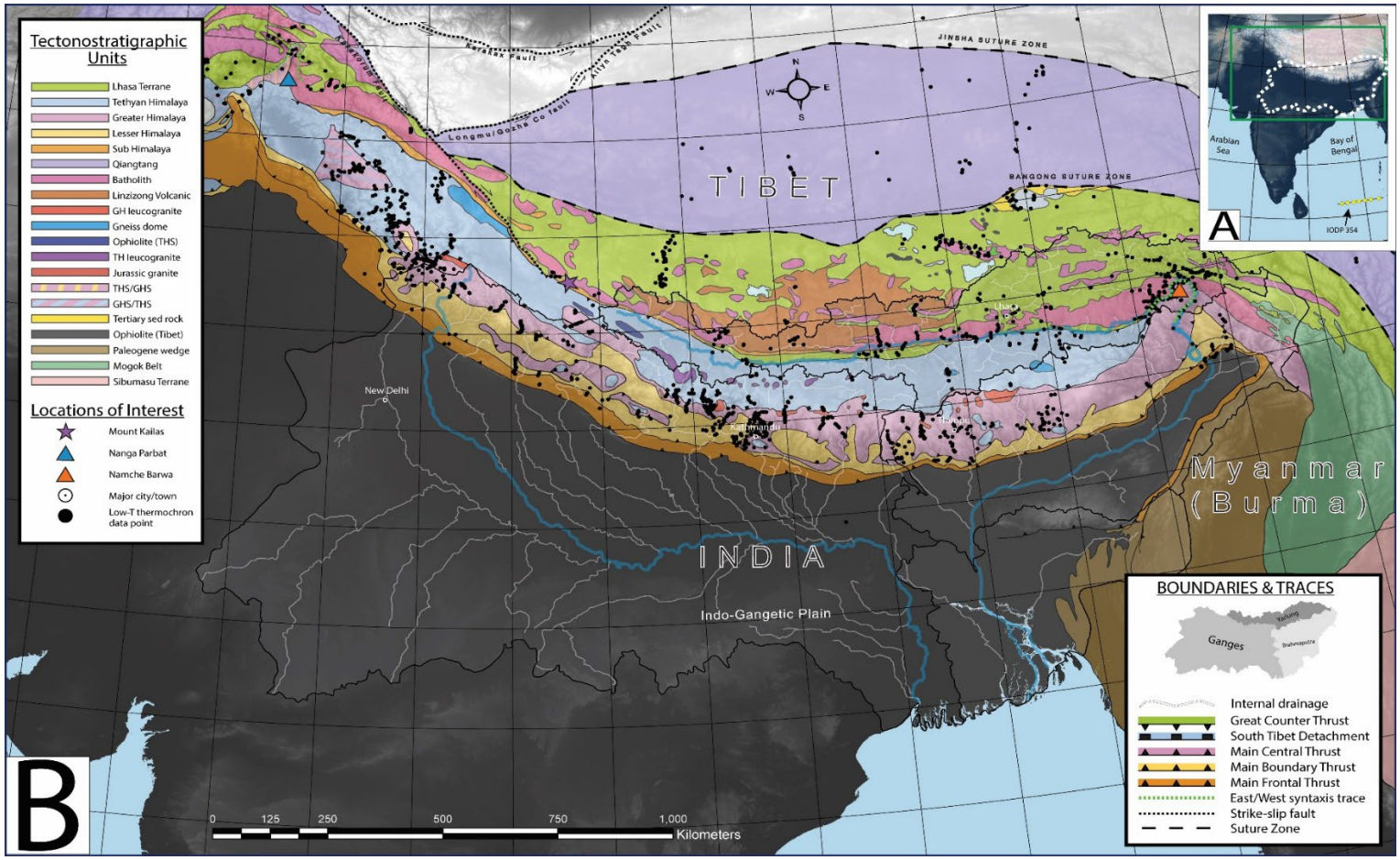


Figure 1: (A) Overview map of the Ganges-Brahmaputra River system drainage and IODP Expedition 354 drilling locations; white stippled outline represents combined Ganges-Brahmaputra drainage area. (B) Overview geological map of the Himalayan-Tibetan orogen and locations of previous low-temperature thermochronology study datapoints. Crustal-scale fault lines and suture zones mark the boundaries between major units and terranes, respectively, with a north-south younging age trend of construction. Ganges and Brahmaputra drainages outlined and shaded in dark and light grey, respectively. Lithotectonic/geologic units, sutures, and faults are modified from Yin and Harrison (2000), Kapp and Decelles (2019), and Zhang et al. (2021).

Ganges-Brahmaputra Rivers

The Ganges-Brahmaputra River system (GBS) is comprised of the collective drainage of the rivers named, including headwaters, tributaries, and the Ganges-Brahmaputra delta (Figure 1A). The Brahmaputra headwaters are fed by the Yarlung River, flowing east along the Yarlung-Suture Zone (YSZ) and Lhasa terrane before redirecting south to drain the Tethyan Himalaya, eastern syntaxis, and southern Tibetan Plateau. Ganges headwaters are located south of the YSZ and drain the Himalayas and Indian plate moving southeastward of this region. Both rivers drain four of the six lithotectonic sequences in tandem: THS, GHS, LHS, and SH. The Lhasa and GB sequences are drained solely by the Yarlung-Brahmaputra. The two rivers converge and carry sediment to the Ganges-Brahmaputra delta before discharging into the northern Bay of Bengal. Similar to Amazonian river dynamics, sand-sized particles are delivered to the main shelf during high sea-level phases, whereas glacial periods and associated low sea-level allow deposition farther out to the shelf margin and the deep sea, thus bypassing the shelf (Blum et al., 2018; Mason et al., 2019).

The Bengal Fan

Sediments that reach the Bay of Bengal encounter journey's end as they are deposited within the Bengal Fan, the world's largest submarine fan by area. The Bengal Fan extends ~2500-3000 km south into the Indian Ocean and is underlain by post-collision sediments deposited ~38 Ma (Najman et al., 2008; Blum et al., 2018). The thickness of Bengal Fan sediments decreases southward from the continental shelf, ranging from ~12 km to <1 km at the distal-most lobe. Fan sediments appear to generally coarsen through time with silt-rich turbidite material dominating the record up to 10 Ma and fine sands thereafter. The modern-day

catchment of the GBS drains a collective 2.6 million km^2 area and rapidly delivers up to 1550 x 10^6 tons/yr of sediment to the Bengal Fan, nearly 80% of eroded material from the Himalaya (France-Lanord et al., 2016; Lupker et al., 2017 and references therein; Huyghe et al., 2020). The deep-sea fan preserves a near-complete record of Himalayan-Tibetan orogenesis and exhumation from the Late Oligocene to present.

Evolution of the Ganges-Brahmaputra River System

The modern-day GBS channels sediment from both Ganges and Brahmaputra sources directly to the Bay of Bengal and ultimately the Bengal Fan. However, this has not been the case for the majority of Himalayan-Tibetan orogenesis. Studies of the paleo-Brahmaputra drainage system have determined primary deposition as far east as the neighboring Nicobar Fan (e.g. Betka et al., 2021). Evidence for far-reaching deposition came from IODP Expedition 362, where a ~15 fold increase in mass accumulation rates recorded at ~9 Ma suggested major input from the Brahmaputra delta to the Nicobar Fan (McNeill et al., 2017; Pickering et al., 2020) while contemporaneously delivering sediment to the Bengal Fan. At this time, the capture of the Yarlung River into the Brahmaputra drainage was well established since Early-Miocene time (Lang and Huntington, 2014), and thus Lhasa and Gangdese detritus are present within post-capture Bengal Fan samples, and especially at the merger of the Brahmaputra and Ganges deltas ~5 – 3 Ma (Govin et al., 2018; Sincavage et al., 2020; Betka et al., 2021) when a direct line of sediment transport would certainly have been established.

Further evidence of increasing Yarlung-Brahmaputra sediment input through time comes from Blum et al (2018), described by U-Pb analyses of Bengal Fan samples that fall within our interest of depositional age ranges. Two end-member samples at 3.6 Ma and 1.5 Ma stratigraphic

ages were established temporally as paleo-Ganges and paleo-Brahmaputra River signals, respectively, signaling a major drainage pattern shift from western to eastern sediment productivity across the PPT. Along with these population signal interpretations, a distinct lack of Tethyan age signals coupled with higher Lhasa and GHS input signals further suggested the transition from Ganges to Brahmaputra dominant sediment delivery.

Apart from these two end-members, all detrital zircon U-Pb dates from the Bengal Fan are of mixed-drainage origins. The most probable first-order cause of these mixed vs singular sediment delivery patterns is *in situ* river avulsions across the delta plain following the Miocene-Pliocene Ganges-Brahmaputra merger (Blum et al., 2018). It is probable that these avulsions may have direct correlations to contemporaneous climatic-tectonic forcing throughout the Miocene-Pleistocene.

Previous Low-Temperature Thermochronology

There have been a multitude of medium and low temperature thermochronology studies conducted across the Himalayan-Tibetan orogen (Dixon et al., *in review*), including application of the apatite (U-Th)/He and fission track and mica argon-argon systems (e.g., Carrapa et al., 2014; Copeland et al., 2014). However, we focus our summary of source region thermochronologic signals on the ZHe system to facilitate direct comparison to our Bengal Fan results. Broad cooling trends across the orogen include 1) a southward-younging distribution of ages from Lhasa to the LHS, and 2) generally recorded onset/acceleration of exhumation during Miocene time continuing into the pre-Pliocene, followed by rapid rate increases that continue into the present (Dixon et al., *in review)*.

Tibetan thermochronology

In Tibet, most studies have found prominent ZHe age modes at c. 50 Ma, ca. 17 Ma and <12 Ma (e.g., Dai et al., 2013; Carrapa et al., 2014; Tremblay et al., 2015; Laskowski et al., 2017; Li et al., 2017; Orme et al., 2019). The 50 Ma mode is found within the GB, which has a wide range of cooling ages between ~6.0-90 Ma, with the >40 Ma ages attributed to variable exhumation rates following major magmatic pulses and younger ages attributed to initiation of rifting/fault block uplift (Dai et al., 2013; Haider et al., 2013; Wolff et al., 2019). The strong population of early ca. 23 Ma and middle Miocene cooling ages ca. 17 Ma is found within both bedrock and detrital records (e.g., Dai et al., 2013; Carrapa et al., 2014; Laskowski et al., 2017; Li et al., 2017; Orme, 2019). Much of the exhumation ca. 23 Ma is attributed to motion and erosion along the Gangdese Thrust and Great Counter Thrust systems (Laskowski et al., 2018; Long and Robinson, 2021). By contrast, the ca. 17 Ma signal has been linked to northward underthrusting of the Indian plate and increased river incision in response to drainage reorganization (Carrapa et al., 2014; Orme, 2019) and rift initiation (e.g. Styron et al., 2015; Laskowski et al., 2017). Zircon (U-Th)/He ages <12 Ma are found within meta-Tethyan rocks and leucogranites (e.g., Laskowski et al., 2017) and active rifts (Styron et al., 2015; Wolff et al., 2019; Wolff et al., 2022; Bian et al., 2022). The exhumation rates determined by these studies along major rifts appear relatively slow until the Pliocene. Footwall exhumation along active rifts record an acceleration between 5-2 Ma (Sundell et al., 2013; Styron et al., 2015) during the PPT.

Himalayan thermochronology

Thermochronometric data from the Himalaya is widespread and wide-ranging, with studies providing variable ZHe results from ~500 ka to 362 Ma (Landry et al., 2016; Colleps et

al., 2018). Studies from southernmost reaches of the THS record cooling ranges from ~1.1–29.6 Ma, and generally follow the trends of its northern counterpart in Tibet. Cooling in the GHS and LHS generally record ages ca. 13-17 Ma (e.g., Deeken et al., 2011; Orme et al., 2015; Carrapa et al., 2016; Schultz et al., 2017), with age ranges from ~0.60–70 Ma in the GHS and ~1–33 Ma in the LHS (Dixon et al., *in review*). Cooling of the northwestern GHS and LHS records ages ca. 14–21 Ma corresponding to nearby MCT movement (Gavillot et al., 2018), while cooling of the GHS in the Bhutan Himalaya has previously been constrained to ca. 5–8 Ma (Adams et al., 2015). In the LHS, general cooling trends reveal older ages in higher elevation regions and younger ages at lower elevations (8-12 Ma and 3.5-6 Ma, respectively) interpreted to reflect variable relief, cooling rates, and oblique to vertical exhumation through time (Thiede et al., 2009). The eastern and western syntaxes record youngest cooling ages. Both apatite and zircon fission-tracks record ages varying from <0.5 – 2 Ma in Nanga Parbat (Zeitler et al., 1985) and biotite $^{40}Ar/^{39}Ar$ and zircon (U-Th)/He and fission-tracks <2 Ma from Namche Barwa bedrock samples, along with detrital fission-tracks as young as 0.1 – 6 Ma from the eastern synatxis drainage (e.g., Burg et al., 1998; Seward and Burg, 2008; Enklemann et al., 2011). Zircon derived from the eastern syntaxis that crystallized at 5 Ma were transported to the fan by 2.5 Ma (Blum et al., 2018; Najman et al., 2019), a key indication of rapid exhumation and cooling in the Pliocene. Cooling trends in the southern Himalaya generally record cooling ages <10 Ma (Jepson et al., 2021 and references therein), supporting rapid exhumation during this period, potentially due to mixed tectonic-climatic forcing. Sub-Himalayan cooling records appear to contain the highest variability in ZHe data from ~6 – 362 Ma (Dixon et al, *in review* and references therein)

which could be attributed to its sedimentary makeup and effective role in recording cumulative Himalayan erosion.

Bengal Fan thermochronology

Although this study presents the first spatially-extensive ZHe Bengal Fan dataset and coupled orogen-wide cooling age data compilation, previous studies of Bengal Fan detrital thermochronology have focused on both white mica $^{40}Ar/^{39}Ar$ and apatite/zircon fission track (AFT/ZFT) analyses. An average central age of ~2.3 ± 1.6 Ma is recorded for apatite fission tracks of Bengal Fan sediments from IODP 354 since ~ 13 Ma, suggesting both rapid exhumation of 1-3 km/Myr and overall negligible storage in the deltaic floodplains (Huyghe et al., 2020). Rutile U-Pb (near-equivalent to biotite $^{40}Ar/^{39}Ar$ closure temperatures) and zircon fission tracks from sediments deposited ~0.63 – 10.55 Ma record decreasing lag time beginning ~3.47 – 3.76 Ma and central ages ranging from ~6.8 – 12.6 Ma, respectively (Najman et al., 2019). White mica $^{40}Ar/^{39}Ar$ from this same study determined minimum ages between 15 – 18 Ma from 1 – 10 Ma depositional ages.

Methodology

Sample Collection and Preparation

A detailed record of IODP Expedition 354 drilling operations can be found in France-Lanord et al., (2016), and is summarized herein. Initial coring of Bengal Fan sediments aboard the JOIDES Resolution included the use of APC/extended core barrel (XCB) at all seven sites along the 8°N transect. Site U1451 also included coring operations using rotary core barrel (RCB) to penetrate the oldest deposits. All transect sites recovered siliciclastic silt-sand and clay

turbidite deposits, with variable amounts of calcareous clays and nannofossil assemblages. Coring site U1451 recovered a complete record of Bengal Fan depositional history reaching into the Oligocene, providing the longest continuous record of Himalayan erosion.

A total of 20 samples across the seven coring sites were collected from the Kochi Core Center, Japan. Heavy mineral separation was conducted on 1-2 kilograms of sediment from each sample at the University of Arizona Laserchron Center (Gehrels et al., 2008).

Zircon (U-Th)/He Low-Temperature Thermochronology

We analyzed zircon for (U-Th)/He thermochronology from these 20 samples to determine the range of cooling ages present in Bengal Fan sediments. In turn, we compared these cooling ages to source ZHe records (Dixon et al., *in review*) to determine regional-scale spatial constraints for provenance and lag-time calculations of Bengal Fan sediments (Figure A1, A-B). Zircon (U-Th)/He thermochronology relies on both the time-dependent production and temperature-sensitive diffusivity of ^{4}He within and through the crystal lattice. At high temperatures (>~220°C), ^{4}He readily diffuses out from the zircon crystal, and is retained at lower temperatures (<~140°C) (Reiners et al., 2004; Guenthner et al., 2013). The temperature range to which zircon is sensitive is a function of several factors, including cooling rate, grain size, and radiation damage, and may range as much as 40-140°C (Guenthner et al., 2013). Broadly, ZHe is sensitive to cooling between 140 – 220°C, or 8-4 km depth assuming a 15 – 25°C/km geothermal gradient.

Five to eight grains were hand-picked from each of the 20 samples for a total of 114 single zircon helium (ZHe) aliquots. Grains were chosen with no apparent inclusions and a minimum ≥60-micron spherical radius (Reiners, 2004). A variety of zircon grain sizes and

morphologies were chosen to limit bias with various detrital populations. ZHe aliquots were picked, photographed, measured, and packed in 1mm Nb foil tubes at the Tectonic Sedimentology and Thermochronology (TeST) laboratory at Montana State University (Bozeman, Montana). Helium degassing and U-Th isotopic analyses were conducted at the Helium Analysis Laboratory (HAL) at the University of Illinois Urbana-Champaign (Urbana, Illinois). ^{4}He molar compositions were determined using a laser microfurnace noble gas extraction vacuum line consisting of diode laser heated degassing and diffusion cells, cryogenic purification steps, and a PrismaPlus QMG 200 mass spectrometer. U and Th molar compositions were determined with a Thermo iCAP quadrupole ICP-MS. Uncertainties of ZHe dates are reported at the 2σ level based on analytical uncertainties of U, Th, and He measurements.

Zircon Double Dating

Eight samples were dated with U-Pb geochronology prior to ZHe analyses on the same grains. Individual detrital zircon grains were selected for mounting, imaging, and U-Th-Pb laser ablation geochronology analyses using a Thermo Fisher Element 2 high-resolution sector ICP-MS, all of which were conducted at the Arizona LaserChron Center (ALC) (Tuscon, Arizona). Backscatter-electron (BSE) images were used to identify zircon grains for placement of 20 micron diameter ablation spots. A total of 300 zircon grains were targeted for U-Pb analyses, and U-Pb ages with >10% discordance were discarded (Vermeesch, 2004; Saylor and Sundell, 2016). Post-laser ablated zircon mounts were then shipped to Montana State University for detrital ZHe analysis preparation. Procedures for single-grain ZHe preparation and analyses were followed as described above, with the exception of the alpha-ejection correction: additional calculations are required for double-dated aliquots due to the nature of U-Pb mount preparation, which results in

up to 50% loss of zircon volume due to grain polishing procedures for laser ablation. Ft corrections for all analyses were calculated following the methods of Farley (2002).

A total of 49 zircon grain aliquots were plucked from U-Pb mounts of 8 out of 20 samples for ZHe analyses. We targeted three major U-Pb crystallization age populations from depositional ages ranging across the Early-Late Pleistocene (0.13 – 1.80 Ma). The U-Pb age ranges represent likely source regions in the rapidly exhuming eastern Himalayan syntaxis (EHS, 0 – 10 Ma), GHS leucogranites (15 – 30 Ma), and GB granitoids (45 – 60 Ma), respectively. One to twelve grains were recovered from each sample, with a maximum of 5 grains per targeted age range.

Both standalone zircon U-Pb and ZHe analyses are powerful tools in provenance studies, constraining interpretations from temporal and spatial perspectives. However, each lack the age constraint that the other provides, thus limiting the effectiveness of provenance interpretations that utilize a single system. The solution to this problem is to conduct both U-Pb and (U-Th)/He analyses on individual zircon grains, known as double-dating, which can greatly refine provenance interpretation (Figure A2). For example, two samples, A and B, have equivalent U-Pb crystallization ages of 100 Ma, inherently hindering provenance differentiation. However, sample A and B have differing (U-Th)/He cooling ages of 50 and 25 Ma, respectively. Thus, both systems together solves the nonunique problem of U-Pb analysis alone. The opposite example would be true as well. Double-dating zircon techniques have proven useful in studies of sediment dispersal systems and tributary fingerprinting (e.g. Meyer et al., 2000; Reiners, 2005).

Similarity Models

Multi-Dimensional Scaling (MDS) MDS is a statistical tool that quantitatively determines similarity and likeness of multiple samples within two and three-dimensional spaces. MDS determines values for the cross-correlation coefficient (similarity) and Kuiper Test V (contradiction) to create a Euclidean (pairwise) distance matrix to calculate and further visualize similarity and dissimilarity, often used in detrital zircon geochronology studies (Vermeesch, 2013; Seraine et al., 2021).

The cross-correlation coefficient (R^2) describes similarity, or how alike pairs of data are to one another. An R^2 value of 1 represents perfect fit/similarity, while 0 represents perfect dissimilarity. The Kuiper Test V describes the opposite of R^2: rather than quantifying similarity, Kuiper V searches for any contradictory evidence in a dataset that negates similarity and wellness of fit between samples. The Kuiper Test V statistic is the sum of the maximum differences between data distributions in positive and negative space. A Kuiper V value of 0 represents perfect similarity, and a value of 1 perfect dissimilarity. For the case of thermochronometric age distributions, MDS testing graphically displays these likeness and similarity values in terms of relative distance. The further away a sample is plotted from another the less similar they are statistically. We conduct MDS for three major dataset comparisons: 1) The 15 single ZHe Bengal Fan samples, 2) Lithotectonic unit ZHe against Epoch supersets, and 3) Epoch supersets against Yarlung-Brahmaputra and Ganges drainage ZHe signals.

We implemented two programs to handle MDS figure syntheses and analytical computations: DZmds (Saylor et al., 2017), which was used to create 2D and 3D plots based on the cross-correlation coefficient and Shepard plots to determine final stress values, and DetritalPy (Sharman et al., 2018) to create heatmaps of samples based on dissimilarity.

Analytical Results

Zircon (U-Th)/He Results

Single-grain ZHe dates were determined for 15 out of 20 samples for a total of 114 dates. One aliquot was found to be an empty Nb tube and was unusable. Three aliquots displayed geologically impossible ages (i.e. negative), with an additional 18 aliquots producing geologically improbable ages that fell below the depositional age of samples. Although it is possible to reset a cooling age through burial and/or reheating processes, this record of the Bengal Fan does not meet any criteria that would result in fully or partially reset cooling ages below depositional age. Altogether, 92 interpretable ages were recovered at 2-8 grains per sample (Appendix B2). Zircon data reveal a wide range of cooling dates from ~0.50 ± 0.01 Ma to 492.5 ± 6.9 Ma. The effective Uranium (eU) in zircon ranged from 10.71–3811.13 ppm. No meaningful correlations were determined between cooling age and spherical radius (Rs) or Rs and eU (Figure B1). No strong correlation occurs between eU and cooling age, though we note a potential trend of ZHe ages >100 Ma containing eU measurements <100 ppm.

Two methods were used to describe shifts in zircon cooling age populations through time. First, kernel density estimates (KDEs) for each of the 15 samples (n = 2-8) were constructed using a bandwidth of 1 Ma (Figure 2A). The second method involved grouping samples based on geologic epoch (Miocene, Pliocene, and Pleistocene, n = 13–64), which allowed for broad changes in cooling age populations to be determined, especially across the PPT (Figure 2B). Miocene samples span the time 6.00 – 6.20 Ma, Pliocene samples from 1.90 – 3.89 Ma, and Pleistocene samples 0.22 – 1.80 Ma. Although the Pleistocene epoch begins ~2.60 Ma, we end

our Pliocene sample set at 1.90 Ma and begin our Pleistocene sampling at 1.80 Ma to encompass initial PPT glaciation.

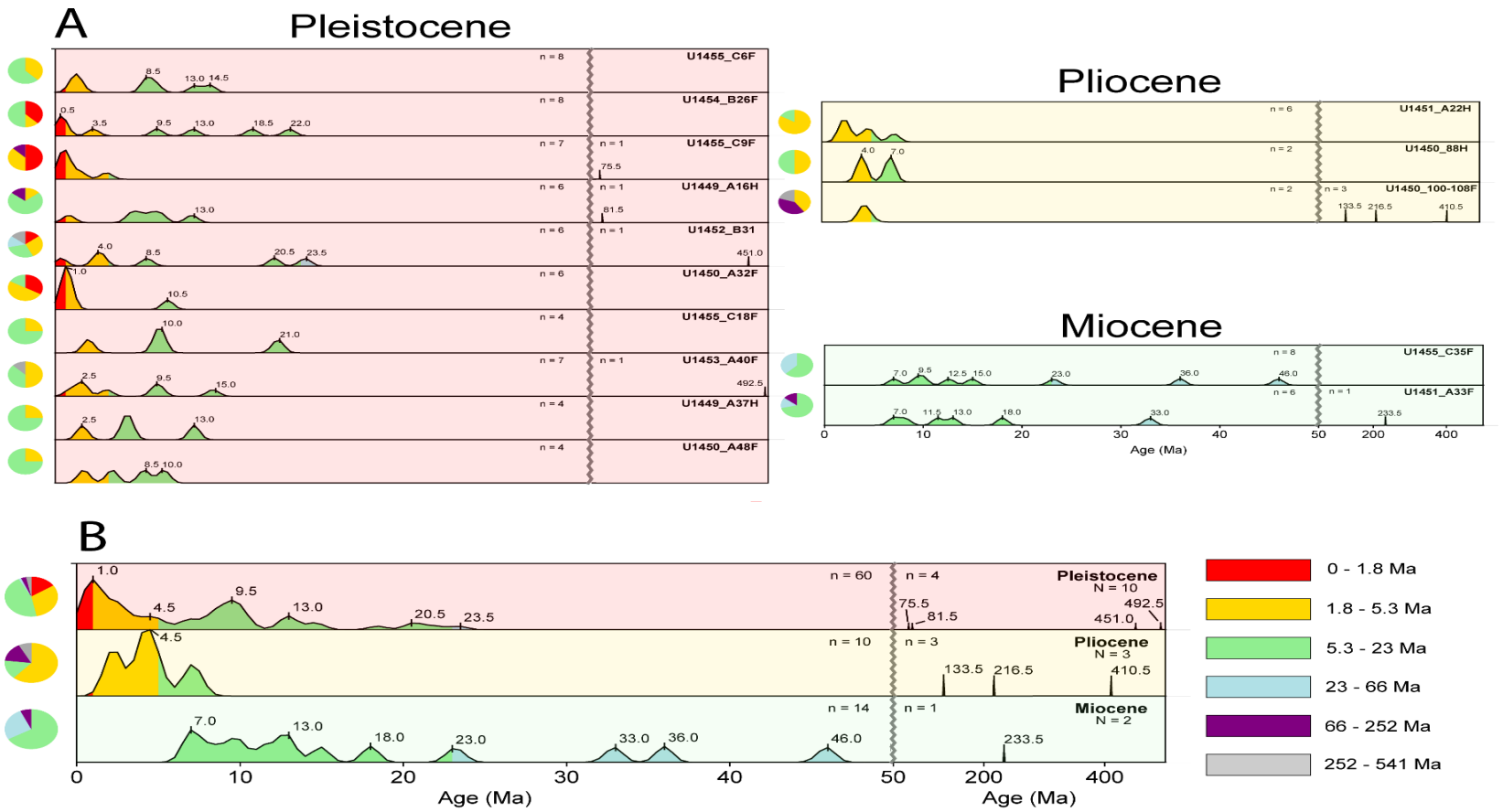


Figure 2: (A) Kernel Density estimates for all single ZHe samples, categorized by epoch. (B) Combined single ZHe samples for Miocene, Pliocene, and Pleistocene depositional ages. Each epoch shows unique ZHe age peaks and appear highly variable to one another, which can be confirmed through multi-dimensional scaling (MDS) methods (see Modeling Results: Multi-Dimensional Scaling for additional information).

Within epochs, Miocene samples show individual cooling ages between 6.96 ± 0.10 Ma to 233.34 ± 2.95 Ma, with notable age modes at ~9.5 Ma, 23 Ma, 33-35 Ma, and 46 Ma; Pliocene samples show individual cooling ages between 2.10 ± 0.04 Ma to 410.38 ± 5.52 Ma, with a major age modes of 4 Ma and 7 Ma; Pleistocene samples show individual cooling ages between 0.50 ± 0.01 Ma to 492.48 ± 6.87 Ma, with age peaks at ~2.5-4 Ma, 9 Ma and 23 - 25 Ma (Figure 2B). Results show a complete loss in Paleocene-Oligocene (>23 – 66 Ma) cooling age populations from Late Miocene-Early Pliocene time, between samples U1455_C35F and U1450_100-108F, with no recovery in younger samples excluding a single grain in sample U1452_B31 at 23.36 ± 0.28 Ma. An increase in Cretaceous and older (>66 Ma) grains accompanies this shift, with Pliocene and Pleistocene samples containing 38% and 50% of these ages, respectively, compared to the single grain from Miocene age samples. KDEs from the Pliocene and Pleistocene samples document an additional shift in cooling ages with an increase in Miocene-age grains (>5.3–23 Ma) beginning in the Early-Pleistocene and remaining consistent up-section. Pleistocene sample U1450_A40F marks the first appearance of ~1 Ma cooling ages which remain prevalent up-section (Figure 3).

Lag-time calculations show a wide range of time between cooling and depositional ages from as long as ~491 Ma to as little as ~69 ka (Figure 3B). Miocene lag-times range from ~0.76–227 Ma, Pliocene lag-times range from ~0.20–406 Ma, and Pleistocene lag-times range from ~0.07–491 Ma. Overall trends show decreasing lag-time from Miocene to Pleistocene time.

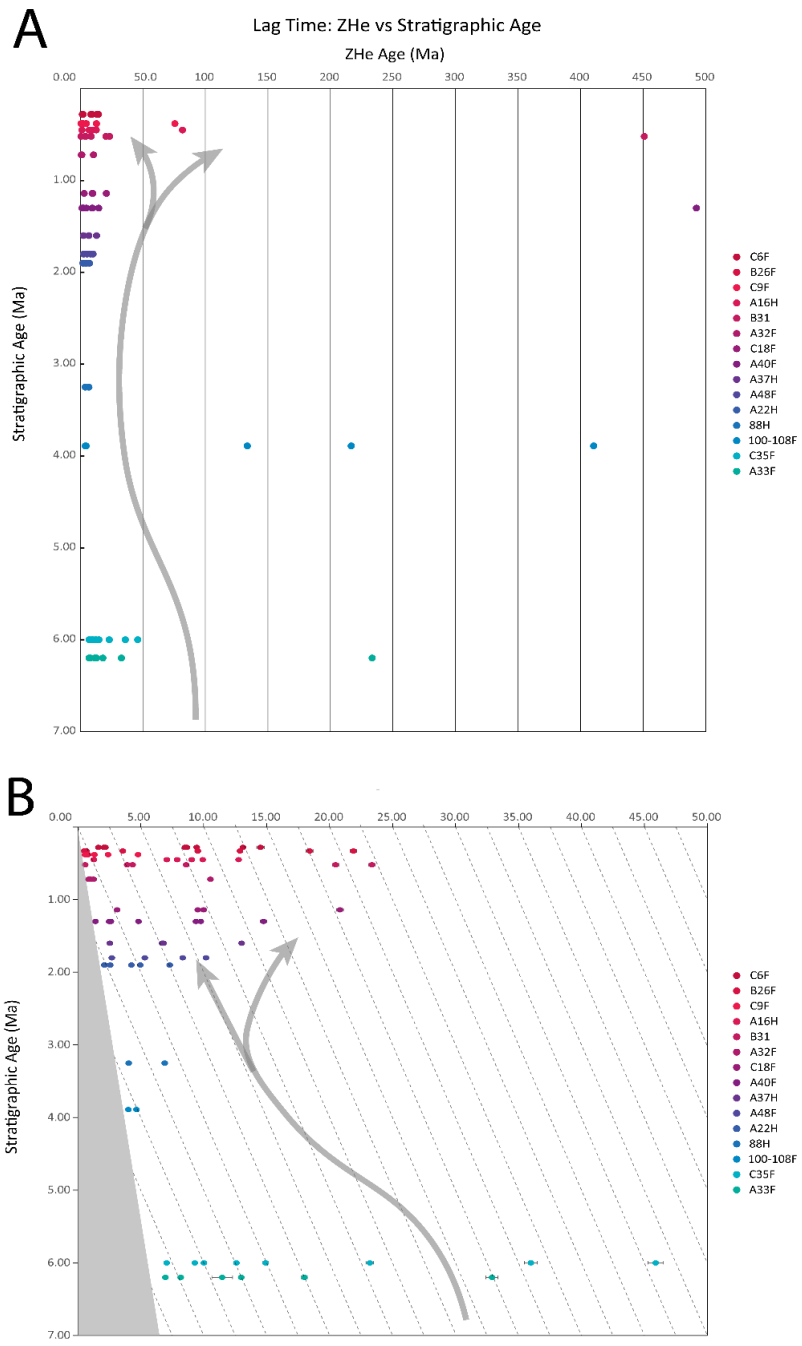


Figure 3: (A) All single ZHe lag times for Bengal Fan sediments. General trends through time show undulation in exhumation rates (black arrows). (B) Focus on post collisional cooling ages <50 Ma, with cooling ages >50 Ma not plotted. Steady state exhumation (dotted black lines) continues through the latest Miocene before increasing rates occur in the Pliocene. Pleistocene samples display mixed exhumation rates, interpreted as sourced from a mixed drainage system of Ganges and Brahmaputra sources.

Double Dating Results

Age data for U-Pb and (U-Th)/He was determined for 8 Pleistocene-age samples, with three targeted U-Pb age ranges per sample: 0-10 Ma, 15-30 Ma, and 45-60 Ma. One to five grains per sample were dated, for a total of 49 He-Pb dates (see Appendix B3 for detailed analytic data and U-Pb dates). Of the 49 He-Pb dates acquired, 8 dates fell within the U-Pb – (U-Th)/He "forbidden zone" (Figure A2), and thus were not interpreted. An additional 5 aliquots were found to be unusable due to one geologically impossible age (i.e. negative), one cooling age below depositional age, and three empty Nb packets, resulting in 36 interpretable ages (Figure 4). For grains with U-Pb dates <10 Ma, 15-30 Ma and 45-60 Ma, ZHe dates range from 1.44–8.26 Ma, 1.35–24.12 Ma, and 0.27–50.55 Ma, respectively. Cooling age ranges appear to be more consistent in the 45-60 Ma and 0-10 Ma U-Pb age groups, while the 15-30 Ma group shows weaker clustering of cooling ages.

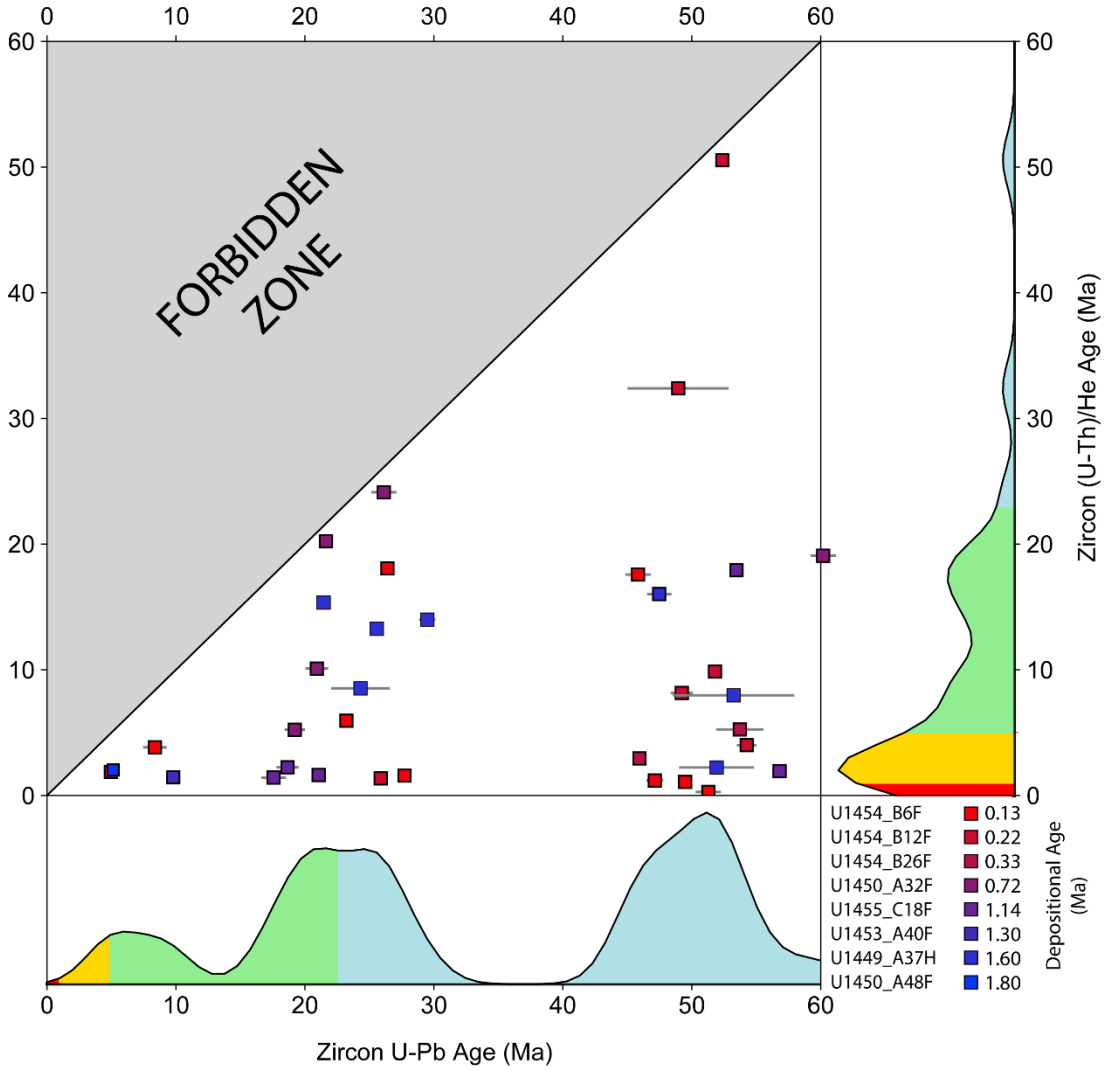


Figure 4: He-Pb double dating KDE plot for 8 Bengal Fan samples. Major ZHe age populations appear to include ~0-11 Ma, ~13-25 Ma. Grains with ZHe cooling ages higher than U-Pb ages were not included due to 1) skewing data/age peaks, and 2) being geologically improbable, and would fall into the grey "forbidden zone". KDEs are calculated and colored following the same scheme as single ZHe populations (Figure 2).

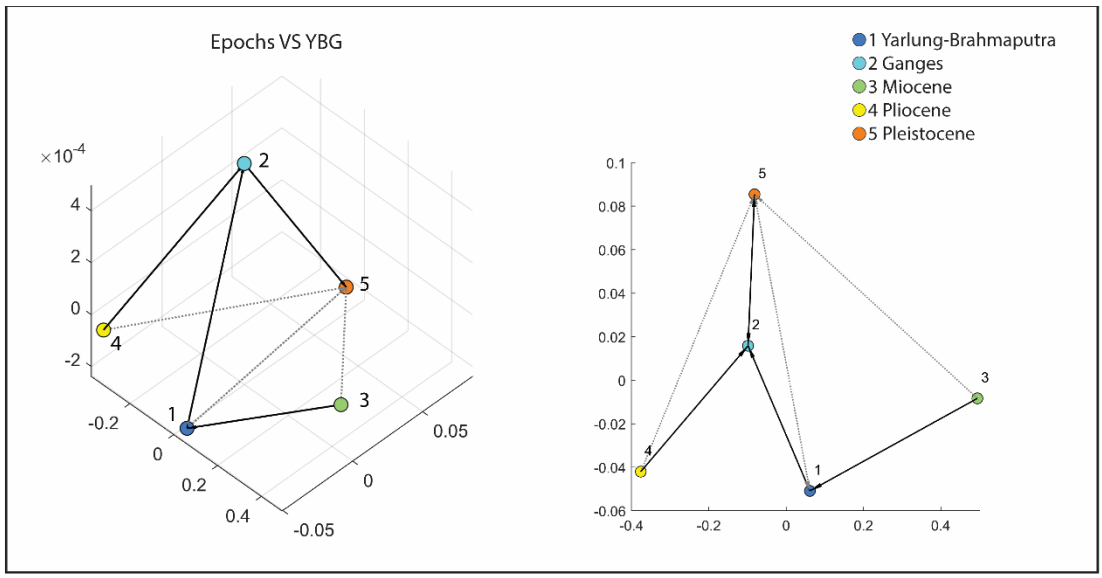
Lag-time calculations were conducted for both U-Pb (crystallization) and ZHe (cooling) age along with ZHe and depositional age. Crystallization-cooling lag-times (U-Pb/ZHe) range from ~54.9–1.4 Ma and cooling-deposition lag-times range from ~0.2–50.3 Ma. For U-Pb age

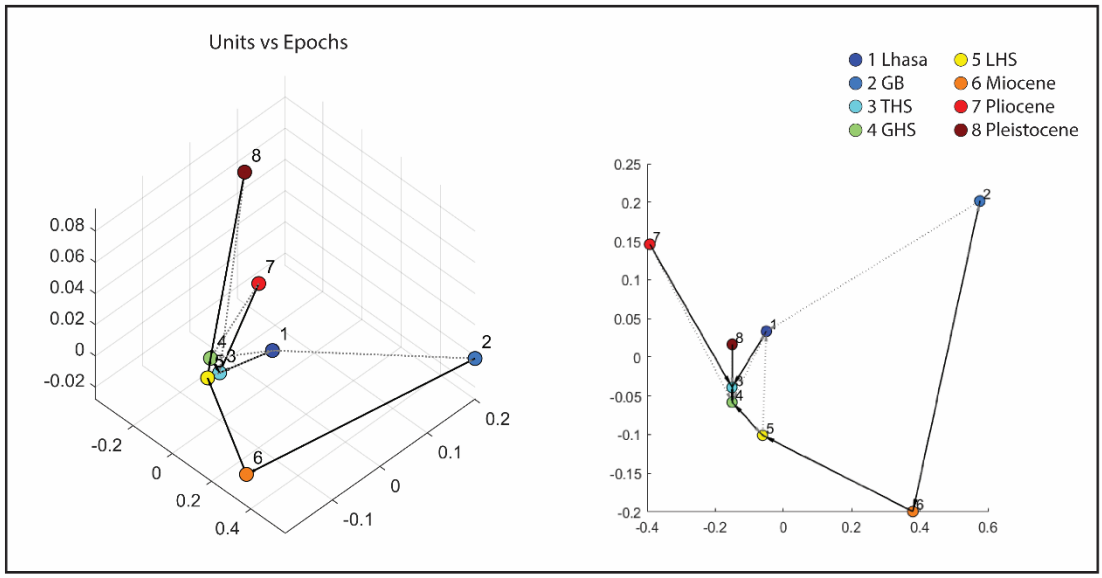
ranges of 45–60 Ma, 15–30 Ma, and 0–10 Ma, U-Pb/ZHe varied from ~1.8–54.9 Ma, ~1.4–26.1 Ma, and ~3.1–8.3 Ma, respectively. Individual U-Pb/ZHe results show a slight increasing trend through time, a reversal of the single ZHe lag-time trends above. Cooling-deposition lag-times (ZHe/D) for the same U-Pb age ranges (in the same order) varied from ~0.2–50.3 Ma, ~0.3–23.4 Ma, and ~0.2–3.7, respectively. Individual ZHe/D results also display a slight increasing trend through time.

Since ~4 Ma, comparisons of ZHe age range and depositional age reveals generally broader range of ZHe data with decreasing depositional age, with a maximum age range of 1.35 ± 0.02 Ma to 50.56 ± 0.53 Ma at 0.22 Ma depositional age (Figure 3). This agrees with the single ZHe results and coincides with increasing U-Pb age ranges.

Multi-Dimensional Scaling

Multi-dimensional scaling (MDS) was implemented to quantitatively compare the various age populations. MDS was performed on the following subsets of data, and in various combinations: (1) Epoch single ZHe dates and a compilation of all dates from the Yarlung-Brahmaputra and Ganges drainages (Figure 5A), (2) Epoch single ZHe dates and a compilation of Himalayan-Tibetan lithotectonic units (Figure 5B), and (3) Himalayan-Tibetan lithotectonic units and drainages (Figure 5C).


Epochs VS YBG
1 Yarlung-Brahmaputra
2 Ganges
3 Miocene
4 Pliocene
5 Pleistocene


Units vs Epochs
1 Lhasa
2 GB
3 THS
4 GHS
5 LHS
6 Miocene
7 Pliocene
8 Pleistocene

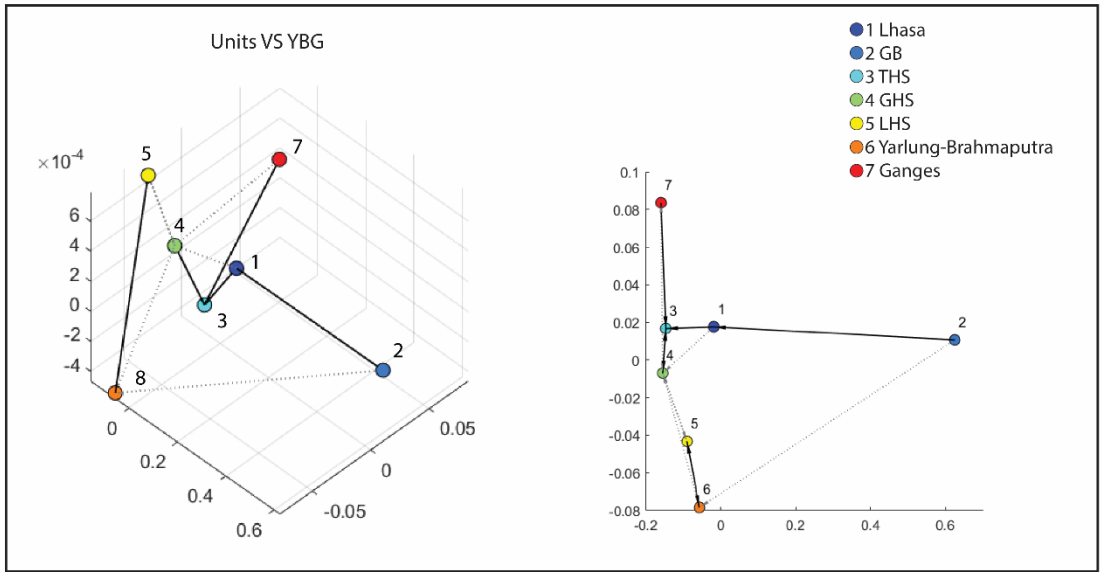

Units VS YBG
1 Lhasa
2 GB
3 THS
4 GHS
5 LHS
6 Yarlung-Brahmaputra
7 Ganges

Figure 5: MDS plots of A) Epochs vs YBG, B) Units vs Epochs, and C) Units vs YBG in 2 and 3-dimensional space. Solid black lines connect nearest-neighbor pairs (most similar), and dotted grey lines connect second nearest-neighbor pairs.

The relative distances between samples plotted in MDS space (Figure 5) are determined by their values of similarity and dissimilarity. Sample pairs that plot closest together are most similar, and those that plot farthest away are most dissimilar, regardless of axis magnitudes. In addition to the MDS space plots above, we chose to visualize our data in heatmaps, where dark colors and high values (Vmax) represent highest sample dissimilarity (Figure 6). Comparisons of epoch data determined a minimum distance value of 0.57 and a maximum of 0.9 for Pliocene-Pleistocene and Miocene-Pliocene samples, respectively. The lack of strongly similar values between the three epochs supports the qualitative dissimilarity between epoch KDEs. Comparisons of lithotectonic units data determined minimum/maximum values of 0.2/1.14 for THS/GHS and GB/GHS pairs, respectively. Separating and comparing the two river drainages against each other gives a dissimilarity value of 0.71 (Figure A4).

Comparing drainage and lithotectonic units datasets determined a minimum and maximum dissimilarity value of 0.1 for LHS and Yarlung-Brahmaputra age populations and 0.69 for GHS and GB age populations. Comparison of drainage and epoch datasets determined minimum and maximum dissimilarity values of 0.26 between Ganges and Pleistocene samples and 0.8 between Miocene and Pliocene samples. Lithotectonic units and epoch dataset comparisons determined dissimilarity values of 0.17 and 0.95 for THS/GHS and GB/Pliocene pairs, respectively. Final stress values for all comparisons ranged from ~0.02 – 0.08, representing good transformation from sample dissimilarity to Cartesian distance (Vermeesch, 2013)

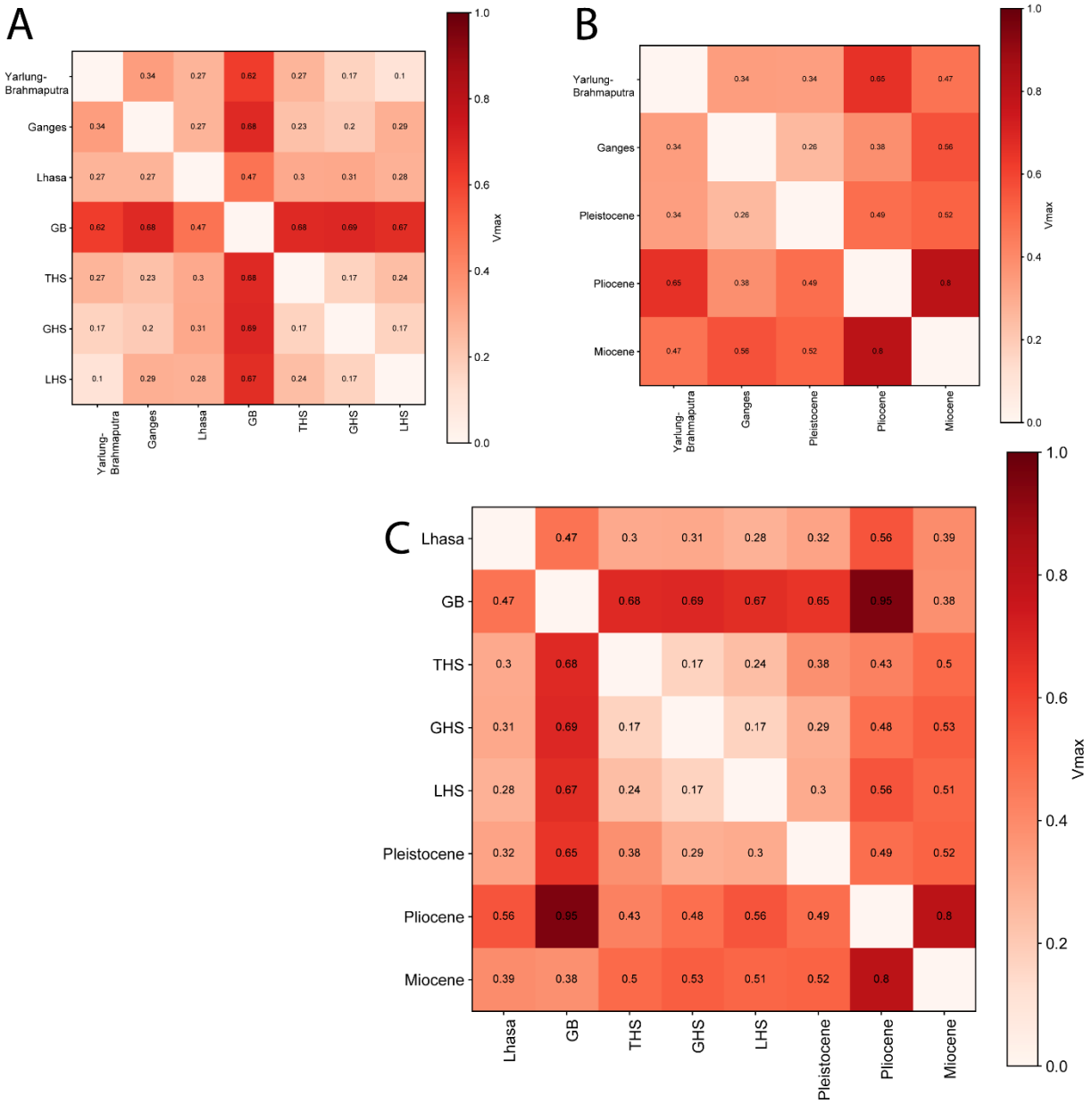


Figure 6: Heat map plots of dissimilarity between samples in MDS space, determined by Kuiper test V values. Pairs are perfectly similar when Vmax = 0 (white) and most dissimilar at Vmax = 1 (dark colors). A) River drainage against lithotectonic units. B) River drainage against Epochs. C) Epochs against lithotectonic units.

First-order interpretation of the three plotting schemes determines the following: Pleistocene samples are most similar to Ganges source signals, while Miocene samples are most similar to Yarlung-Brahmaputra signals. Himalayan source signals (THS, GHS, LHS) share

highly similar age populations, differentiating from Lhasa and (substantially) GB signals. Of particular note, the Yarlung-Brahmaputra shares greatest similarity with LHS ages compared to the Ganges, which is surprising since the spatial extent of the Ganges drainage covers a wider area across the western and central LHS. Overarching trends suggest decreasing single ZHe similarity to Brahmaputra River source signals and increasing Ganges sources from Miocene to Early Pliocene time, with intermittent high-similarity occurrences throughout proceeding time (Figure A4).

Discussion

Miocene-Pleistocene Exhumation Variability

There are two major events over the timeframe of our sample sets that must be taken into account when discussing exhumation in the Himalaya: The onset of EHS rapid exhumation in the Pliocene (e.g. Najman et al., 2019), and major climate regime change across the PPT. Before the former, previous rutile U-Pb and ZFT strongly suggest that Himalayan uplift and exhumation reached a steady-state or static lag-time peak from ~12 – 6 Ma (Najman et al., 2019). The lack of rapid exhumation has been interpreted as passive erosion of GHS material after a period of rapid exhumation ca. ~17 Ma (Laskowski et al., 2018; Najman et al., 2019). Our data from Miocene samples U1451_A33F and U1455_C35F agree with these previous data, where cooling ages are ~1 – 3 Ma older than the depositional age, matching closely with steady erosion through time (Figure 3). By middle Pliocene time, there is a general decrease in ZHe age ranges coupled with faster transport and deposition to the Bengal Fan with increasing appearance of <1 Ma lag times, and thus an increase in exhumation rates. This agrees with the expected increase in exhumation expected with the onset of rapid Himalayan exhumation, both in the EHS and frontal-Himalaya

(Chirouze et al., 2013; Lang et al., 2016). However, the ZHe age spectra (2.10 ± 0.04 Ma to 410.38 ± 5.52 Ma) support a Ganges source of sediments rather than Brahmaputra sources, suggesting that denudation of the frontal-Himalayan outpaced the rapid erosion of the EHS at this time, along with increasing input from source terranes with older rocks in recent time. Approaching and through the duration of the Pleistocene, there is no discernable overall increase or decrease in lag-time, but rather a mixture of very young ZHe ages and older Miocene (>10 Ma) ages. A combination of increasing exhumation in the both frontal-Himalaya and EHS source regions and strengthening climatic forces leading to paleo-river drainage reorganization similar to the modern-day GBS may explain the higher variability in cooling ages seen in the Pleistocene Bengal Fan sediments.

Tectonic-Climate Coupling: Exhumation Acceleration, Monsoon Intensification, and The Pliocene-Pleistocene Transition

Intensive research into the cause-effect relationships between climate and tectonics has resulted in complex models explaining tectono-climatic feedback loops in any given geological setting, and the Himalayan-Tibetan orogen is no exception (England & Molnar, 1990; Jepson et al., 2021). The uplift of the Himalayan orogen is hypothesized and debated to have precipitated major climate change in the Late-Cenozoic via absorption of atmospheric CO_2 through siliciclastic chemical weathering (Raymo and Ruddiman, 1992; Clift and Jonell, 2021), redirection of global wind patterns (Gasse and Derbyshire, 1996), and long-term worldwide cooling (Sarin et al., 1989; Raymo et al., 1992; Colleps et al., 2018). In return, these global climatic transitions are hypothesized and debated to have directly influenced much of the orogens evolution and real or perceived uplift (Beaumont et al., 2001; Reiners et al., 2003; Wobus et al., 2005; Herman et al., 2013). Of particular interest across the lifespan of the orogen

is the PPT, where two instances of major tectonic and climate regime changes have been recorded.

The ZHe ages produced from Pliocene – Pleistocene Bengal Fan samples appear to record these transitions, with age populations of 4 – 9 Ma coinciding with known GHS/LHS peaks of 5 – 8 Ma, respectively, although the 4 Ma peak in the Pliocene aligns greater with known THS peaks. The latter may indicate that parts of the THS were affected by the increase in monsoon intensity, prior to continued topographic growth of the Himalaya and establishment of the modern rain shadow. The Pliocene marks stark, rapid increase in exhumation rates of the frontal Himalaya and syntaxial massifs, most notably with EHS rapid exhumation initiation at a minimum ~5 – 3 Ma (Chirouze et al., 2013; Zeitler et al., 2014; Lang et al., 2016; Najman et al., 2019), marked by cooling age lag-times <1 Ma, and continuing into the present day. Approximately contemporally with rapid exhumation increases in the Himalaya is both onset of glacial-interglacial periods until extensive glaciation ~ 3 Ma (Bartoli et al., 2005) and the intensification of the South Asian Monsoon (SAM), which had been established as a major equatorial climate pattern since the Miocene, with onset at ~10.7 Ma (Jepson et al., 2021). Given the spatial and temporal proximity of the structural and climatic processes across the orogen, this suggests an element of climatic forcing may help to drive rapid exhumation during this period. Dust particles from IODP 359 cores in the Maldives determined an increase in both dust flux and particle size in the timeframe of ~4.0 – 3.3 Ma, coinciding with intensification of the SAM (Lindhorst et al., 2019). Another study reviewing populations of planktonic foraminifera in the Indian Ocean concluded the SAM may have intensified earlier ca. 5.6 – 4.2 Ma cotemporally with the closure of the Indonesian Seaway (Srinivasan and Sinha, 2000). Increasing precipitation

and strengthening wind in the summer months results in intense erosion of the frontal Himalaya, denudating thousands of tons per year of detrital material into both Ganges and Brahmaputra drainages. The frontal Himalaya acts as an orographic barrier to the Tethyan Himalaya and other terranes to the north, and thus intensification of the monsoon should also be recorded by increasing sediment fluxes derived from GHS and LHS sources.

Onset of glaciation in the Pliocene resulted in initially ephemeral periods of cooling and ice sheet coverage in the Himalaya and Tibet before initiation of more complete Northern Hemisphere glaciation (Bartoli et al., 2005; Huntington et al., 2006), followed by additional interglacial periods throughout the Pleistocene. Glaciation would have been most intense in high Himalayan regions and northern terranes in Tibet, encompassing parts of the GHS, THS, GB, and Lhasa terrane. Our lag-time results suggest that sediment may have been stored within or blocked by alpine glaciers, increasing the amount of time between source erosion and deposition to the Bengal Fan, which would then be released during glacial retreat and outwash processes.

We infer from the known tectonic regime and climate intensification during the Pliocene that a coupled tectonic-climatic system greatly affected the overall GBS drainage organization near the Pliocene-Pleistocene transition, as evidenced by the apparent shift from Lhasa and Gangdese dominant sample signals to GHS/LHS source signals within the Bengal Fan record. The increase in GHS/LHS signals and decrease in Lhasa/GB signals may thus be directly related to a mixed climatic-forcing system of monsoon-facilitated frontal Himalaya erosion and glacially impeded south-Tibetan sediment storage. The reappearance of Lhasa and GB characteristic cooling age signals from ~1.30 Ma and onward may be attributed to the extreme, asymmetric ~100,000 glacial/interglacial cycles throughout the Pleistocene into the last glacial period (LGP)

~0.12 Ma. Thus, cooling ages from both the Ganges and Brahmaputra drainages record pre- and post-Pliocene exhumation acceleration and climatic regime change.

Potential Spatial and Numerical Biases in Cooling Age Populations

When compiling data for characterization of Ganges and Brahmaputra river signals, it is important to consider the potential for spatial biases in the distribution of cooling age populations present in both river drainages. Although we require *some* variation in Ganges and Brahmaputra River cooling age signals for strong comparisons to Bengal Fan signals, the distribution of previous ZHe data may have a great effect on the signal of one river against the other, especially for small areas with high (*ad hoc* n > 50 within 100 km radius) concentrations of cooling ages.

The major ~3 Ma age mode and generally Pliocene dominant age populations present in the Ganges signal were initially believed to have been the result of clustered ZHe data in Nepal and surrounding areas, which would inherently contribute larger quantities of this age population to the Ganges river signal, and effectively negate or muddy any potential . Upon investigation of these potential spatial biases in younger age population distributions, the region of Nepal appears to contribute a near-equivalent amount of 1.8 – 5.3 Ma (Pliocene) ages to the Ganges River signal as the Bhutan Himalaya contributes to the Brahmaputra signal. We do note that there are more areas in the northwestern Ganges drainage that contribute these cooling ages to the Ganges signal, though these age signals are widespread and thus do not display anomalous biasing towards the Ganges signal. Interestingly, further investigation into the ~7 Ma age mode dominating the Brahmaputra signal determined that 5.3 – 23 Ma (Miocene) age populations are concentrated in the frontal Bhutan Himalaya. Given the increased strength of the SAM in the Pliocene and Pleistocene, we should expect further additions of these age populations to the

Bengal Fan during this time period. The lack of strong Brahmaputra signals as described before further supports Ganges-dominated sediment delivery from central-western Himalayan denudation during these time periods.

The low n values (n = 2-8) of individual samples from the Bengal Fan introduces computational bias into our interpretations, especially when conducting direct comparisons to the high n valued Ganges and Brahmaputra sample signals (n >200). Although we can ameliorate the robustness of our data comparisons through combining samples into supersets based on geologic epoch, the sheer volume difference in sample size inherently biases similarity/dissimilarity calculations in MDS space, as a single grain from a low n sample may have significant impact upon results. Furthermore, combining samples into epoch supersets coarsens interpretation of provenance and sediment routing shifts through time, although these interpretations are considerably more robust than individual samples. We advise caution when reviewing the conclusions presented in this section. Nevertheless, the age populations present in our Bengal Fan samples reflect those populations present and significant to both Ganges and Brahmaputra River signals, and thus we cannot ignore initial trends in age variability determined in this study.

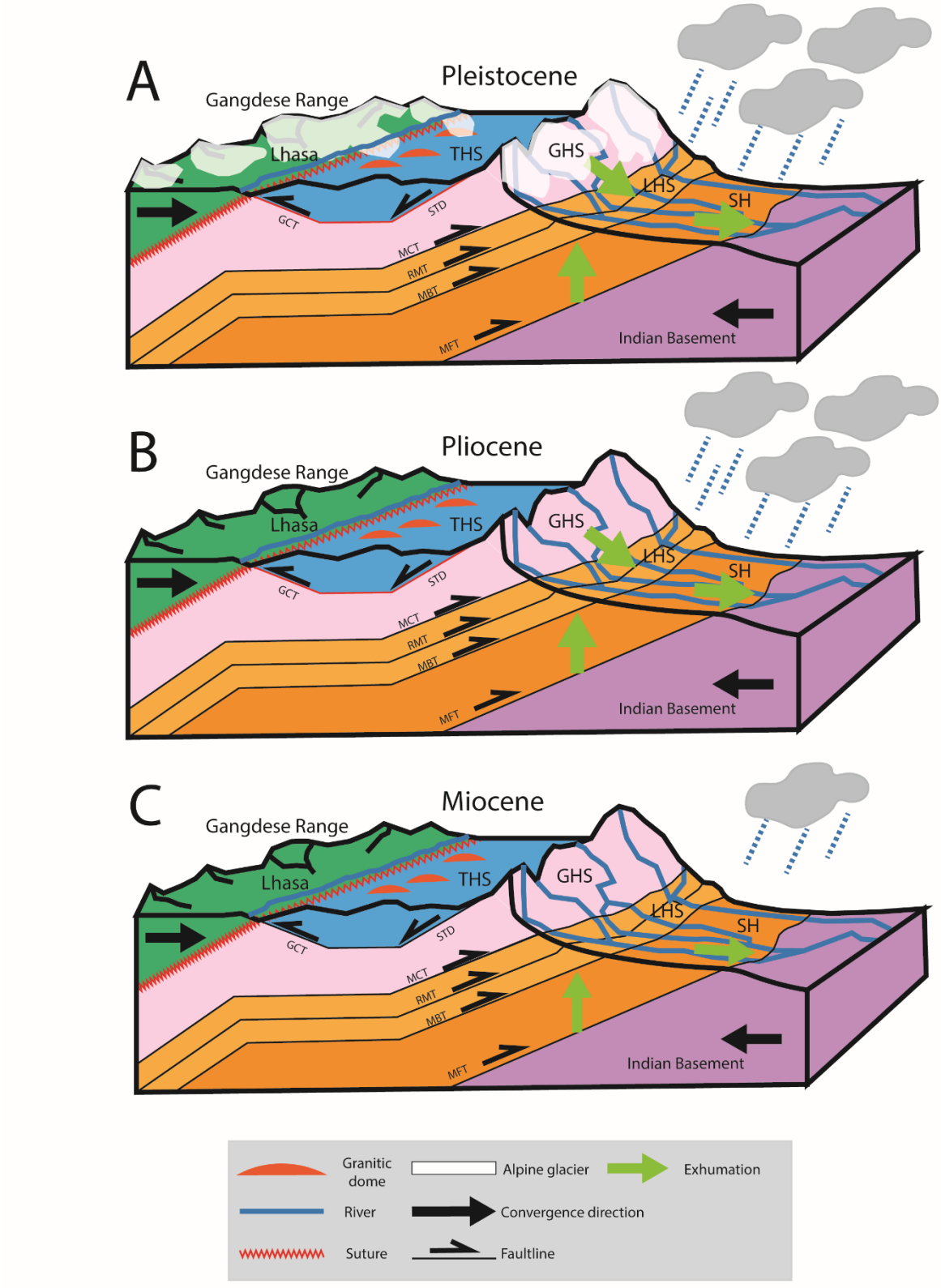

A
Pleistocene
Gangdese Range
Lhasa
THS
GHS
LHS
SH
STD
GCT
MCT
RMT
MBT
MFT
Indian Basement
B
Pliocene
Gangdese Range
Lhasa
THS
GHS
LHS
SH
STD
GCT
MCT
RMT
MBT
MFT
Indian Basement
C
Miocene
Gangdese Range
Lhasa
THS
GHS
LHS
SH
STD
GCT
MCT
RMT
MBT
MFT
Indian Basement
Granitic dome
Alpine glacier
Exhumation
River
Convergence direction
Suture
Faultline

Figure 7: Overview of temporal variability in exhumation and sediment transport mechanisms through tectonic-climatic forcing during Pleistocene (A), Pliocene (B), and Miocene (C) time stamps. Between Miocene-Pliocene time, intensification of the SAM results in increased frontal Himalaya denudation, in tandem with the onset of rapid exhumation in areas such as the EHS. Pliocene-Pleistocene glaciation is hypothesized to have facilitated and inhibited sediment transport and delivery across the orogen. The EHS may have experienced glacial damming along key river systems, resulting in impeded sediment delivery from Lhasa and GB sources.

Provenance Interpretations and Implications

From single ZHe results alone we find increasing probability of Tethyan cooling age signals present across the Pliocene-Pleistocene interglacial period, which is supported by the presence of previously unrecorded Paleozoic ZHe ages within samples that may be derived from crust that did not undergo deformation or reheating throughout the orogen's uplift. We find that the late-Miocene record of Lhasa and Gangdese Batholith cooling signals of Yarlung-Brahmaputra sources ceases by the middle Pliocene, replaced by high-probability Tethyan input. The Tethyan-dominant signal alone does not negate potential input from the Yarlung-Brahmaputra, as the THS is drained by both major drainages via cross-terrane tributaries in both Yarlung-Brahmaputra and Ganges River systems. However, by the Pleistocene, these age signals remain present along with an increase in Miocene (5.3-23 Ma) cooling age populations representative of both GHS and LHS signals found within the Ganges River drainage at higher probabilities. It is not until ~1.30 Ma that a significant Lhasa signal is recorded post-Miocene, and further still at ~500 ka that a return of Gangdese signals is recorded by ZHe analyses. We attribute the increase in GHS/LHS and Ganges-derived source signal similarity of Bengal Fan samples to a mixed tectonic-climatic system involving rapid denudation of the frontal Himalaya due to intensification of precipitation from the SAM (Figure 8). However, the detrital zircon U-Pb record over the same time interval is interpreted to reflect a decrease in THS input in the Pliocene-Pleistocene marked by scarce 400 – 600 Ma ages (Blum et al., 2018), which suggests

that the Ganges river drainage was not the dominant source of sediment delivered to the Bengal Fan at this time. Similarly, where our ZHe data reflects an increase in GHS/LHS material in Bengal Fan sediments, the U-Pb record suggests an opposite trend with increasing <300 Ma age populations representative of Gangdese and Neogene EHS populations that must have been derived from the Brahmaputra drainage (Blum et al., 2018).

Use of double dating analyses is key to reconciliation of these opposite U-Pb and ZHe age population trends. The low n recovery of viable double-dated zircon grains requires caution in consideration of the following interpretations. However, we set out to establish a framework of Bengal Fan provenance herein for future studies to build upon. Initial investigation of Bengal Fan He-Pb samples returned unexpected lag time results for both U-Pb/ZHe and ZHe/stratigraphic age calculations, each displaying a slightly increasing trend through time (Figure 9). One would assume that the onset of rapid exhumation in key regions of the Himalaya (EHS) from the Pliocene to present would result in decreasing lag time trends. Upon consideration of climatic-forcing coinciding with rapid exhumation, we may attribute this increase in lag time to glacial sediment storage processes in southern Tibet, more specifically from Lhasa and Gangdese sources (e.g., Stock et al., 2006). Single ZHe analyses determined the disappearance of Lhasa/GB cooling age populations beginning ~ 3.89 Ma to 1.30 Ma, coinciding with onset and continued intensification of Northern Hemisphere glaciation. Sediment stored for long periods of time between exhumation and deposition would thus cause the apparent increase in ZHe/stratigraphic lag time. Even with the intensification of the SAM eroding frontal Himalayan sources targeting the area encompassed by the Ganges River drainage, pulses of glacially stored sediments released throughout the asymmetric global warming and cooling

periods in the Pleistocene and delivered by the Brahmaputra River drainage may have overridden the Ganges-dominant source signals at specific time intervals. MDS modeling of the Bengal Fan ZHe age signals reveals a similarly suggested pattern of increasing and decreasing similarity to Lhasa and GB source signals across timeframes of ~50 – 100 ka (Figure S5).

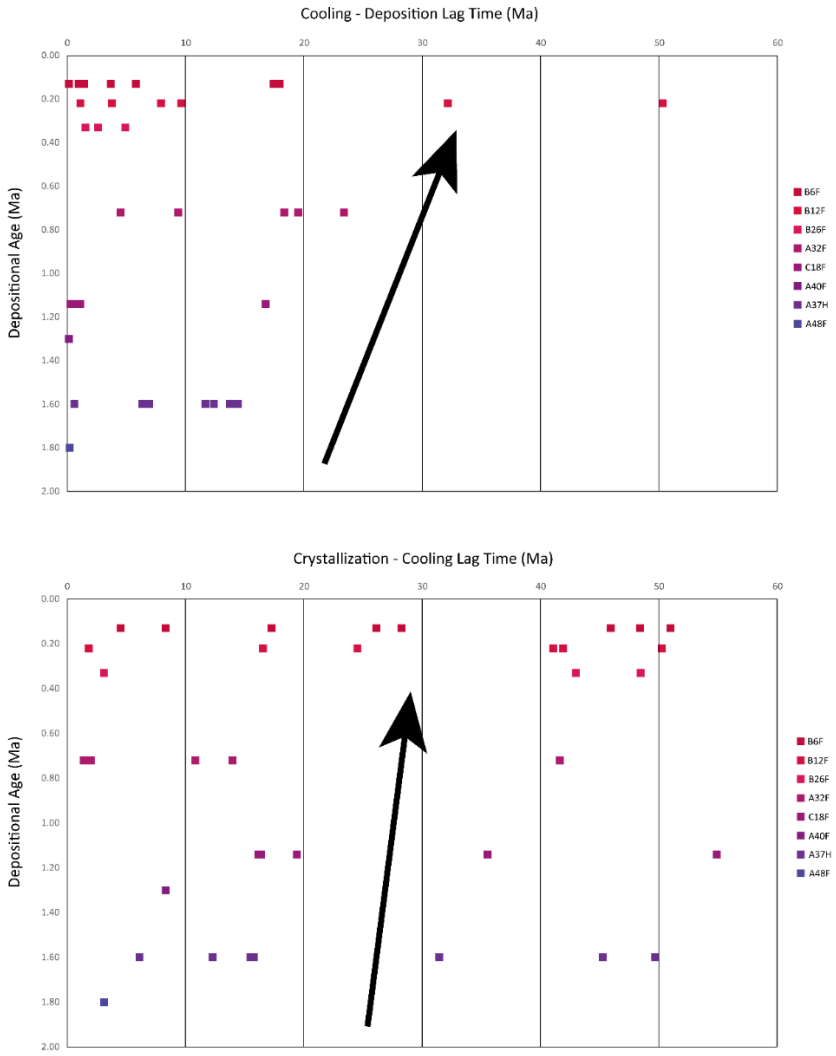


Figure 8: He-Pb lag times calculated for cooling – depositional age (top) and crystallization – cooling age (bottom). General trends are marked by black arrows. Crystallization – cooling lag times appear more variable across Early – Middle Pleistocene time compared with a stronger increasing lag time trend for cooling – deposition.

Reconciliation of increasing U-Pb/ZHe lag time requires additional investigation into known lithotectonic unit U-Pb age spectra. We first begin with initial provenance interpretations. The targeted U-Pb age spectra of 0 – 10 Ma, 15 – 30 Ma, and 45 – 60 Ma was chosen to narrow the uncertainty of errant U-Pb ages to three specific sources, respectively: the eastern Himalayan syntaxis, GHS-derived leucogranites, and Gangdese Batholith signals. The EHS and GB signals need no additional specification for source region as both are drained solely by the Yarlung-Brahmaputra River in the east and no additional information on spatial variation in GB exhumation is available at this time. The GHS leucogranites are the exception: There are a multitude of intruding leucogranites across the extent of the GHS within both the Ganges and Brahmaputra drainages, providing the best opportunity for refined provenance interpretation. Previous studies record leucogranite ZHe cooling age ranges at 10.4 – 12.8 Ma with standard corrections and 14 – 17 Ma with 1-D zonation corrections in the footwall of the South Tibetan Detachment (STDS) in the Everest region of the Himalaya (Burg et al., 1984; Orme et al., 2015), 6.3 – 6.6 Ma in the Bhutan Himalaya (Adams et al., 2015), 6.2 – 8.5 Ma in the Lopu Kangri rift (Laskowski et al., 2017), and 11.0 – 14.3 Ma in the Rongbuk Valley (Schultz et al., 2017). There are many studies utilizing apatite helium (AHe), $^{40}Ar/^{39}Ar$, and AFT/ZFT thermochronometers for these leucogranites (e.g., Wang et al., 2010; Coutand et al., 2014; Jessup et al., 2019), but we avoid these data so as to not mix interpretations across multiple systems.

Of the 15 Bengal Fan He-Pb samples with U-Pb ages 15 – 30 Ma, we acquired five ZHe ages representative of previously determined Everest-region leucogranites (within the Ganges River drainage), with single cooling ages of ~18.1 ± 0.2 Ma, ~15.4 ± 0.3 Ma, ~14.0 ± 0.2 Ma, 13.3 ± 0.2 Ma, and ~10.1 ± 0.1 Ma. Five ZHe ages record cooling from ~1.40 ± 0.02 Ma – 2.20

± 0.04 Ma, which we may attribute to the leucogranites emplaced in the EHS which would be rapidly exhumed following the ~5 – 3 Ma initiation (Najman et al., 2019) and a period of decreased exhumation in the EHS, respectively. One additional grain at ~8.5 ± 0.2 Ma may be representative of either the EHS leucogranites or leucogranites emplaced in the Lopu Kangri fault zone (Laskowski et al., 2017). Two additional ages of ~5.95 ± 0.08 Ma and 5.23 ± 0.08 Ma were acquired as well, and accounting for analytical error in previous samples, may be representative of the Bhutan Himalaya (within the Brahmaputra River drainage), EHS, or Lopu Kangri. Further refinement of these grain sources is not possible without additional mineralogical or compositional information (i.e. enriched/depleted rims/cores, geochemistry, etc.)

Two grains display ZHe ages of 24.1 ± 0.3 Ma and 20.2 ± 0.3 Ma, with corresponding U-Pb ages of 26.1 ± 0.8 Ma and 21.6 ± 0.3, respectively. Currently, there are no known leucogranite samples in the GHS that display these age ranges for the ZHe system; however, Decelles et al (2011) report igneous zircon ~24 – 26 Ma from a tuff bed in the Kailas Formation corresponding to the calculated MDA. The tuffs are attributed to Gangdese volcanism across the northeastern Karakoram Fault (Decelles et al., 2011). Interestingly, there is a sizeable leucogranite intrusion within the Kailas region, ~250 km west from Mt. Kailas (Figure 1). Given the timing of GHS leucogranite intrusions across the orogen of ~30 – 15 Ma (e.g., Searle et al., 1999; Searle et al., 2003; Orme et al., 2015; Wolff et al., 2022) and previous samples displaying near-equivalent U-Pb ages from this region, we hypothesize that leucogranites from this area may be a source of grains with ZHe dates of ~20 – 24 Ma. This interpretation is complicated by the presence of previous muscovite $^{40}Ar/^{39}Ar$ ages of ~15.5 – 15.9 Ma (Vannay et al., 2004), as

we should expect argon ages to be higher than ZHe cooling ages. However, these age differences could be explained by spatial variability in emplacement and cooling rates, or potentially by the effects of inherited cores in leucogranite zircons (e.g., Liu et al., 2022).

These double dating results are thus directly attributable to four source regions across the GHS, narrowing the spatial window of interpretation from ~3000 lateral km to a few hundred km per region and confirming the potential in using zircon (U-Th)/He analyses for powerful Bengal Fan provenance investigation. The data additionally show an easterly-younging trend across the various leucogranites, which may be linked to previously hypothesized deeper crustal processes controlling orogen construction such as asymmetric subduction of Indian lithosphere and slab dynamics (e.g., Piccolo et al., 2018). These refined provenance interpretations, however, are limited by the current ZHe data available surrounding GHS leucogranites. Further still, as Orme et al (2015) demonstrated, U-Th zonation effects on the cooling age of these leucogranite samples may pertain to our samples as well (Appendix A2). However, our detrital record can be further interpreted with future thermochronology studies in the GHS that utilize the ZHe chronometer.

Upon reaching viable interpretation of He-Pb sources of 15 – 30 Ma crystallization and reintroduction of all 36 samples together, the increasing lag-time trend is ameliorated with associated stratigraphic ages. Lag-time calculations for the four 0 – 10 Ma EHS derived samples display a slight increasing trend from ~1.80 – 0.13 Ma. The Everest region-derived samples were deposited between at ~1.60 Ma and ~0.13 Ma, with lag time calculations of ~15.5 Ma and ~6.1 Ma in the Early Pleistocene and ~8 Ma in the Late Pleistocene. The single potential Bhutan Himalaya sample was calculated with a lag time of ~17.3 Ma in the Late Pleistocene.

Calculations for the 45 – 60 Ma Gangdese populations reveal the widest range of U-Pb/ZHe lag times from ~1.8 – 54 Ma, though only one grain was determined to be younger than ~16 Ma at 0.22 Ma deposition. Given that the Gangdese and leucogranite samples fall within the bounds of high-Himalayan glaciation during Pleistocene time, we may contribute the increased lag time from these grains to sediment storage facilitated by increasingly prominent glacial processes (e.g., see Stock et al., 2006); we suggest that these sediments were stored within the Himalayan orographic zone for long periods prior to reaching the shelf margin, as low sea-level associated with glacial periods would facilitate deposition farther onto shelf margins and directly to the Bengal Fan (Mason et al., 2019). Lag-times of the four 0 – 10 Ma EHS derived samples are attributable to both glacial storage processes that and rapid denudation via the SAM, with samples reaching the Fan in <1 Ma ZHe/stratigraphic lag time concurrent with onset of rapid exhumation in the Pliocene and initial enhancement of SAM processes in the Miocene – early Pleistocene.

Conclusions

We demonstrate the capabilities of zircon (U-Th)/He thermochronology in tracking changes in provenance and transportation mechanisms of sediments from the Himalayan-Tibetan orogen to the Bengal Fan. A dataset of 92 single ZHe dates and 36 He-Pb double dates derived from Late-Miocene to Late-Pleistocene samples show distinct shifts in age populations present through time, suggesting a series of major drainage reorganization events in the Ganges-Brahmaputra River system. Our results reveal previously unrecognized Paleozoic ZHe dates from the orogen that we may attribute to the relatively undeformed sections of the Tethyan Himalayan sequence, along with ZHe age population sediment routing trends that add

complexity to previous interpretations derived from U-Pb analyses (Blum et al., 2018). We thus conclude the following:

(1) Late-Miocene ZHe age populations were derived from Brahmaputra River drainage source regions, evidenced by the presence of Gangdese Batholith and Lhasa source signals (Dixon et al., *in review*). From 6.00 – 3.89 Ma, a major drainage shift occurred that resulted in an increase in GHS and LHS age populations derived from Ganges River drainage sources and either an absence or severe decrease in Gangdese/Lhasa Miocene age populations, with the latter not reappearing in the detrital record until ~1.30 Ma in the Early Pleistocene. We thus suggest that the Brahmaputra River dominated Bengal Fan deposition in the Miocene and the Ganges following across the Pliocene-Pleistocene Transition, before a modern day analogous mixed-transport system emerged in the Early Pleistocene.

(2) Although the Pliocene marked the onset of rapid exhumation in the eastern Himalayan syntaxis, we find that the coeval intensification of the South Asian Monsoon during this same period (Lindhorst et al., 2019; Jepson et al., 2021) and onset of Pliocene-Pleistocene glaciation (Bartoli et al., 2005; Huntington et al., 2006; Colleps et al., 2018) triggered an increase in sediment flux from the frontal Himalaya drained by the Ganges River to the Bengal Fan and suppression of sediment delivery from the Yarlung River.

(3) We determined an increase in the <10 Ma ZHe age population derived from the eastern Himalayan syntaxis beginning from Pliocene-Pleistocene time. Overarching lag-time trends decrease through time, coincident with acceleration of exhumation in

the region in the Pliocene, ~5 – 3.3 Ma (Chirouze et al., 2013; Zeitler et al., 2014; Lang et al., 2016; Najman et al., 2019). We suggest that although sediments from the syntaxis were successfully delivered to the Bengal Fan by the Brahmaputra River throughout this time period, the lack of ~17 Ma age populations from the Yarlung-Tsangpo Suture Zone suggests sediment impediment from southern Tibet by glacial activity.

(4) We highlight here the importance of multi-chronometer analyses in studies of sediment provenance. The power of He-Pb double dating techniques is demonstrated, where we suggest that a series of ZHe ages from 15 – 30 Ma leucogranites were derived from four spatially disparate regions of the Greater Himalayan sequence (Decelles et al., 2011; Adams et al., 2015; Orme et al., 2015; Schultz et al., 2017), refining the potential source regions of Bengal Fan sediments from ~ 2500 km^2 of GBS drainage area to a few hundred lateral km across the orogen.

Acknowledgements

We would like to thank Andrew K. Laskowski for contributing his insight and expertise on the geology and structure of southern Tibet while drafting this manuscript. We would also like to thank Dr. William Guenthner and Linda Angeloni of the Helium Analysis Laboratory (HAL) at the University of Illinois Urbana-Champaign for assistance with the generation of this large ZHe dataset. We thank Mike Blum, Mark Pecha, and James Gleason of the University of Kansas, Arizona LaserChron Center, and the University of Michigan, respectively, for their swift communication in shipping and receiving U-Pb samples for double-dating purposes. The authors

would like to thank the National Science Foundation (NSF-GEO-NERC #2026870) for providing funding for this research.

Literature Cited

Adams, B.A., Hodges, K.V., Whipple, K.X., Ehlers, T.A., van Soest, M.C., Wartho, J., 2015. Constraints on the tectonic and landscape evolution of the Bhutan Himalaya from thermochronometry: Late Cenozoic Evolution of Bhutan. Tectonics 34, 1329–1347. https://doi.org/10.1002/2015TC003853

Argand, E., 1977. Tectonics of Asia, Tectonics of Asia. Hafner Press.

Bartoli, G., Sarnthein, M., Weinelt, M., Erlenkeuser, H., Garbe-Schönberg, D., Lea, D.W., 2005. Final closure of Panama and the onset of northern hemisphere glaciation. Earth Planet. Sci. Lett. 237, 33–44. https://doi.org/10.1016/j.epsl.2005.06.020

Beaumont, C., Jamieson, R.A., Nguyen, M.H., Lee, B., 2001. Himalayan tectonics explained by extrusion of a low-viscosity crustal channel coupled to focused surface denudation. Nature 414, 738–742.

Bernet, M., Spiegel, C., 2004. Introduction: Detrital thermochronology, in: Detrital Thermochronology - Provenance Analysis, Exhumation, and Landscape Evolution of Mountain Belts. Geological Society of America. https://doi.org/10.1130/0-8137-2378-7.1

Bhattacharyya, K., Dwivedi, H.V., Das, J.P., Damania, S., 2015. Structural geometry, microstructural and strain analyses of L-tectonites from Paleoproterozoic orthogneiss: Insights into local transport-parallel constrictional strain in the Sikkim Himalayan fold thrust belt. J. Asian Earth Sci. 107, 212–231. https://doi.org/10.1016/j.jseaes.2015.04.038

Blum, M., Rogers, K., Gleason, J., Najman, Y., Cruz, J., Fox, L., 2018. Allogenic and Autogenic Signals in the Stratigraphic Record of the Deep-Sea Bengal Fan. Sci. Rep. 8, 7973. https://doi.org/10.1038/s41598-018-25819-5

Burg, J.P., Brunel, M., Gapais, D., Chen, G.M., Liu, G.H., 1984. Deformation of leucogranites of the crystalline Main Central Sheet in southern Tibet (China). J. Struct. Geol. 6, 535–542. https://doi.org/10.1016/0191-8141(84)90063-4

Cai, F., Ding, L., Yue, Y., 2011. Provenance analysis of upper Cretaceous strata in the Tethys Himalaya, southern Tibet: Implications for timing of India–Asia collision. Earth Planet. Sci. Lett. 305, 195–206. https://doi.org/10.1016/j.epsl.2011.02.055

Carrapa, B., 2009. Tracing exhumation and orogenic wedge dynamics in the European Alps with detrital thermochronology. Geology 37, 1127–1130. https://doi.org/10.1130/G30065A.1

Carrapa, B., Orme, D.A., DeCelles, P.G., Kapp, P., Cosca, M.A., Waldrip, R., 2014. Miocene burial and exhumation of the India-Asia collision zone in southern Tibet: Response to slab dynamics and erosion. Geology 42, 443–446. https://doi.org/10.1130/G35350.1

Cawood, P.A., Johnson, M.R.W., Nemchin, A.A., 2007. Early Palaeozoic orogenesis along the Indian margin of Gondwana: Tectonic response to Gondwana assembly. Earth Planet. Sci. Lett. 255, 70–84. https://doi.org/10.1016/j.epsl.2006.12.006

Chapman, J.B., Kapp, P., 2017. Tibetan Magmatism Database. Geochem. Geophys. Geosystems 18, 4229–4234. https://doi.org/10.1002/2017GC007217

Chirouze, F., Huyghe, P., Van Der Beek, P., Chauvel, C., Chakraborty, T., Dupont-Nivet, G., Bernet, M., 2013. Tectonics, exhumation, and drainage evolution of the eastern Himalaya since 13 Ma from detrital geochemistry and thermochronology, Kameng River Section, Arunachal Pradesh. Geol. Soc. Am. Bull. 125, 523–538. https://doi.org/10.1130/B30697.1

Cina, S.E., Yin, A., Grove, M., Dubey, C.S., Shukla, D.P., Lovera, O.M., Kelty, T.K., Gehrels, G.E., Foster, D.A., 2009. Gangdese arc detritus within the eastern Himalayan Neogene foreland basin: Implications for the Neogene evolution of the Yalu–Brahmaputra River system. Earth Planet. Sci. Lett. 285, 150–162. https://doi.org/10.1016/j.epsl.2009.06.005

Clift, P., Jonell, T., 2021. Himalayan-Tibetan Erosion is not the Cause of Neogene Global Cooling (other). pico. https://doi.org/10.5194/egusphere-egu21-1232

Clift, P.D., Giosan, L., Carter, A., Garzanti, E., Galy, V., Tabrez, A.R., Pringle, M., Campbell, I.H., France-Lanord, C., Blusztajn, J., Allen, C., Alizai, A., Lueckge, A., Danish, M., Rabbani, M.M., Tada, R., Zheng, H., 2010. Monsoon control over erosion patterns in the western Himalaya; possible feed-back into the tectonic evolution. Geol. Soc. Spec. Publ. 342, 185–218. https://doi.org/10.1144/SP342.12

Colleps, C.L., McKenzie, N.R., Stockli, D.F., Hughes, N.C., Singh, B.P., Webb, A.A.G., Myrow, P.M., Planavsky, N.J., Horton, B.K., 2018. Zircon (U-Th)/He Thermochronometric Constraints on Himalayan Thrust Belt Exhumation, Bedrock Weathering, and Cenozoic Seawater Chemistry. Geochem. Geophys. Geosystems 19, 257–271. https://doi.org/10.1002/2017GC007191

Coutand, I., Whipp, D.M., Grujic, D., Bernet, M., Fellin, M.G., Bookhagen, B., Landry, K.R., Ghalley, S.K., Duncan, C., 2014. Geometry and kinematics of the Main Himalayan Thrust and Neogene crustal exhumation in the Bhutanese Himalaya derived from inversion of multithermochronologic data: NEOGENE EXHUMATION OF BHUTAN HIMALAYAS. J. Geophys. Res. Solid Earth 119, 1446–1481. https://doi.org/10.1002/2013JB010891

DeCelles, P.G., Carrapa, B., Gehrels, G.E., Chakraborty, T., Ghosh, P., 2016. Along-strike continuity of structure, stratigraphy, and kinematic history in the Himalayan thrust belt: The view from Northeastern India: EASTERN HIMALAYAN THRUST BELT. Tectonics 35, 2995–3027. https://doi.org/10.1002/2016TC004298

DeCelles, P.G., Gehrels, G.E., Quade, J., LaReau, B., Spurlin, M., 2000. Tectonic Implications of U-Pb Zircon Ages of the Himalayan Orogenic Belt in Nepal. Science 288, 497–499. https://doi.org/10.1126/science.288.5465.497

DeCelles, P.G., Kapp, P., Gehrels, G.E., Ding, L., 2014. Paleocene-Eocene foreland basin evolution in the Himalaya of southern Tibet and Nepal: Implications for the age of initial India-Asia collision: Paleogene Himalayan foreland basin. Tectonics 33, 824–849. https://doi.org/10.1002/2014TC003522

DeCelles, P.G., Kapp, P., Quade, J., Gehrels, G.E., 2011. Oligocene-Miocene Kailas basin, southwestern Tibet: Record of postcollisional upper-plate extension in the Indus-Yarlung suture zone. Geol. Soc. Am. Bull. 123, 1337–1362. https://doi.org/10.1130/B30258.1

DeCelles, P.G., Robinson, D.M., Quade, J., Ojha, T.P., Garzione, C.N., Copeland, P., Upreti, B.N., 2001. Stratigraphy, structure, and tectonic evolution of the Himalayan fold-thrust belt in western Nepal. Tectonics 20, 487–509. https://doi.org/10.1029/2000TC001226

Deeken, A., Thiede, R.C., Sobel, E.R., Hourigan, J.K., Strecker, M.R., 2011. Exhumational variability within the Himalaya of northwest India. Earth Planet. Sci. Lett. 305, 103–114. https://doi.org/10.1016/j.epsl.2011.02.045

England, P., Molnar, P., 1990. Surface uplift, uplift of rocks, and exhumation of rocks. Geology 18, 1173. https://doi.org/10.1130/0091-7613(1990)018<1173:SUUORA>2.3.CO;2

France-Lanord, C., Spiess, V., Klaus, A., Schwenk, T., Adhikari, R.R., Adhikari, S.K., Bahk, J.-J., Baxter, A.T., Cruz, J.W., Das, S.K., Dekens, P., Duleba, W., Fox, L.R., Galy, A., Galy, V., Ge Junyi, Gleason, J.D., Gyawali, B.R., Huyghe, P., Jia Guodong, Lantzsch, H., Manoj, M.C., Martin, Y.M., Meynadier, L., Najman, Y.M.R., Nakajima, A., Ponton, C., Reilly, B.T., Rogers, K.G., Savian, J.F., Selkin, P.A., Weber, M.E., Williams, T., Yoshida, K., 2016. Expedition 354 summary. Proc. Int. Ocean Discov. Program Exped. Rep. 354, 35. https://doi.org/10.14379/iodp.proc.354.101.2016

Gansser, A., 1983. Geology of the Bhutan Himalaya. Denkschr. Schweiz. Naturforschenden Ges. Memoires Soc. Helvetiques Sci. Nat. 96, 181.

Gansser, A., 1964. The geology of the Himalayas, The geology of the Himalayas.

Garver, J.I., Brandon, M.T., Roden-Tice, M., Kamp, P.J.J., 1999. Exhumation history of orogenic highlands determined by detrital fission-track thermochronology. Geol. Soc. Lond. Spec. Publ. 154, 283–304. https://doi.org/10.1144/GSL.SP.1999.154.01.13

Garzanti, E., Baud, A., Mascle, G., Anonymous, 1987. Sedimentary record of the northward flight of India and its collision with Eurasia (Ladakh Himalaya, India). Geodin. Acta 1, 297–312.

Gasse, F., Derbyshire, E., 1996. Environmental changes in the Tibetan Plateau and surrounding areas — Preface. Palaeogeogr. Palaeoclimatol. Palaeoecol. 120, 1–3. https://doi.org/10.1016/0031-0182(95)00030-5

Gavillot, Y., Meigs, A.J., Sousa, F.J., Stockli, D., Yule, D., Malik, M., 2018. Late Cenozoic Foreland-to-Hinterland Low-Temperature Exhumation History of the Kashmir Himalaya. Tectonics 37, 3041–3068. https://doi.org/10.1029/2017TC004668

Gehrels, G., Kapp, P., DeCelles, P., Pullen, A., Blakey, R., Weislogel, A., Ding, L., Guynn, J., Martin, A., McQuarrie, N., Yin, A., 2011. Detrital zircon geochronology of pre-Tertiary strata in the Tibetan-Himalayan orogen: TIBETAN-HIMALAYAN DETRITAL ZIRCONS. Tectonics 30, n/a-n/a. https://doi.org/10.1029/2011TC002868

Gehrels, G.E., DeCelles, P.G., Ojha, T.P., Upreti, B.N., 2006a. Geologic and U-Th-Pb geochronologic evidence for early Paleozoic tectonism in the Kathmandu thrust sheet, central Nepal Himalaya. Geol. Soc. Am. Bull. 118, 185–198. https://doi.org/10.1130/B25753.1

Gehrels, G.E., DeCelles, P.G., Ojha, T.P., Upreti, B.N., 2006b. Geologic and U–Pb geochronologic evidence for early Paleozoic tectonism in the Dadeldhura thrust sheet, far-west Nepal Himalaya. J. Asian Earth Sci. 28, 385–408. https://doi.org/10.1016/j.jseaes.2005.09.012

Gehrels, G.E., Valencia, V.A., Ruiz, J., 2008. Enhanced precision, accuracy, efficiency, and spatial resolution of U-Pb ages by laser ablation-multicollector-inductively coupled plasma-mass spectrometry: TECHNICAL BRIEF. Geochem. Geophys. Geosystems 9, n/a-n/a. https://doi.org/10.1029/2007GC001805

Guenthner, W.R., Reiners, P.W., Ketcham, R.A., Nasdala, L., Giester, G., 2013. Helium diffusion in natural zircon: Radiation damage, anisotropy, and the interpretation of zircon (U-Th)/He thermochronology. Am. J. Sci. 313, 145–198. https://doi.org/10.2475/03.2013.01

Guo, Z., Wilson, M., 2012. The Himalayan leucogranites: Constraints on the nature of their crustal source region and geodynamic setting. Gondwana Res. 22, 360–376. https://doi.org/10.1016/j.gr.2011.07.027

Haider, V.L., Dunkl, I., von Eynatten, H., Ding, L., Frei, D., Zhang, L., 2013. Cretaceous to Cenozoic evolution of the northern Lhasa Terrane and the early Paleogene development of peneplains at Nam Co, Tibetan Plateau. J. Asian Earth Sci. 70–71, 79–98. https://doi.org/10.1016/j.jseaes.2013.03.005

Herman, F., Seward, D., Valla, P.G., Carter, A., Kohn, B., Willett, S.D., Ehlers, T.A., 2013. Worldwide acceleration of mountain erosion under a cooling climate. Nature 504, 423–426. https://doi.org/10.1038/nature12877

Hourigan, J.K., Reiners, P.W., Brandon, M.T., 2005. U-Th zonation-dependent alpha-ejection in (U-Th)/He chronometry. Geochim. Cosmochim. Acta 69, 3349–3365. https://doi.org/10.1016/j.gca.2005.01.024

Hu, X., Garzanti, E., Wang, J., Huang, W., An, W., Webb, A., 2016. The timing of India-Asia collision onset – Facts, theories, controversies. Earth-Sci. Rev. 160, 264–299. https://doi.org/10.1016/j.earscirev.2016.07.014

Hu, X.-M., Garzanti, E., An, W., Hu, X.-F., 2015. Provenance and drainage system of the Early Cretaceous volcanic detritus in the Himalaya as constrained by detrital zircon geochronology. J. Palaeogeogr. 4, 85–98. https://doi.org/10.3724/SP.J.1261.2015.00069

Huntington, K.W., Blythe, A.E., Hodges, K.V., 2006. Climate change and Late Pliocene acceleration of erosion in the Himalaya. Earth Planet. Sci. Lett. 252, 107–118. https://doi.org/10.1016/j.epsl.2006.09.031

Huyghe, P., Bernet, M., Galy, A., Naylor, M., Cruz, J., Gyawali, B.R., Gemignani, L., Mugnier, J.-L., 2020. Rapid exhumation since at least 13 Ma in the Himalaya recorded by detrital apatite fission-track dating of Bengal fan (IODP Expedition 354) and modern Himalayan river sediments. Earth Planet. Sci. Lett. 534, 116078. https://doi.org/10.1016/j.epsl.2020.116078

Jepson, G., Carrapa, B., Gillespie, J., Feng, R., DeCelles, P.G., Kapp, P., Tabor, C.R., Zhu, J., 2021. Climate as the Great Equalizer of Continental-Scale Erosion. Geophys. Res. Lett. 48. https://doi.org/10.1029/2021GL095008

Jessup, M.J., Langille, J.M., Diedesch, T.F., Cottle, J.M., 2019. Gneiss Dome Formation in the Himalaya and southern Tibet. Geol. Soc. Lond. Spec. Publ. 483, 401–422. https://doi.org/10.1144/SP483.15

Kapp, P., DeCelles, P.G., 2019. Mesozoic–Cenozoic geological evolution of the Himalayan-Tibetan orogen and working tectonic hypotheses. Am. J. Sci. 319, 159–254. https://doi.org/10.2475/03.2019.01

Ketcham, R.A., 2005. Forward and Inverse Modeling of Low-Temperature Thermochronometry Data. Rev. Mineral. Geochem. 58, 275–314. https://doi.org/10.2138/rmg.2005.58.11

Kohn, M.J., Paul, S.K., Corrie, S.L., 2009. The lower Lesser Himalayan sequence: A Paleoproterozoic arc on the northern margin of the Indian plate. GSA Bull. 122, 323–335. https://doi.org/10.1130/B26587.1

Kuiper, N.H., 1960. Tests concerning random points on a circle. Indag. Math. Proc. 63, 38–47. https://doi.org/10.1016/S1385-7258(60)50006-0

Landry, K.R., Coutand, I., Whipp, D.M., Grujic, D., Hourigan, J.K., 2016. Late Neogene tectonically driven crustal exhumation of the Sikkim Himalaya: Insights from inversion of multithermochronologic data: Neogene Tectonics of the Sikkim Himalaya. Tectonics 35, 833–859. https://doi.org/10.1002/2015TC004102

Lang, K.A., Huntington, K.W., 2014. Antecedence of the Yarlung–Siang–Brahmaputra River, eastern Himalaya. Earth Planet. Sci. Lett. 397, 145–158. https://doi.org/10.1016/j.epsl.2014.04.026

Lang, K.A., Huntington, K.W., Burmester, R., Housen, B., 2016. Rapid exhumation of the eastern Himalayan syntaxis since the late Miocene. Geol. Soc. Am. Bull. 128, 1403–1422. https://doi.org/10.1130/B31419.1

Laskowski, A.K., Kapp, P., Cai, F., 2018. Gangdese culmination model: Oligocene–Miocene duplexing along the India-Asia suture zone, Lazi region, southern Tibet. GSA Bull. 130, 1355–1376. https://doi.org/10.1130/B31834.1

Laskowski, A.K., Kapp, P., Ding, L., Campbell, C., Liu, X., 2017. Tectonic evolution of the Yarlung suture zone, Lopu Range region, southern Tibet: India-Asia Suture Tectonics, Lopu Range. Tectonics 36, 108–136. https://doi.org/10.1002/2016TC004334

Le Fort, P., 1975. Himalayas; the collided range; present knowledge of the continental arc. Am. J. Sci. Vol. 275-A, 1–44.

Li, G., Kohn, B., Sandiford, M., Xu, Z., 2017. India-Asia convergence: Insights from burial and exhumation of the Xigaze fore-arc basin, south Tibet. J. Geophys. Res. Solid Earth 122, 3430–3449. https://doi.org/10.1002/2017JB014080

Lindhorst, S., Betzler, C., Kroon, D., 2019. Wind variability over the northern Indian Ocean during the past 4 million years – Insights from coarse aeolian dust (IODP exp. 359, site U1467, Maldives). Palaeogeogr. Palaeoclimatol. Palaeoecol. 536, 109371. https://doi.org/10.1016/j.palaeo.2019.109371

Liu, L., Zhu, D.-C., Wang, Q., Cawood, P.A., Stockli, D.F., Stockli, L.D., Lin, C., Zhang, J.-J., Zhang, L.-L., Zhao, Z.-D., 2022. Leucogranite Records Multiple Collisional Orogenies. Geophys. Res. Lett. 49, e2021GL096817. https://doi.org/10.1029/2021GL096817

Long, S.P., Robinson, D.M., 2021. Construction of the Lesser Himalayan–Subhimalayan thrust belt: The primary driver of thickening, exhumation, and high elevations in the Himalayan orogen since the middle Miocene. Geology 49, 1283–1288. https://doi.org/10.1130/G48967.1

Lupker, M., Lavé, J., France-Lanord, C., Christl, M., Bourlès, D., Carcaillet, J., Maden, C., Wieler, R., Rahman, M., Bezbaruah, D., Xiaohan, L., 2017. ¹⁰Be systematics in the Tsangpo-Brahmaputra catchment: the cosmogenic nuclide legacy of the eastern Himalayan syntaxis. Earth Surf. Dyn. 5, 429–449. https://doi.org/10.5194/esurf-5-429-2017

Mason, C.C., Romans, B.W., Stockli, D.F., Mapes, R.W., Fildani, A., 2019. Detrital zircons reveal sea-level and hydroclimate controls on Amazon River to deep-sea fan sediment transfer. Geology 47, 563–567. https://doi.org/10.1130/G45852.1

Meyer, N.R., Garver, J.I., Anonymous, 2000. Zircon fission-track fingerprint of major tributaries to the Mississippi River. Abstr. Programs - Geol. Soc. Am. 32, 59.

Molnar, P., England, P., Martinod, J., 1993. Mantle dynamics, uplift of the Tibetan Plateau, and the Indian monsoon. Rev. Geophys. 31, 357–396. https://doi.org/10.1029/93RG02030

Najman, Y., Bickle, M., BouDagher-Fadel, M., Carter, A., Garzanti, E., Paul, M., Wijbrans, J., Willett, E., Oliver, G., Parrish, R., Akhter, S.H., Allen, R., Ando, S., Chisty, E., Reisberg, L., Vezzoli, G., 2008. The Paleogene record of Himalayan erosion: Bengal Basin, Bangladesh. Earth Planet. Sci. Lett. 273, 1–14. https://doi.org/10.1016/j.epsl.2008.04.028

Najman, Y., Mark, C., Barfod, D.N., Carter, A., Parrish, R., Chew, D., Gemignani, L., 2019. Spatial and temporal trends in exhumation of the Eastern Himalaya and syntaxis as determined from a multitechnique detrital thermochronological study of the Bengal Fan. GSA Bull. 131, 1607–1622. https://doi.org/10.1130/B35031.1

Orme, D.A., 2019. Burial and exhumation history of the Xigaze forearc basin, Yarlung suture zone, Tibet. Geosci. Front. 10, 895–908. https://doi.org/10.1016/j.gsf.2017.11.011

Orme, D.A., Carrapa, B., Kapp, P., 2015a. Sedimentology, provenance and geochronology of the upper Cretaceous-lower Eocene western Xigaze forearc basin, southern Tibet. Basin Res. 27, 387–411. https://doi.org/10.1111/bre.12080

Orme, D.A., Laskowski, A.K., Zilinsky, M.F., Chao, W., Guo, X., Cai, F., Lin, D., 2021. Sedimentology and provenance of newly identified Upper Cretaceous trench basin strata, Dênggar, southern Tibet: Implications for development of the Eurasian margin prior to India–Asia collision. Basin Res. 33, 1454–1473. https://doi.org/10.1111/bre.12521

Orme, D.A., Reiners, P.W., Hourigan, J.K., Carrapa, B., 2015b. Effects of inherited cores and magmatic overgrowths on zircon (U-Th)/He ages and age-eU trends from Greater Himalayan sequence rocks, Mount Everest region, Tibet: EFFECTS OF ZONATION ON AGE-EU TRENDS. Geochem. Geophys. Geosystems 16, 2499–2507. https://doi.org/10.1002/2015GC005818

Parrish, R.R., Hodges, V., 1996. Isotopic constraints on the age and provenance of the Lesser and Greater Himalayan sequences, Nepalese Himalaya. Geol. Soc. Am. Bull. 108, 904–911. https://doi.org/10.1130/0016-7606(1996)108<0904:ICOTAA>2.3.CO;2

Piccolo, A., Faccenda, M., Carosi, R., Montomoli, C., Visonà, D., 2018. Crustal strength control on structures and metamorphism in collisional orogens. Tectonophysics 746, 470–492. https://doi.org/10.1016/j.tecto.2017.09.018

Qin, Q., Huang, H., Wang, T., Guo, R., Zhang, Z., Tong, Y., 2016. Relationship of the Tarim Craton to the Central Asian Orogenic Belt: insights from Devonian intrusions in the northern margin of Tarim Craton, China. Int. Geol. Rev. 58, 2007–2028. https://doi.org/10.1080/00206814.2016.1199289

Raymo, M.E., Ruddiman, W.F., 1992. Tectonic forcing of late Cenozoic climate. Nat. Lond. 359, 117–122.

Raymo, M.E., Tsuchi, R., Ingle, J.C., Jr, 1992. Late Cenozoic evolution of global climate, Pacific Neogene; environment, evolution, and events. University of Tokyo Press.

Reiners, P.W., 2005. (U-Th)/(He-Pb) double dating of detrital zircons. Am. J. Sci. 305, 259–311. https://doi.org/10.2475/ajs.305.4.259

Reiners, P.W., Ehlers, T.A., Mitchell, S.G., Montgomery, D.R., 2003. Coupled spatial variations in precipitation and long-term erosion rates across the Washington Cascades. Nature 426, 645–7. https://doi.org/10.1038/nature02111

Reiners, P.W., Spell, T.L., Nicolescu, S., Zanetti, K.A., 2004. Zircon (U-Th)/He thermochronometry: He diffusion and comparisons with 40Ar/39Ar dating. Geochim. Cosmochim. Acta 68, 1857–1887. https://doi.org/10.1016/j.gca.2003.10.021

Sarin, M.M., Krishnaswami, S., Dilli, K., Somayajulu, B.L.K., Moore, W.S., 1989. Major ion chemistry of the Ganga-Brahmaputra river system; weathering processes and fluxes to the Bay of Bengal. Geochim. Cosmochim. Acta 53, 997–1009. https://doi.org/10.1016/0016-7037(89)90205-6

Saylor, J.E., Sundell, K.E., 2016. Quantifying comparison of large detrital geochronology data sets. Geosphere 12, 203–220. https://doi.org/10.1130/GES01237.1

Saylor, J.E., Sundell, K.E., Sharman, G.R., 2019. Characterizing sediment sources by non-negative matrix factorization of detrital geochronological data. Earth Planet. Sci. Lett. 512, 46–58. https://doi.org/10.1016/j.epsl.2019.01.044

Schultz, M.H., Hodges, K.V., Ehlers, T.A., van Soest, M., Wartho, J.-A., 2017. Thermochronologic constraints on the slip history of the South Tibetan detachment system in the Everest region, southern Tibet. Earth Planet. Sci. Lett. 459, 105–117. https://doi.org/10.1016/j.epsl.2016.11.022

Searle, M.P., Noble, S.R., Hurford, A.J., Rex, D.C., 1999. Age of crustal melting, emplacement and exhumation history of the Shivling Leucogranite, Garhwal Himalaya. Geol. Mag. 136, 513–525. https://doi.org/10.1017/S0016756899002885

Searle, M.P., Simpson, R.L., Law, R.D., Parrish, R.R., Water, D.J., 2003. The structural geometry, metamorphic and magmatic evolution of the Everest massif, High Himalaya of Nepal-South Tibet. J. Geol. Soc. 160, 345.

Seraine, M., Campos, J.E.G., Martins-Ferreira, M.A.C., Alvarenga, C.J.S. de, Chemale, F., Angelo, T.V., Spencer, C., 2021. Multi-dimensional scaling of detrital zircon geochronology constrains basin evolution of the late Mesoproterozoic Paranoá Group, central Brazil. Precambrian Res. 365, 106381. https://doi.org/10.1016/j.precamres.2021.106381

Srinivasan, M.S., Sinha, D.K., 2000. Ocean circulation in the tropical Indo-Pacific during early Pliocene (5.6-4.2 Ma): Paleobiogeographic and isotopic evidence. J. Earth Syst. Sci. 109, 315–328. https://doi.org/10.1007/BF03549815

Stock, G.M., Ehlers, T.A., Farley, K.A., 2006. Where does sediment come from? Quantifying catchment erosion with detrital apatite (U-Th)/He thermochronometry. Geology 34, 725. https://doi.org/10.1130/G22592.1

Styron, R., Taylor, M., Sundell, K., 2015. Accelerated extension of Tibet linked to the northward underthrusting of Indian crust. Nat. Geosci. 8, 131–134. https://doi.org/10.1038/ngeo2336

Sundell, K.E., Saylor, J.E., 2017. Unmixing detrital geochronology age distributions. Geochem. Geophys. Geosystems 18, 2872–2886. https://doi.org/10.1002/2016GC006774

Sundell, K.E., Taylor, M.H., Styron, R.H., Stockli, D.F., Kapp, P., Hager, C., Liu, D., Ding, L., 2013. Evidence for constriction and Pliocene acceleration of east-west extension in the North Lunggar rift region of west central Tibet: NORTH LUNGGAR RIFT, WEST CENTRAL TIBET. Tectonics 32, 1454–1479. https://doi.org/10.1002/tect.20086

Thiede, R.C., Ehlers, T.A., Bookhagen, B., Strecker, M.R., 2009. Erosional variability along the northwest Himalaya. J. Geophys. Res. 114, F01015. https://doi.org/10.1029/2008JF001010

Vermeesch, P., 2013. Multi-sample comparison of detrital age distributions. Chem. Geol. 341, 140–146. https://doi.org/10.1016/j.chemgeo.2013.01.010

Vermeesch, P., 2004. How many grains are needed for a provenance study? Earth Planet. Sci. Lett. 224, 441–451. https://doi.org/10.1016/j.epsl.2004.05.037

Wang, A., Garver, J.I., Wang, G., Smith, J.A., Zhang, K., 2010. Episodic exhumation of the Greater Himalayan Sequence since the Miocene constrained by fission track thermochronology in Nyalam, central Himalaya. Tectonophysics 495, 315–323. https://doi.org/10.1016/j.tecto.2010.09.037

Wobus, C.W., Hodges, K.V., Whipple, K.X., 2003. Has focused denudation sustained active thrusting at the Himalayan topographic front? Geology 31, 861. https://doi.org/10.1130/G19730.1

Wolff, R., Hetzel, R., Dunkl, I., Xu, Q., Bröcker, M., Anczkiewicz, A.A., 2019. High-Angle Normal Faulting at the Tangra Yumco Graben (Southern Tibet) since ~15 Ma. J. Geol. 127, 15–36. https://doi.org/10.1086/700406

Wolff, R., Hetzel, R., Hölzer, K., Dunkl, I., Xu, Q., Anczkiewicz, A.A., Li, Z., 2022a. Rift propagation in south Tibet controlled by underthrusting of India: A case study at the Tangra Yumco graben (south Tibet). J. Geol. Soc. jgs2022-090. https://doi.org/10.1144/jgs2022-090

Wolff, R., Hölzer, K., Hetzel, R., Xu, Q., Dunkl, I., Anczkiewicz, A.A., Li, Z., 2022b. Spatially focused erosion in the High Himalaya and the geometry of the Main Himalayan Thrust in

Central Nepal (85°E) from thermo-kinematic modeling of thermochronological data in the Gyirong region (southern China). Tectonophysics 834, 229378. https://doi.org/10.1016/j.tecto.2022.229378

Yin, A., Harrison, T.M., 2000. Geologic Evolution of the Himalayan-Tibetan Orogen. Annu. Rev. Earth Planet. Sci. 28, 211–280. https://doi.org/10.1146/annurev.earth.28.1.211

Zeitler, P.K., Meltzer, A.S., Brown, L., Kidd, W.S.F., Lim, C., Enkelmann, E., 2014. Tectonics and topographic evolution of Namche Barwa and the easternmost Lhasa block, Tibet, in: Toward an Improved Understanding of Uplift Mechanisms and the Elevation History of the Tibetan Plateau. Geological Society of America. https://doi.org/10.1130/2014.2507(02)

Zhang, P., Mei, L., Jiang, S.-Y., Xu, S., Donelick, R.A., Li, R., Zhang, H., 2021. Erosion and sedimentation in SE Tibet and Myanmar during the evolution of the Burmese continental margin from the Late Cretaceous to Early Neogene. Gondwana Res. 95, 149–175. https://doi.org/10.1016/j.gr.2021.04.005

Zhang, P., Najman, Y., Mei, L., Millar, I., Sobel, E.R., Carter, A., Barfod, D., Dhuime, B., Garzanti, E., Govin, G., Vezzoli, G., Hu, X., 2019. Palaeodrainage evolution of the large rivers of East Asia, and Himalayan-Tibet tectonics. Earth-Sci. Rev. 192, 601–630. https://doi.org/10.1016/j.earscirev.2019.02.003

Zhu, D.-C., Pan, G.-T., Chung, S.-L., Liao, Z.-L., Wang, L.-Q., Li, G.-M., 2008. SHRIMP Zircon Age and Geochemical Constraints on the Origin of Lower Jurassic Volcanic Rocks from the Yeba Formation, Southern Gangdese, South Tibet. Int. Geol. Rev. 50, 442–471. https://doi.org/10.2747/0020-6814.50.5.442

Zhu Dicheng, Wang, Q., Chung, S.-L., Cawood, P.A., Zhao Zhidan, Treloar, P.J., Searle, M.P., 2018. Gangdese magmatism in southern Tibet and India-Asia convergence since 120 Ma. Spec. Publ. - Geol. Soc. Lond. 483, 583–604. https://doi.org/10.1144/SP483.14

CHAPTER FOUR

CONCLUSIONS

The two manuscripts presented in this thesis work (Chapter 2, 3) report on a new orogen-wide low-temperature thermocronology database for the Himalaya and Tibet, *THermO*, and a large ZHe dataset from Bengal Fan sediments comprised of both single and double dated samples. Chapter 2 describes the utility of large regional thermochronology datasets like those available in the *THermO* database, which is demonstrated in four example applications as follows:

(1) Kernel interpolation of regional cooling ages reveals orogen-wide variability in cooling age trends. Young zircon and apatite helium/fission track ages trend towards the Himalayan syntaxes and frontal Himalayas. Both K/Ar and Ar/Ar trends, regardless of mineral system, reveal younging age trends towards the center of the orogen. We suggest that these variations in cooling age trends are indicative of moving foci of Himalayan uplift and exhumation through Miocene-present time.

(2) Investigation of Pliocene-Pleistocene Bengal Fan sediment provenance through apatite fission-tracks reflect shifts in river drainage patterns that we attribute to mixed climatic and tectonic forcing: large-scale rapid denudation of the frontal Himalaya results in increasingly Ganges River-sourced sediments following the Pliocene-Pleistocene Transition, diluting the Brahmaputra River signals that, although present in samples, we would expect to dominate due to rapid exhumation initiation of the EHS.

(3) Region-wide lag time interpretations can be determined through the use of software specializing in calculating exhumation rates from known age and elevation data. We

reference the example of regional AHe/AFT cooling ages across the Himalaya presented by van der Beek and Schildgen (2022) in their *age2exhume* model.

(4) Characterization of known source cooling age signals allows for unknown sink samples to be compared for qualitative and quantitative similarity. We demonstrate the use of DZnmf (Saylor et al., 2019) inverse modeling software and AHe/AFT data to reconstruct and compare potential source regions of unknown sink samples to our known, regional scale sources. The software reconstructed three optimal sources from four unknown sink samples, which showed high levels of similarity to known source signals of the Tethyan Himalaya Sequence, Gangdese Batholith, and Lhasa terrane.

Chapter 3 investigates the provenance of Miocene-Pleistocene Bengal Fan sediments, utilizing 128 total ZHe cooling dates (92 single ZHe analyses, 36 He-Pb double dates) and the *THermO* database described in Chapter 2 to characterize Bengal Fan sediments, Ganges-Brahmaputra river drainage areas, and 5 lithotectonic unit cooling age signals. The Bengal Fan has experienced at least two major shifts in primary provenance and sediment delivery systems, as follows:

(1) From Miocene – Pliocene time, cooling age signals appear most similar to those sourced from the Yarlung-Brahmaputra River, evidenced by the presence of cooling age populations signature of the Lhasa terrane and Gangdese Batholith. Upon reaching the Miocene-Pleistocene transition, cooling age signals become more temporally variable, and the Lhasa/Gangdese signals disappear from the record. This suggests that the Ganges river became the main source of sediments in the Pliocene, which may be attributed to climatic forcing via monsoon intensification around this same time period.

(2) Following the Pliocene-Pleistocene transition, Lhasa and Gangdese signals reappear briefly in the record, and there is an increase in ZHe ages between ~5.3 – 23 Ma. These signals mark the return of Brahmaputra River signals and sediments, although the Ganges River signals continue to dominate the record from the Pleistocene onward.

(3) We attribute the Pliocene-Pleistocene Transition cooling age variability to a mixed tectonic-climatic forcing system. Rapid exhumation initiation in the EHS ~5 – 3 Ma (Najman et al., 2019) results in increasing Lhasa/Gangdese age signals, aligning with previous interpretations from Blum et al (2018). However, the continued and dominant presence of Ganges river signals suggests that climate changes at this time period greatly affected the Bengal Fan sediment delivery system. We suggest that increased denudation in the frontal Himalaya resulted in high flux of sediment volume from the Ganges River drainage, effectively drowning out the Brahmaputra age signals, whose absence was further exacerbated by sediment storage processes in southern Tibet due to cotemporally widespread glaciation.

(4) We successfully demonstrate the capabilities of zircon He-Pb double dating in refining provenance interpretations; U-Pb ages suggestive of GHS and rift-related leucogranites were further refined by ZHe age analyses, revealing four potential regions with leucogranite intrusions to which our Bengal Fan samples may be directly attributable.

This work highlights the complexity of orogen-wide tectonic-climatic feedback loops in determination of the most influential processes affecting exhumation, transport/routing, and deposition of sediments from source to sink. The importance of utilizing multiple mineral systems and chronometers to determine shifts in sediment provenance through time is also

expressed here, as any single system is inherently limited by the very attrbiutes that make it useful in interpretation. Finally, we make a call to action for future researchers to further characterize variability in Himalayan-Tibetan uplift and exhumation through the ZHe system, as it is a powerful low-temperature thermochronometer that has seen relatively low use in this orogenic belt.

CUMULATIVE LITERATURE CITED

Adams, B., Dietsch, C., Owen, L.A., Caffee, M.W., Spotila, J., Haneberg, W.C., 2009. Exhumation and incision history of the Lahul Himalaya, northern India, based on (U-Th)/He thermochronometry and terrestrial cosmogenic nuclide methods. Geomorphology 107, 285–299. https://doi.org/10.1016/j.geomorph.2008.12.017

Adams, B.A., Hodges, K.V., Whipple, K.X., Ehlers, T.A., van Soest, M.C., Wartho, J., 2015. Constraints on the tectonic and landscape evolution of the Bhutan Himalaya from thermochronometry: Late Cenozoic Evolution of Bhutan. Tectonics 34, 1329–1347. https://doi.org/10.1002/2015TC003853

Adlakha, V., Lang, K.A., Patel, R.C., Lal, N., Huntington, K.W., 2013a. Rapid long term erosion in the rain shadow of the Shillong Plateau, eastern Himalaya. Tectonophysics 582, 76–83. https://doi.org/10.1016/j.tecto.2012.09.022

Adlakha, V., Patel, R.C., Kumar, A., Lal, N., Sharma, R., Villa, I.M., Kumar, S., 2018. Tectonic control over exhumation in the Arunachal Himalaya; new constraints from apatite fission track analysis. Spec. Publ. - Geol. Soc. Lond. 481, 65–79. https://doi.org/10.1144/SP481.1

Adlakha, V., Patel, R.C., Lal, N., 2013b. Exhumation and its mechanisms: A review of exhumation studies in the Himalaya. J. Geol. Soc. India 81, 481–502. https://doi.org/10.1007/s12594-013-0064-0

Aoya, M., Wallis, S.R., Terada, K., Lee, J., Kawakami, T., Wang, Y., Heizler, M., 2005. North-south extension in the Tibetan crust triggered by granite emplacement. Geology 33, 853. https://doi.org/10.1130/G21806.1

Argand, E., 1977. Tectonics of Asia, Tectonics of Asia. Hafner Press.

Arita, K., Ganzawa, Y., Ono, Y., Endo, K., Iwata, S., 1997. Thrust tectonics and uplift process of the Nepal Himalaya revealed from fission-track ages. Chigaku Zasshi J. Geogr. 106, 156–167.

Bartoli, G., Sarnthein, M., Weinelt, M., Erlenkeuser, H., Garbe-Schönberg, D., Lea, D.W., 2005. Final closure of Panama and the onset of northern hemisphere glaciation. Earth Planet. Sci. Lett. 237, 33–44. https://doi.org/10.1016/j.epsl.2005.06.020

Beaumont, C., Jamieson, R.A., Nguyen, M.H., Lee, B., 2001. Himalayan tectonics explained by extrusion of a low-viscosity crustal channel coupled to focused surface denudation. Nature 414, 738–742.

Bernet, M., Spiegel, C., 2004. Introduction: Detrital thermochronology, in: Detrital Thermochronology - Provenance Analysis, Exhumation, and Landscape Evolution of Mountain Belts. Geological Society of America. https://doi.org/10.1130/0-8137-2378-7.1

Bhattacharyya, K., Dwivedi, H.V., Das, J.P., Damania, S., 2015. Structural geometry, microstructural and strain analyses of L-tectonites from Paleoproterozoic orthogneiss: Insights

into local transport-parallel constrictional strain in the Sikkim Himalayan fold thrust belt. J. Asian Earth Sci. 107, 212–231. https://doi.org/10.1016/j.jseaes.2015.04.038

Bian, S., Gong, J., Zuza, A.V., Yang, R., Chen, L., Ji, J., Yu, X., Tian, Y., Yu, Z., Cheng, X., Lin, X., Chen, H., 2022. Along-Strike Variation in the Initiation Timing of the North-Trending Rifts in Southern Tibet as Revealed From the Yadong-Gulu Rift. Tectonics 41. https://doi.org/10.1029/2021TC007091

Bian, S., Gong, J., Zuza, A.V., Yang, R., Tian, Y., Ji, J., Chen, H., Xu, Q., Chen, L., Lin, X., Cheng, X., Tu, J., Yu, X., 2020. Late Pliocene onset of the Cona rift, eastern Himalaya, confirms eastward propagation of extension in Himalayan-Tibetan orogen. Earth Planet. Sci. Lett. 544, 116383. https://doi.org/10.1016/j.epsl.2020.116383

Blum, M., Rogers, K., Gleason, J., Najman, Y., Cruz, J., Fox, L., 2018. Allogenic and Autogenic Signals in the Stratigraphic Record of the Deep-Sea Bengal Fan. Sci. Rep. 8, 7973. https://doi.org/10.1038/s41598-018-25819-5

Blythe, A.E., Burbank, D.W., Carter, A., Schmidt, K., Putkonen, J., 2007. Plio-Quaternary exhumation history of the central Nepalese Himalaya: 1. Apatite and zircon fission track and apatite [U-Th]/He analyses: CENTRAL NEPAL PLIO-QUATERNARY EXHUMATION. Tectonics 26, n/a-n/a. https://doi.org/10.1029/2006TC001990

Bojar, A.-V., Fritz, H., Nicolescu, S., Bregar, M., Gupta, R.P., 2005. Timing and mechanisms of Central Himalayan exhumation: discriminating between tectonic and erosion processes. Terra Nova 17, 427–433. https://doi.org/10.1111/j.1365-3121.2005.00629.x

Bollinger, L., Avouac, J.P., Beyssac, O., Catlos, E.J., Harrison, T.M., Grove, M., Goffé, B., Sapkota, S., 2004. Thermal structure and exhumation history of the Lesser Himalaya in central Nepal: THERMAL STRUCTURE OF THE LESSER HIMALAYA. Tectonics 23, n/a-n/a. https://doi.org/10.1029/2003TC001564

Burbank, D.W., Blythe, A.E., Putkonen, J., Pratt-Sitaula, B., Gabet, E., Oskin, M., Barros, A., Ojha, T.P., 2003. Decoupling of erosion and precipitation in the Himalayas. Nature 426, 652–655. https://doi.org/10.1038/nature02187

Burg, J.P., Brunel, M., Gapais, D., Chen, G.M., Liu, G.H., 1984. Deformation of leucogranites of the crystalline Main Central Sheet in southern Tibet (China). J. Struct. Geol. 6, 535–542. https://doi.org/10.1016/0191-8141(84)90063-4

Burg, J.-P., Nievergelt, P., Oberli, F., Seward, D., Davy, P., Maurin, J.-C., Diao Zhizhong, Meier, M., Gaetani, M., Windley, B., 1998. The Namche Barwa syntaxis; evidence for exhumation related to compressional crustal folding. J. Asian Earth Sci. 16, 239–252.

Burg, J.P., Nievergelt, P., Oberli, F., Seward, D., Ristedt, H., Matter, A., Pfiffner, O.A., 1998. Erosion of crustal folds in the Himalayan syntaxes. Terra Nostra Bonn 98–1, 5.

Burke, W.B., Laskowski, A.K., Orme, D.A., Sundell, K.E., Taylor, M.H., Guo, X., Ding, L., 2021. Record of Crustal Thickening and Synconvergent Extension from the Dajiamang Tso Rift, Southern Tibet. Geosciences 11, 209. https://doi.org/10.3390/geosciences11050209

Cai, F., Ding, L., Yue, Y., 2011. Provenance analysis of upper Cretaceous strata in the Tethys Himalaya, southern Tibet: Implications for timing of India–Asia collision. Earth Planet. Sci. Lett. 305, 195–206. https://doi.org/10.1016/j.epsl.2011.02.055

Carrapa, B., 2009. Tracing exhumation and orogenic wedge dynamics in the European Alps with detrital thermochronology. Geology 37, 1127–1130. https://doi.org/10.1130/G30065A.1

Carrapa, B., Faiz bin Hassim, M., Kapp, P.A., DeCelles, P.G., Gehrels, G., 2017. Tectonic and erosional history of southern Tibet recorded by detrital chronological signatures along the Yarlung River drainage. Geol. Soc. Am. Bull. 129, 570–581. https://doi.org/10.1130/B31587.1

Carrapa, B., Orme, D.A., DeCelles, P.G., Kapp, P., Cosca, M.A., Waldrip, R., 2014. Miocene burial and exhumation of the India-Asia collision zone in southern Tibet: Response to slab dynamics and erosion. Geology 42, 443–446. https://doi.org/10.1130/G35350.1

Carrapa, B., Robert, X., DeCelles, P.G., Orme, D.A., Thomson, S.N., Schoenbohm, L.M., 2016. Asymmetric exhumation of the Mount Everest region: Implications for the tectono-topographic evolution of the Himalaya. Geology 44, 611–614. https://doi.org/10.1130/G37756.1

Catlos, E.J., Harrison, T.M., Kohn, M.J., Grove, M., Ryerson, F.J., Manning, C.E., Upreti, B.N., 2001. Geochronologic and thermobarometric constraints on the evolution of the Main Central Thrust, central Nepal Himalaya. J. Geophys. Res. Solid Earth 106, 16177–16204. https://doi.org/10.1029/2000JB900375

Cawood, P.A., Johnson, M.R.W., Nemchin, A.A., 2007. Early Palaeozoic orogenesis along the Indian margin of Gondwana: Tectonic response to Gondwana assembly. Earth Planet. Sci. Lett. 255, 70–84. https://doi.org/10.1016/j.epsl.2006.12.006

Célérier, J., Harrison, T.M., Beyssac, O., Herman, F., Dunlap, W.J., Webb, A.A.G., 2009. The Kumaun and Garwhal Lesser Himalaya, India: Part 2. Thermal and deformation histories. Geol. Soc. Am. Bull. 121, 1281–1297. https://doi.org/10.1130/B26343.1

Chapman, J.B., Kapp, P., 2017. Tibetan Magmatism Database. Geochem. Geophys. Geosystems 18, 4229–4234. https://doi.org/10.1002/2017GC007217

Chirouze, F., Bernet, M., Huyghe, P., Erens, V., Dupont-Nivet, G., Senebier, F., 2012. Detrital thermochronology and sediment petrology of the middle Siwaliks along the Muksar Khola section in eastern Nepal. J. Asian Earth Sci. 44, 94–106. https://doi.org/10.1016/j.jseaes.2011.01.009

Chirouze, F., Huyghe, P., Van Der Beek, P., Chauvel, C., Chakraborty, T., Dupont-Nivet, G., Bernet, M., 2013. Tectonics, exhumation, and drainage evolution of the eastern Himalaya since

13 Ma from detrital geochemistry and thermochronology, Kameng River Section, Arunachal Pradesh. Geol. Soc. Am. Bull. 125, 523–538. https://doi.org/10.1130/B30697.1

Cina, S.E., Yin, A., Grove, M., Dubey, C.S., Shukla, D.P., Lovera, O.M., Kelty, T.K., Gehrels, G.E., Foster, D.A., 2009. Gangdese arc detritus within the eastern Himalayan Neogene foreland basin: Implications for the Neogene evolution of the Yalu–Brahmaputra River system. Earth Planet. Sci. Lett. 285, 150–162. https://doi.org/10.1016/j.epsl.2009.06.005

Clark, R.J., 2005. Structural constraints on the exhumation of the Tso Morari Dome, NW Himalaya (Master's). Struct. Constraints Exhum. Tso Morari Dome NW Himalaya. University of Wisconsin at Madison.

Clift, P., Jonell, T., 2021. Himalayan-Tibetan Erosion is not the Cause of Neogene Global Cooling (other). pico. https://doi.org/10.5194/egusphere-egu21-1232

Clift, P.D., Giosan, L., Carter, A., Garzanti, E., Galy, V., Tabrez, A.R., Pringle, M., Campbell, I.H., France-Lanord, C., Blusztajn, J., Allen, C., Alizai, A., Lueckge, A., Danish, M., Rabbani, M.M., Tada, R., Zheng, H., 2010. Monsoon control over erosion patterns in the western Himalaya; possible feed-back into the tectonic evolution. Geol. Soc. Spec. Publ. 342, 185–218. https://doi.org/10.1144/SP342.12

Coleman, M.E., Hodges, K.V., 1998. Contrasting Oligocene and Miocene thermal histories from the hanging wall and footwall of the South Tibetan detachment in the central Himalaya from ^{40}Ar/^{39}Ar thermochronology, Marsyandi Valley, central Nepal. Tectonics 17, 726–740. https://doi.org/10.1029/98TC02777

Colleps, C.L., McKenzie, N.R., Stockli, D.F., Hughes, N.C., Singh, B.P., Webb, A.A.G., Myrow, P.M., Planavsky, N.J., Horton, B.K., 2018a. Zircon (U-Th)/He Thermochronometric Constraints on Himalayan Thrust Belt Exhumation, Bedrock Weathering, and Cenozoic Seawater Chemistry. Geochem. Geophys. Geosystems 19, 257–271. https://doi.org/10.1002/2017GC007191

Colleps, C.L., McKenzie, N.R., Stockli, D.F., Hughes, N.C., Singh, B.P., Webb, A.A.G., Myrow, P.M., Planavsky, N.J., Horton, B.K., 2018b. Zircon (U-Th)/He Thermochronometric Constraints on Himalayan Thrust Belt Exhumation, Bedrock Weathering, and Cenozoic Seawater Chemistry. Geochem. Geophys. Geosystems 19, 257–271. https://doi.org/10.1002/2017GC007191

Copeland, P., Harrison, T.M., Hodges, K.V., Maruejol, P., Le Fort, P., Pecher, A., 1991. An early Pliocene thermal disturbance of the Main Central Thrust, central Nepal; implications for Himalayan tectonics. J. Geophys. Res. 96, 8475–8500. https://doi.org/10.1029/91JB00178

Copeland, P., Harrison, T.M., Pan, Y., Kidd, W.S.F., Roden, M., Zhang, Y., 1995. Thermal evolution of the Gangdese batholith, southern Tibet: A history of episodic unroofing. Tectonics 14, 223–236. https://doi.org/10.1029/94TC01676

Copeland, P., Harrison, T.M., Parrish, R.R., Burchfiel, B.C., Hodges, K.V., Kidd, W.S.F., Anonymous, 1987. Constraints on the age of normal faulting, north face of Mt. Everest; implications for Oligo-Miocene uplift. Eos Trans. Am. Geophys. Union 68, 1444.

Copeland, P., Mark Harrison, T., Le Fort, P., 1990. Age and cooling history of the Manaslu granite: implications for Himalayan tectonics. J. Volcanol. Geotherm. Res. 44, 33–50. https://doi.org/10.1016/0377-0273(90)90010-D

Coutand, I., Whipp, D.M., Grujic, D., Bernet, M., Fellin, M.G., Bookhagen, B., Landry, K.R., Ghalley, S.K., Duncan, C., 2014. Geometry and kinematics of the Main Himalayan Thrust and Neogene crustal exhumation in the Bhutanese Himalaya derived from inversion of multithermochronologic data: NEOGENE EXHUMATION OF BHUTAN HIMALAYAS. J. Geophys. Res. Solid Earth 119, 1446–1481. https://doi.org/10.1002/2013JB010891

Cross, E.A., III, 2014. The structure, stratigraphy, and evolution of the Lesser Himalaya of central Nepal (Master's). Struct. Stratigr. Evol. Lesser Himalaya Cent. Nepal. University of Arizona.

Crouzet, C., Dunkl, I., Paudel, L., Árkai, P., Rainer, T.M., Balogh, K., Appel, E., 2007. Temperature and age constraints on the metamorphism of the Tethyan Himalaya in Central Nepal: A multidisciplinary approach. J. Asian Earth Sci. 30, 113–130. https://doi.org/10.1016/j.jseaes.2006.07.014

Dai, J., Fox, M., Han, X., Tremblay, M.M., Xu, S., Shuster, D.L., Liu, B., Zhang, J., Wang, C., 2021. Two Stages of Accelerated Exhumation in the Middle Reach of the Yarlung River, Southern Tibet Since the Mid-Miocene. Tectonics 40. https://doi.org/10.1029/2020TC006618

Dai, J., Fox, M., Shuster, D.L., Hourigan, J., Han, X., Li, Y., Wang, C., 2020. Burial and exhumation of the Hoh Xil Basin, northern Tibetan Plateau: Constraints from detrital (U-Th)/He ages. Basin Res. 32, 894–915. https://doi.org/10.1111/bre.12405

Dai, J., Wang, C., Hourigan, J., Santosh, M., 2013. Insights into the early Tibetan Plateau from (U–Th)/He thermochronology. J. Geol. Soc. 170, 917–927. https://doi.org/10.1144/jgs2012-076

DeCelles, P.G., Carrapa, B., Gehrels, G.E., Chakraborty, T., Ghosh, P., 2016. Along-strike continuity of structure, stratigraphy, and kinematic history in the Himalayan thrust belt: The view from Northeastern India: EASTERN HIMALAYAN THRUST BELT. Tectonics 35, 2995–3027. https://doi.org/10.1002/2016TC004298

DeCelles, P.G., Carrapa, B., Ojha, T.P., Gehrels, G.E., Collins, D., 2020. Structural and thermal evolution of the Himalayan thrust belt in midwestern Nepal. Spec. Pap. - Geol. Soc. Am. 547, 79. https://doi.org/10.1130/2020.2547(01)

DeCelles, P.G., Gehrels, G.E., Quade, J., LaReau, B., Spurlin, M., 2000. Tectonic Implications of U-Pb Zircon Ages of the Himalayan Orogenic Belt in Nepal. Science 288, 497–499. https://doi.org/10.1126/science.288.5465.497

DeCelles, P.G., Kapp, P., Gehrels, G.E., Ding, L., 2014. Paleocene-Eocene foreland basin evolution in the Himalaya of southern Tibet and Nepal: Implications for the age of initial India-Asia collision: Paleogene Himalayan foreland basin. Tectonics 33, 824–849. https://doi.org/10.1002/2014TC003522

DeCelles, P.G., Kapp, P., Quade, J., Gehrels, G.E., 2011. Oligocene-Miocene Kailas basin, southwestern Tibet: Record of postcollisional upper-plate extension in the Indus-Yarlung suture zone. Geol. Soc. Am. Bull. 123, 1337–1362. https://doi.org/10.1130/B30258.1

DeCelles, P.G., Robinson, D.M., Quade, J., Ojha, T.P., Garzione, C.N., Copeland, P., Upreti, B.N., 2001. Stratigraphy, structure, and tectonic evolution of the Himalayan fold-thrust belt in western Nepal. Tectonics 20, 487–509. https://doi.org/10.1029/2000TC001226

Deeken, A., Thiede, R.C., Sobel, E.R., Hourigan, J.K., Strecker, M.R., 2011. Exhumational variability within the Himalaya of northwest India. Earth Planet. Sci. Lett. 305, 103–114. https://doi.org/10.1016/j.epsl.2011.02.045

Dewey, J.F., Shackleton, R.M., Chengfa, C., Yiyin, S., Chengfa, C., Shackleton, R.M., Dewey, J.F., Jixiang, Y., 1988. The tectonic evolution of the Tibetan Plateau. Philos. Trans. R. Soc. Lond. Ser. Math. Phys. Sci. 327, 379–413. https://doi.org/10.1098/rsta.1988.0135

Dezes, P.J., Vannay, J.C., Steck, A., Bussy, F., Cosca, M., 1999. Synorogenic extension; quantitative constraints on the age and displacement of the Zanskar shear zone (Northwest Himalaya). Geol. Soc. Am. Bull. 111, 364–374. https://doi.org/10.1130/0016-7606(1999)111<0364:SEQCOT>2.3.CO;2

Ding, L., Dalai, Z., Yin, A., Kapp, P., Harrison, T.M., 2001. Cenozoic structural and metamorphic evolution of the eastern Himalayan syntaxis (Namche Barwa). Earth Planet. Sci. Lett. 192, 423–438. https://doi.org/10.1016/S0012-821X(01)00463-0

Dunkl, I., Antolin, B., Wemmer, K., Rantitsch, G., Kienast, M., Montomoli, C., Ding, L., Carosi, R., Appel, E., El Bay, R., Xu, Q., von Eynatten, H., Gloaguen, R., Ratschbacher, L., 2011. Metamorphic evolution of the Tethyan Himalayan flysch in SE Tibet. Geol. Soc. Spec. Publ. 353, 45–69. https://doi.org/10.1144/SP353.4

Edwards, R.M., 1995. (super 40) Ar/ (super 39) Ar geochronology of the Main Central Thrust (MCT) region; evidence for late Miocene to Pliocene disturbances along the MCT, Marsyangdi River valley, west-central Nepal Himalaya. J. Nepal Geol. Soc. 10, 41–46.

England, P., Molnar, P., 1990. Surface uplift, uplift of rocks, and exhumation of rocks. Geology 18, 1173. https://doi.org/10.1130/0091-7613(1990)018<1173:SUUORA>2.3.CO;2

Enkelmann, E., Ehlers, T.A., Zeitler, P.K., Hallet, B., 2011. Denudation of the Namche Barwa antiform, eastern Himalaya. Earth Planet. Sci. Lett. 307, 323–333. https://doi.org/10.1016/j.epsl.2011.05.004

Eugster, P., Thiede, R.C., Scherler, D., Stübner, K., Sobel, E.R., Strecker, M.R., 2018. Segmentation of the Main Himalayan Thrust Revealed by Low-Temperature Thermochronometry in the Western Indian Himalaya. Tectonics 37, 2710–2726. https://doi.org/10.1029/2017TC004752

Fan, S., Murphy, M.A., Whipp, D.M., Saylor, J.E., Copeland, P., Hoxey, A.K., Taylor, M.H., Stockli, D.F., 2022. Megathrust Heterogeneity, Crustal Accretion, and a Topographic Embayment in the Western Nepal Himalaya: Insights From the Inversion of Thermochronological Data. Tectonics 41. https://doi.org/10.1029/2021TC007071

Finnegan, N.J., Hallet, B., Montgomery, D.R., Zeitler, P.K., Stone, J.O., Anders, A.M., Yuping, L., 2008. Coupling of rock uplift and river incision in the Namche Barwa-Gyala Peri massif, Tibet. Geol. Soc. Am. Bull. 120, 142–155. https://doi.org/10.1130/B26224.1

Foster, D.A., Gleadow, A.J.W., Mortimer, G., 1994. Rapid Pliocene exhumation in the Karakoram (Pakistan), revealed by fission-track thermochronology of the K2 gneiss. Geol. Boulder 22, 19–22. https://doi.org/10.1130/0091-7613(1994)022<0019:RPEITK>2.3.CO;2

Fox, M., Herman, F., Willett, S.D., May, D.A., 2014. A linear inversion method to infer exhumation rates in space and time from thermochronometric data. Earth Surf. Dyn. 2, 47–65. https://doi.org/10.5194/esurf-2-47-2014

France-Lanord, C., Spiess, V., Klaus, A., Schwenk, T., Adhikari, R.R., Adhikari, S.K., Bahk, J.-J., Baxter, A.T., Cruz, J.W., Das, S.K., Dekens, P., Duleba, W., Fox, L.R., Galy, A., Galy, V., Ge Junyi, Gleason, J.D., Gyawali, B.R., Huyghe, P., Jia Guodong, Lantzsch, H., Manoj, M.C., Martin, Y.M., Meynadier, L., Najman, Y.M.R., Nakajima, A., Ponton, C., Reilly, B.T., Rogers, K.G., Savian, J.F., Selkin, P.A., Weber, M.E., Williams, T., Yoshida, K., 2016. Expedition 354 summary. Proc. Int. Ocean Discov. Program Exped. Rep. 354, 35. https://doi.org/10.14379/iodp.proc.354.101.2016

Gallagher, K., 2012. Transdimensional inverse thermal history modeling for quantitative thermochronology: TRANSDIMENSIONAL INVERSE THERMAL HISTORY. J. Geophys. Res. Solid Earth 117, n/a-n/a. https://doi.org/10.1029/2011JB008825

Gansser, A., 1983. Geology of the Bhutan Himalaya. Denkschr. Schweiz. Naturforschenden Ges. Memoires Soc. Helvetiques Sci. Nat. 96, 181.

Gansser, A., 1964. The geology of the Himalayas, The geology of the Himalayas.

Garver, J.I., Brandon, M.T., Roden-Tice, M., Kamp, P.J.J., 1999. Exhumation history of orogenic highlands determined by detrital fission-track thermochronology. Geol. Soc. Lond. Spec. Publ. 154, 283–304. https://doi.org/10.1144/GSL.SP.1999.154.01.13

Garzanti, E., Baud, A., Mascle, G., Anonymous, 1987. Sedimentary record of the northward flight of India and its collision with Eurasia (Ladakh Himalaya, India). Geodin. Acta 1, 297–312.

Gasse, F., Derbyshire, E., 1996. Environmental changes in the Tibetan Plateau and surrounding areas — Preface. Palaeogeogr. Palaeoclimatol. Palaeoecol. 120, 1–3. https://doi.org/10.1016/0031-0182(95)00030-5

Gautam, P., Koshimizu, S., 1991. Zircon & apatite fission track dating of the Ampipal alkaline massif, the Nepal Lesser Himalaya. J. Nepal Geol. Soc. 7, 1–8.

Gavillot, Y., Meigs, A.J., Sousa, F.J., Stockli, D., Yule, D., Malik, M., 2018. Late Cenozoic Foreland-to-Hinterland Low-Temperature Exhumation History of the Kashmir Himalaya. Tectonics 37, 3041–3068. https://doi.org/10.1029/2017TC004668

Ge, Y., Li, Y., Wang, X., Qian, X., Zhang, J., Zhou, A., Liu-Zeng, J., 2018. Oligocene-Miocene burial and exhumation of the southernmost Gangdese mountains from sedimentary and thermochronological evidence. Tectonophysics 723, 68–80. https://doi.org/10.1016/j.tecto.2017.12.003

Ge, Y.-K., Dai, J.-G., Wang, C.-S., Li, Y.-L., Xu, G.-Q., Danisik, M., 2017. Cenozoic thermo-tectonic evolution of the Gangdese batholith constrained by low-temperature thermochronology. Gondwana Res. 41, 451–462. https://doi.org/10.1016/j.gr.2016.05.006

Gehrels, G., Kapp, P., DeCelles, P., Pullen, A., Blakey, R., Weislogel, A., Ding, L., Guynn, J., Martin, A., McQuarrie, N., Yin, A., 2011. Detrital zircon geochronology of pre-Tertiary strata in the Tibetan-Himalayan orogen: TIBETAN-HIMALAYAN DETRITAL ZIRCONS. Tectonics 30, n/a-n/a. https://doi.org/10.1029/2011TC002868

Gehrels, G.E., DeCelles, P.G., Ojha, T.P., Upreti, B.N., 2006a. Geologic and U-Th-Pb geochronologic evidence for early Paleozoic tectonism in the Kathmandu thrust sheet, central Nepal Himalaya. Geol. Soc. Am. Bull. 118, 185–198. https://doi.org/10.1130/B25753.1

Gehrels, G.E., DeCelles, P.G., Ojha, T.P., Upreti, B.N., 2006b. Geologic and U–Pb geochronologic evidence for early Paleozoic tectonism in the Dadeldhura thrust sheet, far-west Nepal Himalaya. J. Asian Earth Sci. 28, 385–408. https://doi.org/10.1016/j.jseaes.2005.09.012

Gehrels, G.E., Valencia, V.A., Ruiz, J., 2008. Enhanced precision, accuracy, efficiency, and spatial resolution of U-Pb ages by laser ablation-multicollector-inductively coupled plasma-mass spectrometry: TECHNICAL BRIEF. Geochem. Geophys. Geosystems 9, n/a-n/a. https://doi.org/10.1029/2007GC001805

Ghoshal, S., McQuarrie, N., Robinson, D.M., Adhikari, D.P., Morgan, L.E., Ehlers, T.A., 2020. Constraining Central Himalayan (Nepal) Fault Geometry Through Integrated Thermochronology and Thermokinematic Modeling. Tectonics 39. https://doi.org/10.1029/2020TC006399

Godin, L., Parrish, R.R., Brown, R.L., Hodges, K.V., 2001. Crustal thickening leading to exhumation of the Himalayan Metamorphic core of central Nepal: Insight from U-Pb Geochronology and ^{40}Ar/^{39}Ar Thermochronology. Tectonics 20, 729–747. https://doi.org/10.1029/2000TC001204

Gong Junfeng, Ji Jianqing, Han Baofu, Chen, J., Sun Dongxia, Li, B., Zhou, J., Tu Jiyao, Dalai, Z., 2012. Early subduction-exhumation and late channel flow of the Greater Himalayan Sequence; implications from the Yadong section in the eastern Himalaya. Int. Geol. Rev. 54, 1184–1202. https://doi.org/10.1080/00206814.2011.626604

Gourbet, L., Mahéo, G., Shuster, D.L., Tripathy-Lang, A., Leloup, P.H., Paquette, J.-L., 2016. River network evolution as a major control for orogenic exhumation: Case study from the western Tibetan plateau. Earth Planet. Sci. Lett. 456, 168–181. https://doi.org/10.1016/j.epsl.2016.09.037

Govin, G., van der Beek, P., Najman, Y., Millar, I., Gemignani, L., Huyghe, P., Dupont-Nivet, G., Bernet, M., Mark, C., Wijbrans, J., 2020. Early onset and late acceleration of rapid exhumation in the Namche Barwa syntaxis, eastern Himalaya. Geology 48, 1139–1143. https://doi.org/10.1130/G47720.1

Grujic, D., Ashley, K.T., Coble, M.A., Coutand, I., Kellett, D.A., Larson, K.P., Whipp, D.M., Gao, M., Whynot, N., 2020. Deformational Temperatures Across the Lesser Himalayan Sequence in Eastern Bhutan and Their Implications for the Deformation History of the Main Central Thrust. Tectonics 39. https://doi.org/10.1029/2019TC005914

Grujic, D., Coutand, I., Bookhagen, B., Bonnet, S., Blythe, A., Duncan, C., 2006. Climatic forcing of erosion, landscape, and tectonics in the Bhutan Himalayas. Geol. Boulder 34, 801–804. https://doi.org/10.1130/G22648.1

Guenthner, W.R., Reiners, P.W., Ketcham, R.A., Nasdala, L., Giester, G., 2013. Helium diffusion in natural zircon: Radiation damage, anisotropy, and the interpretation of zircon (U-Th)/He thermochronology. Am. J. Sci. 313, 145–198. https://doi.org/10.2475/03.2013.01

Guillot, S., Pecher, A., Le Fort, P., Anonymous, 1994. Comparison of the emplacement of some High-Himalayan leucogranites (Mugu-Mustang, Manaslu and Kula-Kangri). J. Nepal Geol. Soc. 10, Special issue, 61.

Guo, Z., Wilson, M., 2012. The Himalayan leucogranites: Constraints on the nature of their crustal source region and geodynamic setting. Gondwana Res. 22, 360–376. https://doi.org/10.1016/j.gr.2011.07.027

Haider, V.L., Dunkl, I., von Eynatten, H., Ding, L., Frei, D., Zhang, L., 2013. Cretaceous to Cenozoic evolution of the northern Lhasa Terrane and the early Paleogene development of peneplains at Nam Co, Tibetan Plateau. J. Asian Earth Sci. 70–71, 79–98. https://doi.org/10.1016/j.jseaes.2013.03.005

Haproff, P.J., Odlum, M.L., Zuza, A.V., Yin, A., Stockli, D.F., 2020. Structural and thermochronologic constraints on the Cenozoic tectonic development of the northern Indo-Burma Ranges. Tectonics 39, Article e2020TC006231. https://doi.org/10.1029/2020TC006231

Hein, C.J., Galy, V., Galy, A., France-Lanord, C., Kudrass, H., Schwenk, T., 2017. Post-glacial climate forcing of surface processes in the Ganges–Brahmaputra river basin and implications for carbon sequestration. Earth Planet. Sci. Lett. 478, 89–101. https://doi.org/10.1016/j.epsl.2017.08.013

Herman, F., Copeland, P., Avouac, J.-P., Bollinger, L., Mahéo, G., Le Fort, P., Rai, S., Foster, D., Pêcher, A., Stüwe, K., Henry, P., 2010. Exhumation, crustal deformation, and thermal structure of the Nepal Himalaya derived from the inversion of thermochronological and thermobarometric data and modeling of the topography. J. Geophys. Res. 115, B06407. https://doi.org/10.1029/2008JB006126

Herman, F., Seward, D., Valla, P.G., Carter, A., Kohn, B., Willett, S.D., Ehlers, T.A., 2013. Worldwide acceleration of mountain erosion under a cooling climate. Nature 504, 423–426. https://doi.org/10.1038/nature12877

Hetzel, R., Dunkl, I., Haider, V., Strobl, M., von Eynatten, H., Ding, L., Frei, D., 2011. Peneplain formation in southern Tibet predates the India-Asia collision and plateau uplift. Geol. Boulder 39, 983–986. https://doi.org/10.1130/G32069.1

Hodges, K.V., Bowring, S.A., Davidek, K.L., Hawkins, D., Krol, M., 1998. Evidence for rapid displacement on Himalayan normal faults and the importance of tectonic denudation in the evolution of mountain ranges. Geol. Boulder 26, 483–486. https://doi.org/10.1130/0091-7613(1998)026<0483:EFRDOH>2.3.CO;2

Hodges, K.V., Hames, W.E., Olszewski, W., Burchfiel, B.C., Royden, L.H., Chen, Z., 1994. Thermobarometric and (super 40) Ar/ (super 39) Ar geochronologic constraints on Eohimalayan metamorphism in the Dinggye area, southern Tibet. Contrib. Mineral. Petrol. 117, 151–163.

Hourigan, J.K., Reiners, P.W., Brandon, M.T., 2005. U-Th zonation-dependent alpha-ejection in (U-Th)/He chronometry. Geochim. Cosmochim. Acta 69, 3349–3365. https://doi.org/10.1016/j.gca.2005.01.024

Hu, X., Garzanti, E., Wang, J., Huang, W., An, W., Webb, A., 2016. The timing of India-Asia collision onset – Facts, theories, controversies. Earth-Sci. Rev. 160, 264–299. https://doi.org/10.1016/j.earscirev.2016.07.014

Hu, X.-M., Garzanti, E., An, W., Hu, X.-F., 2015. Provenance and drainage system of the Early Cretaceous volcanic detritus in the Himalaya as constrained by detrital zircon geochronology. J. Palaeogeogr. 4, 85–98. https://doi.org/10.3724/SP.J.1261.2015.00069

Huntington, K.W., Blythe, A.E., Hodges, K.V., 2006. Climate change and Late Pliocene acceleration of erosion in the Himalaya. Earth Planet. Sci. Lett. 252, 107–118. https://doi.org/10.1016/j.epsl.2006.09.031

Huyghe, P., Bernet, M., Galy, A., Naylor, M., Cruz, J., Gyawali, B.R., Gemignani, L., Mugnier, J.-L., 2020. Rapid exhumation since at least 13 Ma in the Himalaya recorded by detrital apatite

fission-track dating of Bengal fan (IODP Expedition 354) and modern Himalayan river sediments. Earth Planet. Sci. Lett. 534, 116078. https://doi.org/10.1016/j.epsl.2020.116078

Jain, A.K., Kumar, D., Singh, S., Kumar, A., Lal, N., 2000. Timing, quantification and tectonic modelling of Pliocene-Quaternary movements in the NW Himalaya; evidence from fission track dating. Earth Planet. Sci. Lett. 179, 437–451. https://doi.org/10.1016/S0012-821X(00)00133-3

Jepson, G., Carrapa, B., Gillespie, J., Feng, R., DeCelles, P.G., Kapp, P., Tabor, C.R., Zhu, J., 2021. Climate as the Great Equalizer of Continental-Scale Erosion. Geophys. Res. Lett. 48. https://doi.org/10.1029/2021GL095008

Jessup, M.J., Langille, J.M., Diedesch, T.F., Cottle, J.M., 2019. Gneiss Dome Formation in the Himalaya and southern Tibet. Geol. Soc. Lond. Spec. Publ. 483, 401–422. https://doi.org/10.1144/SP483.15

Ji, W.-Q., Wu, F.-Y., Chung, S.-L., Li, J.-X., Liu, C.-Z., 2009. Zircon U–Pb geochronology and Hf isotopic constraints on petrogenesis of the Gangdese batholith, southern Tibet. Chem. Geol. 262, 229–245. https://doi.org/10.1016/j.chemgeo.2009.01.020

Jia Dong, Li, Y., Yan, B., Li, Z., Wang Maomao, Chen Zhuxin, Zhang, Y., Chen, H., Xia Qunke, Xu Yixian, 2020. The Cenozoic thrusting sequence of the Longmen Shan fold-and-thrust belt, eastern margin of the Tibetan Plateau; insights from low-temperature thermochronology. J. Asian Earth Sci. 198, Article 104381. https://doi.org/10.1016/j.jseaes.2020.104381

Jolivet, M., Brunel, M., Seward, D., Xu, Z., Yang, J., Roger, F., Tapponnier, P., Malavieille, J., Arnaud, N., Wu, C., 2001. Mesozoic and Cenozoic tectonics of the northern edge of the Tibetan plateau: fission-track constraints. Tectonophysics 343, 111–134. https://doi.org/10.1016/S0040-1951(01)00196-2

Kang, W., Xu Xiwei, Yu, G., Tan Xibin, Kang, L., Luo Jiahong, Zhang, W., 2019. Differential late-Cenozoic uplift across the Dongjiu-Milin fault zone in the eastern Himalayan Syntaxis revealed by low-temperature thermochronology. J. Asian Earth Sci. 179, 189–199. https://doi.org/10.1016/j.jseaes.2019.04.022

Kapp, J.L.D., 2005. Nyainqentanglha Shan: A window into the tectonic, thermal, and geochemical evolution of the Lhasa block, southern Tibet. J. Geophys. Res. 110, B08413. https://doi.org/10.1029/2004JB003330

Kapp, P., DeCelles, P.G., 2019. Mesozoic–Cenozoic geological evolution of the Himalayan-Tibetan orogen and working tectonic hypotheses. Am. J. Sci. 319, 159–254. https://doi.org/10.2475/03.2019.01

Kellett, D.A., Grujic, D., Coutand, I., Cottle, J., Mukul, M., 2013. The South Tibetan detachment system facilitates ultra rapid cooling of granulite-facies rocks in Sikkim Himalaya: S. TIBETAN DETACHMENT, SIKKIM HIMALAYA. Tectonics 32, 252–270. https://doi.org/10.1002/tect.20014

Ketcham, R.A., 2005. Forward and Inverse Modeling of Low-Temperature Thermochronometry Data. Rev. Mineral. Geochem. 58, 275–314. https://doi.org/10.2138/rmg.2005.58.11

Khanal, S., 2014. Structural and kinematic evolution of the Himalayan thrust belt, central Nepal (Ph.D.). ProQuest Diss. Theses. The University of Alabama, Ann Arbor.

Kirby, E., Reiners, P.W., Krol, M.A., Whipple, K.X., Hodges, K.V., Farley, K.A., Tang, W., Chen, Z., 2002. Late Cenozoic evolution of the eastern margin of the Tibetan Plateau: Inferences from ^{40} Ar/ ^{39} Ar and (U-Th)/He thermochronology: LATE CENOZOIC EVOLUTION OF EASTERN TIBET. Tectonics 21, 1-1-1–20. https://doi.org/10.1029/2000TC001246

Kirstein, L.A., Foeken, J.P.T., van der Beek, P., Stuart, F.M., Phillips, R.J., 2009. Cenozoic unroofing history of the Ladakh Batholith, western Himalaya, constrained by thermochronology and numerical modelling. J. Geol. Soc. 166, 667–678. https://doi.org/10.1144/0016-76492008-107

Kirstein, L.A., Sinclair, H., Stuart, F.M., Dobson, K., 2006. Rapid early Miocene exhumation of the Ladakh batholith, western Himalaya. Geology 34, 1049. https://doi.org/10.1130/G22857A.1

Kohn, M.J., Paul, S.K., Corrie, S.L., 2009. The lower Lesser Himalayan sequence: A Paleoproterozoic arc on the northern margin of the Indian plate. GSA Bull. 122, 323–335. https://doi.org/10.1130/B26587.1

Krishna, K.S., Ismaiel, M., Srinivas, K., Gopala Rao, D., Mishra, J., Saha, D., 2016. Sediment Pathways and Emergence of Himalayan Source Material in the Bay of Bengal. Curr. Sci. 110, 363. https://doi.org/10.18520/cs/v110/i3/363-372

Kuiper, N.H., 1960. Tests concerning random points on a circle. Indag. Math. Proc. 63, 38–47. https://doi.org/10.1016/S1385-7258(60)50006-0

Kumar, A., Lal, N., Jain, A.K., Sorkhabi, R.B., 1995. Late Cenozoic-Quaternary thermo-tectonic history of Higher Himalayan Crystalline (HHC) in Kishtwar-Padar-Zanskar region, NW Himalaya; evidence from fission track ages. J. Geol. Soc. India 45, 375–391.

Lai, Q., Ding, L., Wang, H., Yue, Y., Cai, F., 2007. Constraining the stepwise migration of the eastern Tibetan Plateau margin by apatite fission track thermochronology. Sci. China Ser. Earth Sci. 50, 172–183. https://doi.org/10.1007/s11430-007-2048-7

Lal, N., Mehta, Y.P., Kumar, D., Kumar, A., Jain, A.K., Manickavasagam, R.M., 1999. Cooling and exhumation history of the Mandi Granite and adjoining tectonic units, Himachal Pradesh, and estimation of closure temperature from external surface of zircon. Gondwana Res. Group Mem. 6, 207–216.

Lama Sherpa, T., DeCelles, P.G., Carrapa, B., Anonymous, 2019. Exhumation history of the Bhumichula Plateau; a relict low relief surface in the Himalayan thrust belt of Nepal? Abstr. Programs - Geol. Soc. Am. 51, Abstract no. 283-10.

Landry, K.R., Coutand, I., Whipp, D.M., Grujic, D., Hourigan, J.K., 2016a. Late Neogene tectonically driven crustal exhumation of the Sikkim Himalaya: Insights from inversion of multithermochronologic data: Neogene Tectonics of the Sikkim Himalaya. Tectonics 35, 833–859. https://doi.org/10.1002/2015TC004102

Landry, K.R., Coutand, I., Whipp, D.M., Grujic, D., Hourigan, J.K., 2016b. Late Neogene tectonically driven crustal exhumation of the Sikkim Himalaya: Insights from inversion of multithermochronologic data: Neogene Tectonics of the Sikkim Himalaya. Tectonics 35, 833–859. https://doi.org/10.1002/2015TC004102

Lang, K.A., Huntington, K.W., 2014. Antecedence of the Yarlung–Siang–Brahmaputra River, eastern Himalaya. Earth Planet. Sci. Lett. 397, 145–158. https://doi.org/10.1016/j.epsl.2014.04.026

Lang, K.A., Huntington, K.W., Burmester, R., Housen, B., 2016. Rapid exhumation of the eastern Himalayan syntaxis since the late Miocene. Geol. Soc. Am. Bull. 128, 1403–1422. https://doi.org/10.1130/B31419.1

Laskowski, A.K., Kapp, P., Cai, F., 2018. Gangdese culmination model: Oligocene–Miocene duplexing along the India-Asia suture zone, Lazi region, southern Tibet. GSA Bull. 130, 1355–1376. https://doi.org/10.1130/B31834.1

Laskowski, A.K., Kapp, P., Ding, L., Campbell, C., Liu, X., 2017. Tectonic evolution of the Yarlung suture zone, Lopu Range region, southern Tibet: India-Asia Suture Tectonics, Lopu Range. Tectonics 36, 108–136. https://doi.org/10.1002/2016TC004334

Le Fort, P., 1975. Himalayas; the collided range; present knowledge of the continental arc. Am. J. Sci. Vol. 275-A, 1–44.

Leary, R.J., DeCelles, P.G., Quade, J., Gehrels, G.E., Waanders, G., 2016. The Liuqu Conglomerate, southern Tibet: Early Miocene basin development related to deformation within the Great Counter Thrust system. Lithosphere 8, 427–450. https://doi.org/10.1130/L542.1

Lee, J., Hacker, B.R., Dinklage, W.S., Wang, Y., Gans, P., Calvert, A., Wan, J., Chen, W., Blythe, A.E., McClelland, W., 2000. Evolution of the Kangmar Dome, southern Tibet: Structural, petrologic, and thermochronologic constraints. Tectonics 19, 872–895. https://doi.org/10.1029/1999TC001147

Li, G., Kohn, B., Sandiford, M., Xu, Z., 2017. India-Asia convergence: Insights from burial and exhumation of the Xigaze fore-arc basin, south Tibet. J. Geophys. Res. Solid Earth 122, 3430–3449. https://doi.org/10.1002/2017JB014080

Li, G., Kohn, B., Sandiford, M., Xu, Z., Tian, Y., Seiler, C., 2016. Synorogenic morphotectonic evolution of the Gangdese batholith, South Tibet: Insights from low-temperature thermochronology: EXHUMATION OF GANGDESE BATHOLITH. Geochem. Geophys. Geosystems 17, 101–112. https://doi.org/10.1002/2015GC006047

Li, G., Kohn, B.P., Sandiford, M., Ma Zeliang, Xu Zhiqin, 2018. Post-collisional exhumation of the Indus-Yarlung suture zone and northern Tethyan Himalaya, Saga, SW Tibet. Gondwana Res. 64, 1–10. https://doi.org/10.1016/j.gr.2018.06.006

Li, G., Tian, Y., Kohn, B.P., Sandiford, M., Xu Zhiqin, Cai Zhihui, 2015. Cenozoic low temperature cooling history of the northern Tethyan Himalaya in Zedang, SE Tibet and its implications. Tectonophysics 643, 80–93. https://doi.org/10.1016/j.tecto.2014.12.014

Li, H.-A., Dai, J.-G., Xu, S.-Y., Liu, B.-R., Han, X., Wang, Y.-N., Wang, C.-S., 2019. The formation and expansion of the eastern Proto-Tibetan Plateau: Insights from low-temperature thermochronology. J. Asian Earth Sci. 183, 103975. https://doi.org/10.1016/j.jseaes.2019.103975

Lindhorst, S., Betzler, C., Kroon, D., 2019. Wind variability over the northern Indian Ocean during the past 4 million years – Insights from coarse aeolian dust (IODP exp. 359, site U1467, Maldives). Palaeogeogr. Palaeoclimatol. Palaeoecol. 536, 109371. https://doi.org/10.1016/j.palaeo.2019.109371

Liu, L., Zhu, D.-C., Wang, Q., Cawood, P.A., Stockli, D.F., Stockli, L.D., Lin, C., Zhang, J.-J., Zhang, L.-L., Zhao, Z.-D., 2022. Leucogranite Records Multiple Collisional Orogenies. Geophys. Res. Lett. 49, e2021GL096817. https://doi.org/10.1029/2021GL096817

Long, S.P., McQuarrie, N., Tobgay, T., Coutand, I., Cooper, F.J., Reiners, P.W., Wartho, J.-A., Hodges, K., Anonymous, 2012. Variable shortening rates in the Bhutan thrust belt; implications for strain partitioning in the eastern Himalayan-Tibetan orogenic system. Am. Geophys. Union Fall Meet. 2012, Abstract T51F-2661.

Long, S.P., McQuarrie, N., Tobgay, T., Reiners, P.W., Anonymous, 2010. Preliminary timing constraints on Lesser Himalayan duplex development from zircon (U-Th)/He thermochronometry, eastern Bhutan. Abstr. Programs - Geol. Soc. Am. 42, 665.

Long, S.P., Robinson, D.M., 2021. Construction of the Lesser Himalayan–Subhimalayan thrust belt: The primary driver of thickening, exhumation, and high elevations in the Himalayan orogen since the middle Miocene. Geology 49, 1283–1288. https://doi.org/10.1130/G48967.1

Lu, L., Zhao, Z., Wu Zhenhan, Cheng, Q., Ye Peisheng, 2015. Fission track thermochronology evidence for the Cretaceous and Paleogene tectonic event of Nyainrong Microcontinent, Tibet. Acta Geol. Sin. Engl. Ed. 89, 133–144. https://doi.org/10.1111/1755-6724.12400

Lupker, M., Lavé, J., France-Lanord, C., Christl, M., Bourlès, D., Carcaillet, J., Maden, C., Wieler, R., Rahman, M., Bezbaruah, D., Xiaohan, L., 2017. ¹⁰Be systematics in the Tsangpo-Brahmaputra catchment: the cosmogenic nuclide legacy of the eastern Himalayan syntaxis. Earth Surf. Dyn. 5, 429–449. https://doi.org/10.5194/esurf-5-429-2017

Macfarlane, A.M., 1993. Chronology of tectonic events in the crystalline core of the Himalaya, Langtang National Park, central Nepal. Tectonics 12, 1004–1025. https://doi.org/10.1029/93TC00916

Macfarlane, A.M., Hodges, K.V., Lux, D., 1992. A structural analysis of the Main Central Thrust zone, Langtang National Park, central Nepal Himalaya. Geol. Soc. Am. Bull. 104, 1389–1402. https://doi.org/10.1130/0016-7606(1992)104<1389:ASAOTM>2.3.CO;2

Malusà, M.G., Fitzgerald, P.G., 2020. The geologic interpretation of the detrital thermochronology record within a stratigraphic framework, with examples from the European Alps, Taiwan and the Himalayas. Earth-Sci. Rev. 201, 103074. https://doi.org/10.1016/j.earscirev.2019.103074

Maluski, H., Matte, P., Brunel, M., Xiao Xusheng, 1988. Argon 39 - argon 40 dating of metamorphic and plutonic events in the North and High Himalaya belts (southern Tibet, China). Tectonics 7, 299–326. https://doi.org/10.1029/TC007i002p00299

Maluski, H., Proust, F., Xiao, X.C., 1982. 39Ar/40 Ar dating of the trans-Himalayan calc-alkaline magmatism of southern Tibet. Nature 298, 152–154. https://doi.org/10.1038/298152a0

Mamani, M., Worner, G., Sempere, T., 2010. Geochemical variations in igneous rocks of the Central Andean orocline (13 S to 18 S): Tracing crustal thickening and magma generation through time and space. Geol. Soc. Am. Bull. 122, 162–182. https://doi.org/10.1130/B26538.1

Mason, C.C., Romans, B.W., Stockli, D.F., Mapes, R.W., Fildani, A., 2019. Detrital zircons reveal sea-level and hydroclimate controls on Amazon River to deep-sea fan sediment transfer. Geology 47, 563–567. https://doi.org/10.1130/G45852.1

McCallister, A.T., Taylor, M.H., Murphy, M.A., Styron, R.H., Stockli, D.F., 2014. Thermochronologic constraints on the late Cenozoic exhumation history of the Gurla Mandhata metamorphic core complex, Southwestern Tibet: GURLA MANDHATA, SW TIBET. Tectonics 33, 27–52. https://doi.org/10.1002/2013TC003302

McDermott, J.A., Hodges, K.V., Whipple, K.X., Soest, M.C. van, HurtadoJr., and J.M., 2015. Evidence for Pleistocene Low-Angle Normal Faulting in the Annapurna-Dhaulagiri Region, Nepal. J. Geol. 123, 133–151.

McQuarrie, N., Eizenhöfer, P.R., Long, S.P., Tobgay, T., Ehlers, T.A., Blythe, A.E., Morgan, L.E., Gilmore, M.E., Dering, G.M., 2019. The Influence of Foreland Structures on Hinterland Cooling: Evaluating the Drivers of Exhumation in the Eastern Bhutan Himalaya. Tectonics 38, 3282–3310. https://doi.org/10.1029/2018TC005340

McQuarrie, N., Tobgay, T., Long, S.P., Reiners, P.W., Cosca, M.A., 2014. Variable exhumation rates and variable displacement rates: Documenting recent slowing of Himalayan shortening in western Bhutan. Earth Planet. Sci. Lett. 386, 161–174. https://doi.org/10.1016/j.epsl.2013.10.045

Metcalfe, R.P., Treloar, P.J., Searle, M.P., 1993. Pressure, temperature and time constraints on metamorphism across the Main Central Thrust zone and high Himalayan slab in the Garhwal Himalaya. Geol. Soc. Spec. Publ. 74, 485–509.

Meyer, N.R., Garver, J.I., Anonymous, 2000. Zircon fission-track fingerprint of major tributaries to the Mississippi River. Abstr. Programs - Geol. Soc. Am. 32, 59.

Molnar, P., England, P., Martinod, J., 1993. Mantle dynamics, uplift of the Tibetan Plateau, and the Indian monsoon. Rev. Geophys. 31, 357–396. https://doi.org/10.1029/93RG02030

Morell, K.D., Sandiford, M., Kohn, B., Codilean, A., Fülöp, R.-H., Ahmad, T., 2017. Current strain accumulation in the hinterland of the northwest Himalaya constrained by landscape analyses, basin-wide denudation rates, and low temperature thermochronology. Tectonophysics 721, 70–89. https://doi.org/10.1016/j.tecto.2017.09.007

Nadin, E.S., Martin, A.J., 2012. Apatite thermochronometry within a knickzone near the Higher Himalaya front, central Nepal: No resolvable fault motion in the past one million years: APATITE THERMOCHRONOMETRY, CENTRAL NEPAL. Tectonics 31, n/a-n/a. https://doi.org/10.1029/2011TC003000

Najman, Y., Bickle, M., BouDagher-Fadel, M., Carter, A., Garzanti, E., Paul, M., Wijbrans, J., Willett, E., Oliver, G., Parrish, R., Akhter, S.H., Allen, R., Ando, S., Chisty, E., Reisberg, L., Vezzoli, G., 2008. The Paleogene record of Himalayan erosion: Bengal Basin, Bangladesh. Earth Planet. Sci. Lett. 273, 1–14. https://doi.org/10.1016/j.epsl.2008.04.028

Najman, Y., Mark, C., Barfod, D.N., Carter, A., Parrish, R., Chew, D., Gemignani, L., 2019. Spatial and temporal trends in exhumation of the Eastern Himalaya and syntaxis as determined from a multitechnique detrital thermochronological study of the Bengal Fan. GSA Bull. 131, 1607–1622. https://doi.org/10.1130/B35031.1

Nakajima, T., Kawakami, T., Iwano, H., Danhara, T., Sakai, H., 2022. Denudation Process of Crystalline Nappes in a Continental Collision Zone Constrained by Inversion of Fission-Track Data and Thermokinematic Forward Modeling: An Example From Eastern Nepalese Himalaya. J. Geophys. Res. Solid Earth 127. https://doi.org/10.1029/2021JB023630

Orme, D.A., 2019. Burial and exhumation history of the Xigaze forearc basin, Yarlung suture zone, Tibet. Geosci. Front. 10, 895–908. https://doi.org/10.1016/j.gsf.2017.11.011

Orme, D.A., Carrapa, B., Kapp, P., 2015a. Sedimentology, provenance and geochronology of the upper Cretaceous-lower Eocene western Xigaze forearc basin, southern Tibet. Basin Res. 27, 387–411. https://doi.org/10.1111/bre.12080

Orme, D.A., Laskowski, A.K., Zilinsky, M.F., Chao, W., Guo, X., Cai, F., Lin, D., 2021. Sedimentology and provenance of newly identified Upper Cretaceous trench basin strata, Dênggar, southern Tibet: Implications for development of the Eurasian margin prior to India–Asia collision. Basin Res. 33, 1454–1473. https://doi.org/10.1111/bre.12521

Orme, D.A., Reiners, P.W., Hourigan, J.K., Carrapa, B., 2015b. Effects of inherited cores and magmatic overgrowths on zircon (U-Th)/He ages and age-eU trends from Greater Himalayan sequence rocks, Mount Everest region, Tibet: EFFECTS OF ZONATION ON AGE-EU TRENDS. Geochem. Geophys. Geosystems 16, 2499–2507. https://doi.org/10.1002/2015GC005818

Ouimet, W., Whipple, K., Royden, L., Reiners, P., Hodges, K., Pringle, M., 2010. Regional incision of the eastern margin of the Tibetan Plateau. Lithosphere 2, 50–63. https://doi.org/10.1130/L57.1

Parrish, R.R., Hodges, V., 1996. Isotopic constraints on the age and provenance of the Lesser and Greater Himalayan sequences, Nepalese Himalaya. Geol. Soc. Am. Bull. 108, 904–911. https://doi.org/10.1130/0016-7606(1996)108<0904:ICOTAA>2.3.CO;2

Patel, R.C., Adlakha, V., Singh, P., Kumar, Y., Lal, N., 2011. Geology, structural and exhumation history of the Higher Himalayan Crystallines in Kumaon Himalaya, India. J. Geol. Soc. India 77, 47–72. https://doi.org/10.1007/s12594-011-0008-5

Patel, R.C., Carter, A., 2009. Exhumation history of the Higher Himalayan Crystalline along Dhauliganga-Goriganga river valleys, NW India: New constraints from fission track analysis: EXHUMATION HISTORY OF KUMAON HIMALAYA. Tectonics 28, n/a-n/a. https://doi.org/10.1029/2008TC002373

Patel, R.C., Kumar, Y., Lal, N., Kumar, A., Arita, K., Yin, A., Singh, S., Okada, H., 2007. Thermotectonic history of the Chiplakot crystalline belt in the Lesser Himalaya, Kumaon, India; constraints from apatite fission-track thermochronology. J. Asian Earth Sci. 29, 430–439. https://doi.org/10.1016/j.jseaes.2006.04.008

Patel, R.C., Singh, P., Lal, N., 2015. Thrusting and back-thrusting as post-emplacement kinematics of the Almora klippe: Insights from Low-temperature thermochronology. Tectonophysics 653, 41–51. https://doi.org/10.1016/j.tecto.2015.03.025

Pebam, J., Adlakha, V., Jain, A.K., Patel, R.C., Lal, N., Singh, S., Kumar, R., Devrani, R., 2021. Apatite and zircon fission-track thermochronology constraining the interplay between tectonics, topography and exhumation, Arunachal Himalaya. J. Earth Syst. Sci. 130, 178. https://doi.org/10.1007/s12040-021-01667-2

Piccolo, A., Faccenda, M., Carosi, R., Montomoli, C., Visonà, D., 2018. Crustal strength control on structures and metamorphism in collisional orogens. Tectonophysics 746, 470–492. https://doi.org/10.1016/j.tecto.2017.09.018

Puniya, M.K., Patel, R.C., Pant, P.D., 2019. Structural and thermochronological studies of the Almora klippe, Kumaun, NW India: implications for crustal thickening and exhumation of the NW Himalaya. Geol. Soc. Lond. Spec. Publ. 481, 81–110. https://doi.org/10.1144/SP481-2017-74

Qin, Q., Huang, H., Wang, T., Guo, R., Zhang, Z., Tong, Y., 2016. Relationship of the Tarim Craton to the Central Asian Orogenic Belt: insights from Devonian intrusions in the northern margin of Tarim Craton, China. Int. Geol. Rev. 58, 2007–2028. https://doi.org/10.1080/00206814.2016.1199289

Rai, S.P., Noble, J., Singh, D., Rawat, Y.S., Kumar, B., 2021. Spatiotemporal variability in stable isotopes of the Ganga River and factors affecting their distributions. CATENA 204, 105360. https://doi.org/10.1016/j.catena.2021.105360

Raymo, M.E., Ruddiman, W.F., 1992. Tectonic forcing of late Cenozoic climate. Nat. Lond. 359, 117–122.

Raymo, M.E., Tsuchi, R., Ingle, J.C., Jr, 1992. Late Cenozoic evolution of global climate, Pacific Neogene; environment, evolution, and events. University of Tokyo Press.

Reid, A.J., Fowler, A.P., Phillips, D., Wilson, C.J.L., 2005. Thermochronology of the Yidun Arc, central eastern Tibetan Plateau: constraints from 40Ar/39Ar K-feldspar and apatite fission track data. J. Asian Earth Sci. 25, 915–935. https://doi.org/10.1016/j.jseaes.2004.09.002

Reiners, P.W., 2005. (U-Th)/(He-Pb) double dating of detrital zircons. Am. J. Sci. 305, 259–311. https://doi.org/10.2475/ajs.305.4.259

Reiners, P.W., Ehlers, T.A., Mitchell, S.G., Montgomery, D.R., 2003. Coupled spatial variations in precipitation and long-term erosion rates across the Washington Cascades. Nature 426, 645–7. https://doi.org/10.1038/nature02111

Reiners, P.W., Spell, T.L., Nicolescu, S., Zanetti, K.A., 2004. Zircon (U-Th)/He thermochronometry: He diffusion and comparisons with 40Ar/39Ar dating. Geochim. Cosmochim. Acta 68, 1857–1887. https://doi.org/10.1016/j.gca.2003.10.021

Robert, X., van der Beek, P., Braun, J., Perry, C., Dubille, M., Mugnier, J.-L., 2009. Assessing Quaternary reactivation of the Main Central thrust zone (central Nepal Himalaya); new thermochronologic data and numerical modeling. Geol. Boulder 37, 731–734. https://doi.org/10.1130/G25736A.1

Robert, X., van der Beek, P., Braun, J., Perry, C., Mugnier, J.-L., 2011. Control of detachment geometry on lateral variations in exhumation rates in the Himalaya: Insights from low-temperature thermochronology and numerical modeling. J. Geophys. Res. 116, B05202. https://doi.org/10.1029/2010JB007893

Robinson, D.M., DeCelles, P.G., Copeland, P., 2006. Tectonic evolution of the Himalayan thrust belt in western Nepal; implications for channel flow models. Geol. Soc. Am. Bull. 118, 865–885, 1 sheet. https://doi.org/10.1130/B25911.1

Rohrmann, A., Kapp, P., Carrapa, B., Reiners, P.W., Guynn, J., Ding, L., Heizler, M., 2011. Thermochronologic evidence for plateau formation in central Tibet by 45 Ma. Geol. Boulder 40, 187–190. https://doi.org/10.1130/G32530.1

Sakai H., Imayama T., Yoshida K., Asahi K., 2017. Tectonics of the Himalayas. J. Geol. Soc. Jpn. 123, 403–421. https://doi.org/10.5575/geosoc.2017.0026

Sakai, H., Iwano, H., Danhara, T., Hirata, T., Takigami, Y., 2013. Emplacement of hot Lesser Himalayan nappes from 15 to 10 Ma in the Jumla-Surkhet region, western Nepal, and their thermal imprint on the underlying Early Miocene fluvial Dumri Formation: Emplacement of hot Himalayan nappes. Isl. Arc 22, 361–381. https://doi.org/10.1111/iar.12030

Sakai, H., Sawada, M., Takigami, Y., Orihashi, Y., Danhara, T., Iwano, H., Kuwahara, Y., Dong Qi, Cai Huawei, Li, J., Gautam, P., Watanabe, T., Nishi, H., Yasunari, T., 2005. Geology of the summit limestone of Mount Qomolangma (Everest) and cooling history of the Yellow Band under the Qomolangma Detachment. Isl. Arc 14, 297–310.

Salameh, E., Frappart, F., Papa, F., Güntner, A., Venugopal, V., Getirana, A., Prigent, C., Aires, F., Labat, D., Laignel, B., 2017. Fifteen Years (1993–2007) of Surface Freshwater Storage Variability in the Ganges-Brahmaputra River Basin Using Multi-Satellite Observations. Water 9, 245. https://doi.org/10.3390/w9040245

Salvi, D., Mathew, G., Kohn, B., Pande, K., Borgohain, B., 2020. Thermochronological insights into the thermotectonic evolution of Mishmi hills across the Dibang Valley, NE Himalayan Syntaxis. J. Asian Earth Sci. 190. https://doi.org/10.1016/j.jseaes.2019.104158

Sanchez, V.I., Murphy, M.A., Robinson, A.C., Lapen, T.J., Heizler, M.T., Ivanov, A.V. (Ivanov, Aleksei V.)., Deverchere, J., Ernst, R., Gladkochub, D.P., 2013. Tectonic evolution of the India-Asia suture zone since middle Eocene time, Lopukangri area, south-central Tibet. J. Asian Earth Sci. 62, 205–220. https://doi.org/10.1016/j.jseaes.2012.09.004

Sarin, M.M., Krishnaswami, S., Dilli, K., Somayajulu, B.L.K., Moore, W.S., 1989. Major ion chemistry of the Ganga-Brahmaputra river system; weathering processes and fluxes to the Bay of Bengal. Geochim. Cosmochim. Acta 53, 997–1009. https://doi.org/10.1016/0016-7037(89)90205-6

Saylor, J.E., Sundell, K.E., 2016. Quantifying comparison of large detrital geochronology data sets. Geosphere 12, 203–220. https://doi.org/10.1130/GES01237.1

Saylor, J.E., Sundell, K.E., Sharman, G.R., 2019. Characterizing sediment sources by non-negative matrix factorization of detrital geochronological data. Earth Planet. Sci. Lett. 512, 46–58. https://doi.org/10.1016/j.epsl.2019.01.044

Schärer, U., Xu, R.-H., Allègre, C.J., 1984. UPb geochronology of Gangdese (Transhimalaya) plutonism in the Lhasa-Xigaze region, Tibet. Earth Planet. Sci. Lett. 69, 311–320. https://doi.org/10.1016/0012-821X(84)90190-0

Schlup M., Carter A., Cosca M., Steck A., 2003. Exhumation history of eastern Ladakh revealed by 40Ar/39Ar and fission-track ages: the Indus River–Tso Morari transect, NW Himalaya. J. Geol. Soc. 160, 385–399. https://doi.org/10.1144/0016-764902-084

Schultz, M.H., Hodges, K.V., Ehlers, T.A., van Soest, M., Wartho, J.-A., 2017. Thermochronologic constraints on the slip history of the South Tibetan detachment system in the Everest region, southern Tibet. Earth Planet. Sci. Lett. 459, 105–117. https://doi.org/10.1016/j.epsl.2016.11.022

Searle, M.P., Noble, S.R., Hurford, A.J., Rex, D.C., 1999. Age of crustal melting, emplacement and exhumation history of the Shivling Leucogranite, Garhwal Himalaya. Geol. Mag. 136, 513–525. https://doi.org/10.1017/S0016756899002885

Searle, M.P., Simpson, R.L., Law, R.D., Parrish, R.R., Water, D.J., 2003. The structural geometry, metamorphic and magmatic evolution of the Everest massif, High Himalaya of Nepal-South Tibet. J. Geol. Soc. 160, 345.

Seraine, M., Campos, J.E.G., Martins-Ferreira, M.A.C., Alvarenga, C.J.S. de, Chemale, F., Angelo, T.V., Spencer, C., 2021. Multi-dimensional scaling of detrital zircon geochronology constrains basin evolution of the late Mesoproterozoic Paranoá Group, central Brazil. Precambrian Res. 365, 106381. https://doi.org/10.1016/j.precamres.2021.106381

Seward, D., Burg, J.P., Sorkhabi, R., Heydari, E., 2008. Growth of the Namche Barwa Syntaxis and associated evolution of the Tsangpo Gorge; constraints from structural and thermochronological data. Tectonophysics 451, 282–289. https://doi.org/10.1016/j.tecto.2007.11.057

Shen, T., Wang, G., Leloup, P.H., van der Beek, P., Bernet, M., Cao, K., Wang, A., Liu, C., Zhang, K., 2016. Controls on Cenozoic exhumation of the Tethyan Himalaya from fission-track thermochronology and detrital zircon U-Pb geochronology in the Gyirong basin area, southern Tibet: The Tethyan Himalaya Cenozoic Exhumation. Tectonics 35, 1713–1734. https://doi.org/10.1002/2016TC004149

Shen, T., Wang, G., van der Beek, P., Bernet, M., Chen, Y., Zhang, P., Wang, A., Cao, K., 2022. Impacts of late Miocene normal faulting on Yarlung Tsangpo River evolution, southeastern Tibet. GSA Bull. https://doi.org/10.1130/B36210.1

Singh, P., Patel, R.C., 2017. Post-emplacement kinematics and exhumation history of the Almora klippe of the Kumaun–Garhwal Himalaya, NW India: revealed by fission track thermochronology. Int. J. Earth Sci. 106, 2189–2202. https://doi.org/10.1007/s00531-016-1422-0

Singh, P., Patel, R.C., Lal, N., 2012. Plio-Plistocene in-sequence thrust propagation along the Main Central Thrust zone (Kumaon–Garhwal Himalaya, India): New thermochronological data. Tectonophysics 574–575, 193–203. https://doi.org/10.1016/j.tecto.2012.08.015

Sobel, E.R., Hilley, G.E., Strecker, M.R., 2003. Formation of internally drained contractional basins by aridity-limited bedrock incision: FORMATION OF INTERNALLY DRAINED BASINS. J. Geophys. Res. Solid Earth 108. https://doi.org/10.1029/2002JB001883

Sorkhabi, R.B., Stump, E., Foland, K.A., Jain, A.K., Burg, J.-P., 1996. Fission-track and (super 40) Ar/ (super 39) Ar evidence for episodic denudation of the Gangotri granites in the Garhwal Higher Himalaya, India. Tectonophysics 260, 187–199.

Srinivasan, M.S., Sinha, D.K., 2000. Ocean circulation in the tropical Indo-Pacific during early Pliocene (5.6-4.2 Ma): Paleobiogeographic and isotopic evidence. J. Earth Syst. Sci. 109, 315–328. https://doi.org/10.1007/BF03549815

Stock, G.M., Ehlers, T.A., Farley, K.A., 2006. Where does sediment come from? Quantifying catchment erosion with detrital apatite (U-Th)/He thermochronometry. Geology 34, 725. https://doi.org/10.1130/G22592.1

Streule, M.J., Carter, A., Searle, M.P., Cottle, J.M., 2012. Constraints on brittle field exhumation of the Everest-Makalu section of the Greater Himalayan Sequence: Implications for models of crustal flow: EVEREST-MAKALU FISSION TRACK DATA. Tectonics 31, n/a-n/a. https://doi.org/10.1029/2011TC003062

Stübner, K., Grujic, D., Dunkl, I., Thiede, R., Eugster, P., 2018. Pliocene episodic exhumation and the significance of the Munsiari thrust in the northwestern Himalaya. Earth Planet. Sci. Lett. 481, 273–283. https://doi.org/10.1016/j.epsl.2017.10.036

Stübner, K., Ratschbacher, L., Rutte, D., Stanek, K., Minaev, V., Wiesinger, M., Gloaguen, R., Project TIPAGE members, 2013. The giant Shakhdara migmatitic gneiss dome, Pamir, India-Asia collision zone: 1. Geometry and kinematics: SHAKHDARA DOME: GEOMETRY AND KINEMATICS. Tectonics n/a-n/a. https://doi.org/10.1002/tect.20057

Stuewe, K., Grasemann, B., 2001. The influence of Himalayan topography on low-T geochronology. J. Asian Earth Sci. 19, 65.

Styron, R., Taylor, M., Sundell, K., 2015. Accelerated extension of Tibet linked to the northward underthrusting of Indian crust. Nat. Geosci. 8, 131–134. https://doi.org/10.1038/ngeo2336

Styron, R.H., Taylor, M.H., Sundell, K.E., Stockli, D.F., Oalmann, J.A.G., Möller, A., McCallister, A.T., Liu, D., Ding, L., 2013. Miocene initiation and acceleration of extension in the South Lunggar rift, western Tibet: Evolution of an active detachment system from structural mapping and (U-Th)/He thermochronology: SOUTH LUNGGAR RIFT, SW TIBET. Tectonics n/a-n/a. https://doi.org/10.1002/tect.20053

Sundell, K.E., Saylor, J.E., 2017. Unmixing detrital geochronology age distributions. Geochem. Geophys. Geosystems 18, 2872–2886. https://doi.org/10.1002/2016GC006774

Sundell, K.E., Taylor, M.H., Styron, R.H., Stockli, D.F., Kapp, P., Hager, C., Liu, D., Ding, L., 2013. Evidence for constriction and Pliocene acceleration of east-west extension in the North Lunggar rift region of west central Tibet: NORTH LUNGGAR RIFT, WEST CENTRAL TIBET. Tectonics 32, 1454–1479. https://doi.org/10.1002/tect.20086

Taylor, M., Forte, A., Laskowski, A., Ding, L., 2021. Active Uplift of Southern Tibet Revealed. GSA Today 31, 4–10. https://doi.org/10.1130/GSATG487A.1

Thiede, R., Robert, X., Stübner, K., Dey, S., Faruhn, J., 2017. Sustained out-of-sequence shortening along a tectonically active segment of the Main Boundary thrust: The Dhauladhar Range in the northwestern Himalaya. Lithosphere 9, 715–725. https://doi.org/10.1130/L630.1

Thiede, R.C., Arrowsmith, J.R., Bookhagen, B., McWilliams, M., Sobel, E.R., Strecker, M.R., Anonymous, 2006. Timing of dome formation and extension in the Tethyan Himalaya, Leo Pargil, NW India. Terra Nostra Bonn 2006–3, 98.

Thiede, R.C., Arrowsmith, J.R., Bookhagen, B., McWilliams, M.O., Sobel, E.R., Strecker, M.R., 2005. From tectonically to erosionally controlled development of the Himalayan Orogen. Geol. Boulder 33, 689–692. https://doi.org/10.1130/G21483AR.1

Thiede, R.C., Bookhagen, B., Arrowsmith, J.R., Sobel, E.R., Strecker, M.R., 2004. Climatic control on rapid exhumation along the Southern Himalayan Front. Earth Planet. Sci. Lett. 222, 791–806. https://doi.org/10.1016/j.epsl.2004.03.015

Thiede, R.C., Ehlers, T.A., 2013. Large spatial and temporal variations in Himalayan denudation. Earth Planet. Sci. Lett. 371–372, 278–293. https://doi.org/10.1016/j.epsl.2013.03.004

Thiede, R.C., Ehlers, T.A., Bookhagen, B., Strecker, M.R., 2009. Erosional variability along the northwest Himalaya. J. Geophys. Res. 114, F01015. https://doi.org/10.1029/2008JF001010

Tremblay, M.M., Fox, M., Schmidt, J.L., Tripathy-Lang, A., Wielicki, M.M., Harrison, T.M., Zeitler, P.K., Shuster, D.L., 2015. Erosion in southern Tibet shut down at ∼10 Ma due to enhanced rock uplift within the Himalaya. Proc. Natl. Acad. Sci. 112, 12030–12035. https://doi.org/10.1073/pnas.1515652112

Tshering, P., 2007. Detrital muscovite thermochronology in two drainage basins in western Bhutan (Master's). Detrital Muscovite Thermochronology Two Drain. Basins West. Bhutan. Massachusetts Institute of Technology.

van der Beek, P., Litty, C., Baudin, M., Mercier, J., Robert, X., Hardwick, E., 2016. Contrasting tectonically driven exhumation and incision patterns, western versus central Nepal Himalaya. Geology 44, 327–330. https://doi.org/10.1130/G37579.1

van der Beek, P., Robert, X., Mugnier, J.-L., Bernet, M., Huyghe, P., Labrin, E., 2006. Late Miocene - Recent exhumation of the central Himalaya and recycling in the foreland basin assessed by apatite fission-track thermochronology of Siwalik sediments, Nepal: Recent

exhumation of the central Himalaya. Basin Res. 18, 413–434. https://doi.org/10.1111/j.1365-2117.2006.00305.x

van der Beek, P., Schildgen, T.F., 2022. Short Communication: age2exhume – A Matlab script to calculate steady-state vertical exhumation rates from thermochronologic ages in regional datasets and application to the Himalaya (preprint). Geochronological data analysis/statistics/modelling. https://doi.org/10.5194/egusphere-2022-888

van der Beek, P., Van Melle, J., Guillot, S., Pêcher, A., Reiners, P.W., Nicolescu, S., Latif, M., 2009. Eocene Tibetan plateau remnants preserved in the northwest Himalaya. Nat. Geosci. 2, 364–368. https://doi.org/10.1038/ngeo503

Vannay, J.-C., Grasemann, B., Rahn, M., Frank, W., Carter, A., Baudraz, V., Cosca, M., 2004. Miocene to Holocene exhumation of metamorphic crustal wedges in the NW Himalaya: Evidence for tectonic extrusion coupled to fluvial erosion: TECTONICS AND EROSION IN THE NW HIMALAYA. Tectonics 23, n/a-n/a. https://doi.org/10.1029/2002TC001429

Vannay, J.C., Hodges, K.V., 1996. Tectonometamorphic evolution of the Himalayan metamorphic core between the Annapurna and Dhaulagiri, central Nepal. J. Metamorph. Geol. 14, 635–656.

Vermeesch, P., 2013. Multi-sample comparison of detrital age distributions. Chem. Geol. 341, 140–146. https://doi.org/10.1016/j.chemgeo.2013.01.010

Vermeesch, P., 2004. How many grains are needed for a provenance study? Earth Planet. Sci. Lett. 224, 441–451. https://doi.org/10.1016/j.epsl.2004.05.037

Walker, J.D., Geissman, J.W., Bowring, S.A., Babcock, L.E., 2013. The Geological Society of America Geologic Time Scale. Geol. Soc. Am. Bull. 125, 259–272. https://doi.org/10.1130/B30712.1

Walker, J.D., Martin, M.W., Bowring, S.A., Searle, M.P., Waters, D.J., Hodges, K.V., 1999. Metamorphism, melting, and extension; age constraints from the High Himalayan slab of Southeast Zanskar and Northwest Lahaul. J. Geol. 107, 473–495.

Wang, A., Garver, J.I., Wang, G., Smith, J.A., Zhang, K., 2010. Episodic exhumation of the Greater Himalayan Sequence since the Miocene constrained by fission track thermochronology in Nyalam, central Himalaya. Tectonophysics 495, 315–323. https://doi.org/10.1016/j.tecto.2010.09.037

Wang, A., Min, K., Wang Guocan, Cao, K., Shen Tianyi, Jiang Pengfei, Wei Jiangwei, 2019. Slow exhumation of the Greater Himalaya in the Yadong region, the transition between the central and eastern Himalaya, during the late Neogene. J. Geol. Soc. Lond. 176, 1207–1217. https://doi.org/10.1144/jgs2018-186

Wang, C., Ding, L., Zhang, L.-Y., Kapp, P., Pullen, A., Yue, Y.-H., 2016. Petrogenesis of Middle–Late Triassic volcanic rocks from the Gangdese belt, southern Lhasa terrane: Implications for early subduction of Neo-Tethyan oceanic lithosphere. Lithos 262, 320–333. https://doi.org/10.1016/j.lithos.2016.07.021

Wang, Y., Zhang, X., Sun, L., Wan Jinglin, Arita, K., Yin, A., Singh, S., Okada, H., 2007. Cooling history and tectonic exhumation stages of the south-central Tibetan Plateau (China); constrained by (super 40) Ar/ (super 39) Ar and apatite fission-track thermochronology. J. Asian Earth Sci. 29, 266–282. https://doi.org/10.1016/j.jseaes.2005.11.001

Wang, Y., Zheng Jianjing, Zheng Youwei, Liu, X., Sun, G., 2015. Early Cenozoic Altyn Mountains uplift recorded by detrital zircon fission track age in northwestern Qaidam Basin. Jilin Daxue Xuebao Diqiu Kexue Ban J. Jilin Univ. Earth Sci. Ed. 45, 1447–1459. https://doi.org/10.13278/j.cnki.jjuese.201505116

Wang, Z., Li, T., Zhang, J., Liu, Y., Ma, Z., 2008. The uplifting process of the Bogda Mountain during the Cenozoic and its tectonic implication. Sci. China Ser. Earth Sci. 51, 579–593. https://doi.org/10.1007/s11430-008-0038-z

Warren, C.J., Singh, A.K., Roberts, N.M.W., Regis, D., Halton, A.M., Singh, R.B., 2014. Timing and conditions of peak metamorphism and cooling across the Zimithang Thrust, Arunachal Pradesh, India. Lithos 200–201, 94–110. https://doi.org/10.1016/j.lithos.2014.04.005

Wiesmayr, G., Grasemann, B., 2002. Eohimalayan fold and thrust belt; implications for the geodynamic evolution of the NW-Himalaya (India). Tectonics 21, 18. https://doi.org/10.1029/2002TC001363

Wobus, C.W., Hodges, K.V., Whipple, K.X., 2003. Has focused denudation sustained active thrusting at the Himalayan topographic front? Geology 31, 861. https://doi.org/10.1130/G19730.1

Wolff, R., Hetzel, R., Dunkl, I., Xu, Q., Bröcker, M., Anczkiewicz, A.A., 2019. High-Angle Normal Faulting at the Tangra Yumco Graben (Southern Tibet) since ~15 Ma. J. Geol. 127, 15–36. https://doi.org/10.1086/700406

Wolff, R., Hetzel, R., Hölzer, K., Dunkl, I., Xu, Q., Anczkiewicz, A.A., Li, Z., 2022a. Rift propagation in south Tibet controlled by underthrusting of India: A case study at the Tangra Yumco graben (south Tibet). J. Geol. Soc. jgs2022-090. https://doi.org/10.1144/jgs2022-090

Wolff, R., Hölzer, K., Hetzel, R., Xu, Q., Dunkl, I., Anczkiewicz, A.A., Li, Z., 2022b. Spatially focused erosion in the High Himalaya and the geometry of the Main Himalayan Thrust in Central Nepal (85°E) from thermo-kinematic modeling of thermochronological data in the Gyirong region (southern China). Tectonophysics 834, 229378. https://doi.org/10.1016/j.tecto.2022.229378

Wu, C., Yin, A., Zuza, A.V., Zhang, J., Liu, W., Ding, L., 2016. Pre-Cenozoic geologic history of the central and northern Tibetan Plateau and the role of Wilson cycles in constructing the Tethyan orogenic system. Lithosphere 8, 254–292. https://doi.org/10.1130/L494.1

Xu, Y., Zhang, K., Wang Guocan, Jiang Shangsong, Chen Fenning, Xiang Shuyuan, Dupont-Nivet, G., Hoorn, C., Clift, P., An, Y., 2012. Extended stratigraphy, palynology and depositional environments record the initiation of the Himalayan Gyirong Basin (Neogene China). J. Asian Earth Sci. 44, 77–93. https://doi.org/10.1016/j.jseaes.2011.04.007

Xu Zhiqin, Wang, Q., Pecher, A., Liang Fenghua, Qi Xuexiang, Cai Zhihui, Li Huaqi, Zeng Lingsen, Cao, H., 2013. Orogen-parallel ductile extension and extrusion of the Greater Himalaya in the late Oligocene and Miocene. Tectonics 32, 191–215. https://doi.org/10.1002/tect.20021

Yang, R., Herman, F., Liu, T., Biswas, R.H., Fellin, M.G., Tian, Y., Gong, J., Jiao, R., Maden, C., Chen, H., 2021. Enhanced Quaternary exhumation in the Namche Barwa syntaxis, eastern Himalaya. Geology 49, 958–962. https://doi.org/10.1130/G48595.1

Yin, A., 2010. Cenozoic tectonic evolution of Asia: A preliminary synthesis. Tectonophysics 488, 293–325. https://doi.org/10.1016/j.tecto.2009.06.002

Yin, A., 2006. Cenozoic tectonic evolution of the Himalayan orogen as constrained by along-strike variation of structural geometry, exhumation history, and foreland sedimentation. Earth-Sci. Rev. 76, 1–131. https://doi.org/10.1016/j.earscirev.2005.05.004

Yin, A., Dubey, C.S., Kelty, T.K., Webb, A.A.G., Harrison, T.M., Chou, C.Y., Celerier, J., 2010. Geologic correlation of the Himalayan orogen and Indian craton: Part 2. Structural geology, geochronology, and tectonic evolution of the Eastern Himalaya. Geol. Soc. Am. Bull. 122, 360–395. https://doi.org/10.1130/B26461.1

Yin, A., Harrison, T.M., 2000. Geologic Evolution of the Himalayan-Tibetan Orogen. Annu. Rev. Earth Planet. Sci. 28, 211–280. https://doi.org/10.1146/annurev.earth.28.1.211

Yuan, W., Deng, J., Zheng, Q., Dong, J., Bao, Z., Eizenhoefer, P.R., Xu, X., Huang, Z., 2009. Apatite fission track constraints on the Neogene tectono-thermal history of Nimu area, southern Gangdese terrane, Tibet Plateau. Isl. Arc 18, 488–495. https://doi.org/10.1111/j.1440-1738.2009.00669.x

Yuan, W., Dong, J., Shicheng, W., Carter, A., 2006. Apatite fission track evidence for Neogene uplift in the eastern Kunlun Mountains, northern Qinghai–Tibet Plateau, China. J. Asian Earth Sci. 27, 847–856. https://doi.org/10.1016/j.jseaes.2005.09.002

Zeitler, P.K., 1985. Cooling history of the NW Himalaya, Pakistan. Tectonics 4, 127–151. https://doi.org/10.1029/TC004i001p00127

Zeitler, P.K., Meltzer, A.S., Brown, L., Kidd, W.S.F., Lim, C., Enkelmann, E., 2014. Tectonics and topographic evolution of Namche Barwa and the easternmost Lhasa block, Tibet, in: Toward

an Improved Understanding of Uplift Mechanisms and the Elevation History of the Tibetan Plateau. Geological Society of America. https://doi.org/10.1130/2014.2507(02)

Zhang, P., Mei, L., Jiang, S.-Y., Xu, S., Donelick, R.A., Li, R., Zhang, H., 2021. Erosion and sedimentation in SE Tibet and Myanmar during the evolution of the Burmese continental margin from the Late Cretaceous to Early Neogene. Gondwana Res. 95, 149–175. https://doi.org/10.1016/j.gr.2021.04.005

Zhang, P., Najman, Y., Mei, L., Millar, I., Sobel, E.R., Carter, A., Barfod, D., Dhuime, B., Garzanti, E., Govin, G., Vezzoli, G., Hu, X., 2019. Palaeodrainage evolution of the large rivers of East Asia, and Himalayan-Tibet tectonics. Earth-Sci. Rev. 192, 601–630. https://doi.org/10.1016/j.earscirev.2019.02.003

Zhao, Z., Lu, L., Wu Zhenhan, Hu Daogong, 2017. Cenozoic uplift process in Gangdese Belt, Xizang; evidence from thermal history modeling of apatite fission track. Dizhi Tongbao Geol. Bull. China 36, 1553–1561.

Zhu, D.-C., Pan, G.-T., Chung, S.-L., Liao, Z.-L., Wang, L.-Q., Li, G.-M., 2008. SHRIMP Zircon Age and Geochemical Constraints on the Origin of Lower Jurassic Volcanic Rocks from the Yeba Formation, Southern Gangdese, South Tibet. Int. Geol. Rev. 50, 442–471. https://doi.org/10.2747/0020-6814.50.5.442

Zhu, D.-C., Zhao, Z.-D., Pan, G.-T., Lee, H.-Y., Kang, Z.-Q., Liao, Z.-L., Wang, L.-Q., Li, G.-M., Dong, G.-C., Liu, B., 2009. Early cretaceous subduction-related adakite-like rocks of the Gangdese Belt, southern Tibet: Products of slab melting and subsequent melt–peridotite interaction? J. Asian Earth Sci. 34, 298–309. https://doi.org/10.1016/j.jseaes.2008.05.003

Zhu Dicheng, Wang, Q., Chung, S.-L., Cawood, P.A., Zhao Zhidan, Treloar, P.J., Searle, M.P., 2018. Gangdese magmatism in southern Tibet and India-Asia convergence since 120 Ma. Spec. Publ. - Geol. Soc. Lond. 483, 583–604. https://doi.org/10.1144/SP483.14

APPENDICES

APPENDIX A

DETAILED METHODOLOGY AND ANALYTICAL PARAMETERS

Appendix A1: Zircon (U-Th)/He Thermochronology

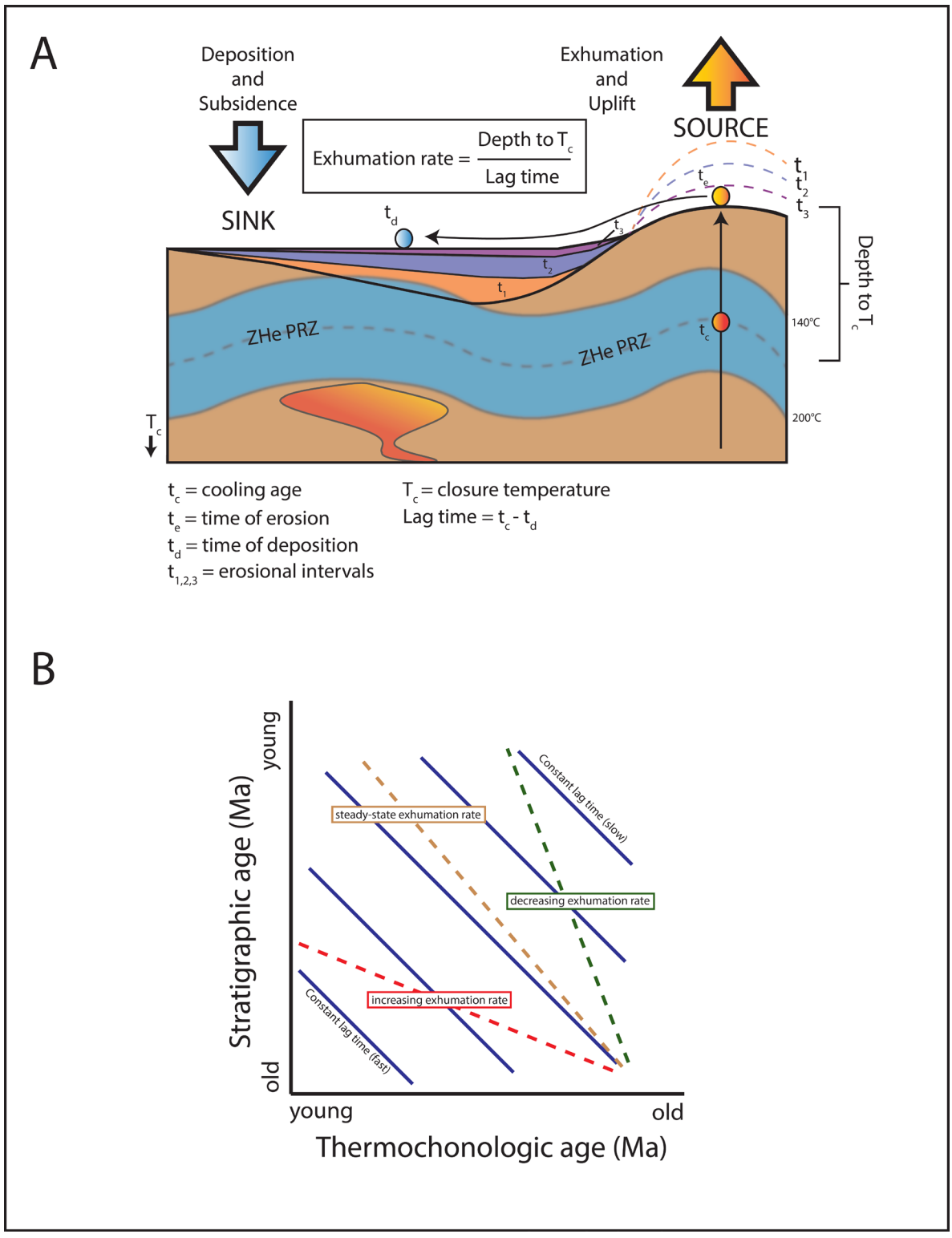


Figure A1: (A) Conceptual model of the lag-time approach using detrital thermochronology modified from Malusà & Fitzgerald (2020) and references therein. A package of rock is exhumed through the zircon helium partial retention zone (ZHe PRZ) and subsequently the zircon closure temperature (T_c) range at time t_c (cooling age). The package is exhumed to the surface at time t_e and is subsequently uplifted, eroded, and deposited in an adjacent sedimentary basin at time t_d. An estimate of average exhumation rate of the rock package can then be determined by first taking the difference between time t_c and t_d (lag-time) and using it as the divisor of the depth measured to the zone of T_c. Further burial of material in a basin may result in reheating within or below the PRZ, thus partially or fully resetting a cooling age. (B) Lag-time diagram comparing stratigraphic and thermochronologic ages (Ma). Equivalent lag-time (1-1) is represented by blue lines. Increasing exhumation is indicated by decreasing lag-time values (red), constant values represent steady-state exhumation (yellow) and decreasing exhumation rates are indicated by increasing lag-time values (green). These rates can be used to infer an orogenic belt's condition as under constructional, steady-state, or decay stages of evolution (Malusà & Fitzgerald, 2020; Carrapa et al, 2009).

Appendix A2: Zircon He-Pb Double-Dating

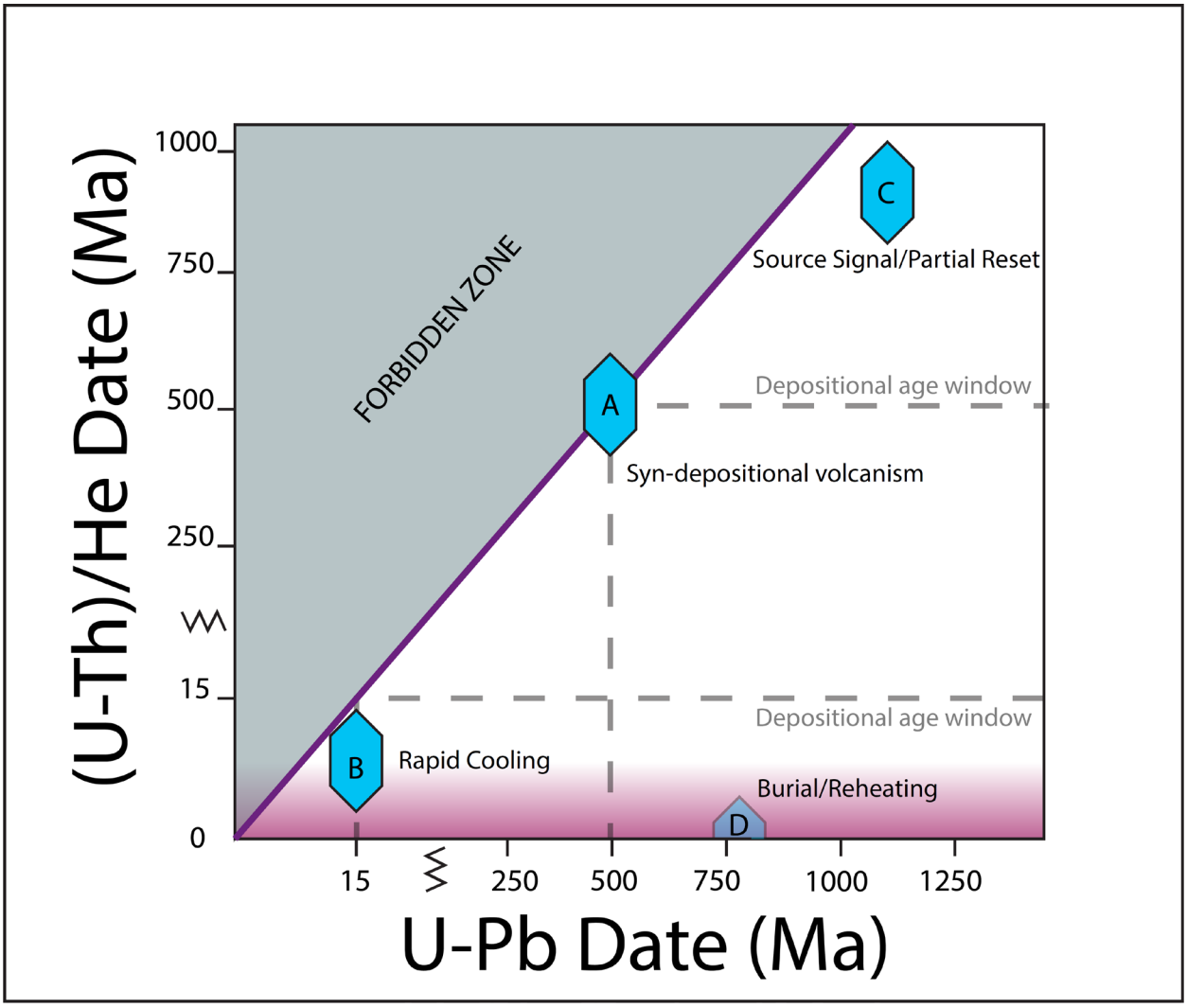


Figure A2: Detrital zircon double-dating assumes crystallization is achieved before or in conjunction with deposition. **(A)** Concordant correlations are interpreted as rock which experienced volcanism during deposition; **(B)** Zircon with U-Pb dates slightly older than He dates can be interpreted as experiencing rapid cooling [e.g. the eastern syntaxis experiences lag times <1 m.y. (Najman et al., 2019)]; **(C)** Zircon retaining original source signals are interpreted from He ages greater than apparent depositional age; Partially reset crystals are described by He dates that are younger than the depositional age but maintain a crystallization date above the depositional age; **(D)** Burial and reheating results in crystals that fall below the depositional age window due to helium diffusion at high temperatures; due to the generally rapid exhumation rates and shallow burial of zircon in the region, the probability of reheating by burial within the Bengal Fan is likely negligible for this study. Crystals that display crystallization age below cooling age are geologically impossible, and thus fall into the "forbidden zone".

Appendix A3: Multi-Dimensional Scaling Heat Maps

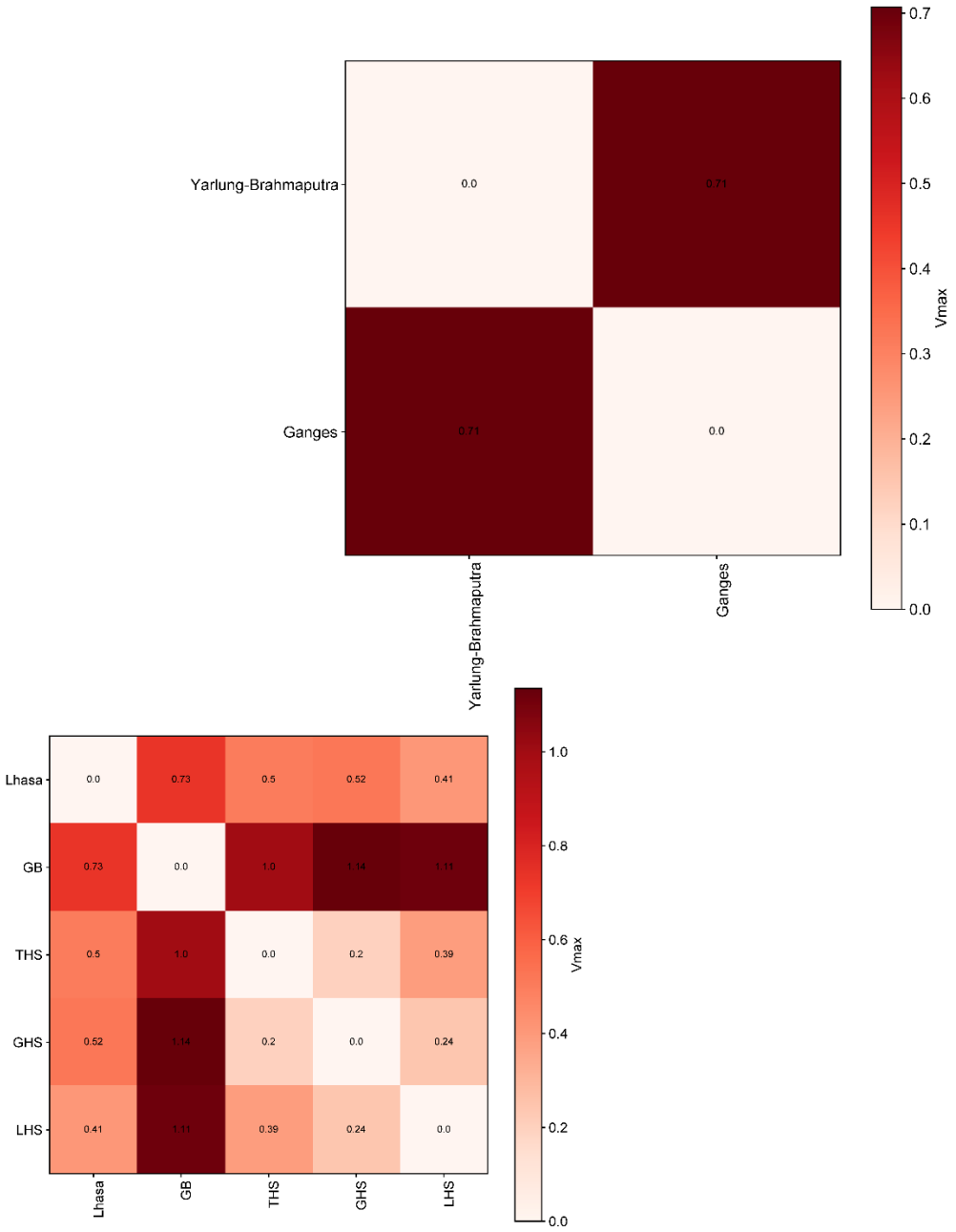


Figure A4: Additional heatmap plots utilizing Euclidean distance values. Pairs are perfectly similar when Vmax = 0 (light colors) and most dissimilar at Vmax = ∞ (dark colors). Top-right: River drainages are highly dissimilar in MDS space, demonstrating high potential for ZHe differentiation between drainages. Bottom-left: Lithotectonic units show generally increasing similarity with decreasing north-south distance.

APPENDIX B

DETAILED ANALYTICAL RESULTS

Appendix B1: Bengal Fan single Zircon (U-Th)/He Results: Table 1

*Set to 1000°C, reached 760 at 100% **ZHe age below depositional age **empty Nb packet ****negative age, Ft $^{147}Sm = 1$

Sample Name	Depth (mbsf)	Rs (um)	eU (ppm)	U (ppm)	Th (ppm)	nmol 4He/g	Ft 238U	Ft 235U	Ft 232Th	Corrected Age (Ma)	1s ± age (Ma)	Depositional Age (Ma)
U1455_C6F_Zr1	32	58.82	637.85	610.19	117.70	23.56	0.79	0.79	0.76	8.66	0.11	0.28
U1455_C6F_Zr2	32	59.34	214.83	199.02	67.29	7.81	0.79	0.79	0.76	8.50	0.10	0.28
U1455_C6F_Zr3	32	57.23	1585.25	1387.53	841.39	87.95	0.79	0.79	0.76	13.11	0.14	0.28
U1455_C6F_Zr4	32	60.42	304.58	285.57	80.86	2.86	0.80	0.80	0.77	2.19	0.03	0.28
U1455_C6F_Zr5	32	61.90	690.55	662.03	121.36	28.20	0.80	0.80	0.77	9.45	0.11	0.28
U1455_C6F_Zr6	32	55.68	787.15	749.81	158.91	6.87	0.78	0.78	0.75	2.07	0.03	0.28
U1455_C6F_Zr7	32	69.74	925.26	874.79	214.76	6.69	0.82	0.82	0.80	1.63	0.02	0.28
U1455_C6F_Zr8	32	49.71	464.98	412.89	221.64	27.46	0.76	0.76	0.72	14.51	0.30	0.28
U1454_B26F_Zr1	130	69.55	433.60	375.13	248.81	24.72	0.82	0.82	0.80	12.89	0.17	0.33
U1454_B26F_Zr2	130	68.37	1176.93	1026.75	639.03	3.52	0.82	0.82	0.79	0.68	0.01	0.33
U1454_B26F_Zr3	130	68.93	122.84	110.59	52.12	10.00	0.82	0.82	0.80	18.41	0.27	0.33
U1454_B26F_Zr4	130	71.76	462.15	443.42	79.70	1.02	0.83	0.83	0.80	0.49	0.01	0.33
U1454_B26F_Zr5	130	50.94	718.74	666.20	223.56	2.02	0.76	0.76	0.73	0.69	0.02	0.33
U1454_B26F_Zr6	130	52.14	1487.64	1311.98	747.51	134.45	0.77	0.77	0.73	21.89	0.27	0.33
U1452_B26_Zr7	130	54.03	2783.11	2728.04	234.32	41.52	0.78	0.78	0.74	3.57	0.05	0.33
U1452_B26_Zr8	130	51.70	90.51	72.44	76.89	3.54	0.77	0.77	0.73	9.53	0.16	0.33
U1455_C9F_Zr1	47	45.35	1258.84	1229.86	123.34	11.97	0.74	0.74	0.70	2.40	0.03	0.38
U1455_C9F_Zr2	47	50.63	762.65	593.68	719.04	236.06	0.76	0.76	0.73	75.58	0.87	0.38
U1455_C9F_Zr3	47	65.58	934.98	796.21	590.52	3.02	0.81	0.81	0.79	0.74	0.01	0.38
U1455_C9F_Zr4	47	59.37	410.32	401.39	37.99	2.31	0.79	0.79	0.76	1.32	0.02	0.38
U1455_C9F_Zr5	47	51.74	468.27	411.20	242.84	1.57	0.77	0.77	0.73	0.81	0.02	0.38
U1455_C9F_Zr6	47	57.28	666.00	645.28	88.20	13.51	0.79	0.79	0.76	4.78	0.06	0.38
U1455_C9F_Zr7	47	66.61	1442.10	1202.02	1021.63	5.10	0.82	0.82	0.79	0.81	0.01	0.38
U1455_C9F_Zr8	47	72.03	478.11	449.79	120.48	1.23	0.83	0.83	0.80	0.58	0.01	0.38
U1449_A16H_Zr1	82	58.78	663.80	615.79	204.30	3.61	0.79	0.79	0.76	1.28	0.08	0.45
U1449_A16H_Zr2	82	48.40	504.43	485.67	79.84	26.08	0.75	0.75	0.72	12.78	0.18	0.45
U1449_A16H_Zr3	82	74.88	708.20	642.33	280.33	25.09	0.84	0.84	0.81	7.89	0.11	0.45
U1449_A16H_Zr4***	82	57.49	0.22	0.21	0.04	0.00	0.79	0.79	0.76	3.71	5.68	0.45
U1449_A16H_Zr5	82	45.53	826.37	759.13	286.12	32.47	0.74	0.74	0.70	9.92	0.13	0.45
U1449_A16H_Zr6	82	50.56	374.39	339.93	146.65	13.86	0.76	0.76	0.73	9.05	0.12	0.45
U1449_A16H_Zr7	82	49.72	1040.57	1011.30	124.56	349.21	0.76	0.76	0.72	81.70	1.06	0.45
U1449_A16H_Zr8	82	41.73	836.10	735.70	427.23	22.68	0.72	0.72	0.68	7.07	0.10	0.45
U1452_B31_Zr1	160	62.58	621.47	569.90	219.44	1.58	0.80	0.80	0.78	0.59	0.01	0.52
U1452_B31_Zr2	160	54.00	2662.17	2542.52	509.15	259.92	0.78	0.78	0.74	23.36	0.28	0.52

Table 1 (cont.)

Sample Name	Depth (mbsf)	Rs (um)	eU (ppm)	U (ppm)	Th (ppm)	nmol 4He/g	Ft 238U	Ft 235U	Ft 232Th	Corrected Age (Ma)	1s ± age (Ma)	Depositional Age (Ma)
U1452_B31_Zr3	160	46.69	683.44	572.57	471.78	1273.58	0.74	0.74	0.71	450.83	4.88	0.52
U1452_B31_Zr4	160	44.23	1080.00	1017.00	268.07	86.92	0.73	0.73	0.69	20.48	0.24	0.52
U1452_B31_Zr5	160	42.34	1820.21	1745.31	318.74	60.62	0.72	0.72	0.68	8.61	0.11	0.52
U1452_B31_Zr6	160	40.35	617.36	581.85	151.13	9.17	0.71	0.71	0.67	3.91	0.06	0.52
UI1452_B31_Zr7**	160	43.75	1048.55	982.83	279.67	1.84	0.73	0.73	0.69	0.45	0.02	0.52
UI1452_B31_Zr8	160	44.01	636.67	578.21	248.73	10.85	0.73	0.73	0.69	4.36	0.07	0.52
U1450_A32F-Zr1	154	50.02	488.17	469.34	80.13	20.99	0.76	0.72	0.72	10.54	0.16	0.72
U1450_A32F-Zr2	154	52.56	275.47	265.78	41.23	0.98	0.77	0.74	0.74	0.86	0.02	0.72
U1450_A32F-Zr3	154	52.42	1226.58	1205.87	88.12	4.80	0.77	0.74	0.74	0.95	0.01	0.72
U1450_A32F-Zr4	154	46.62	97.22	90.47	28.71	0.48	0.74	0.71	0.71	1.24	0.06	0.72
U1450_A32F-Zr5	154	42.49	607.87	583.04	105.69	2.96	0.72	0.68	0.68	1.26	0.03	0.72
U1450_A32F-Zr6	154	42.49	909.66	756.43	652.05	3.58	0.72	0.68	0.68	1.02	0.02	0.72
U1450_A32F-Zr7**	154	51.67	1104.98	976.95	544.82	2.46	0.77	0.73	0.73	0.54	0.01	0.72
U1450_A32F-Zr8****	154	53.10	0.36	0.34	0.10	12.87	0.77	0.74	0.74	-27350.48	1197.47	0.72
U1455_C18F_Zr2**	92	52.08	201.24	187.70	57.63	0.66	0.77	0.73	0.73	0.79	0.02	1.14
U1455_C18F_Zr3	92	52.48	977.96	922.74	234.99	84.24	0.77	0.74	0.74	20.82	0.28	1.14
U1455_C18F_Zr4**	92	40.31	402.36	368.41	144.48	1.56	0.71	0.67	0.67	1.03	0.03	1.14
U1455_C18F_Zr5	92	49.17	723.97	659.43	274.64	27.93	0.76	0.72	0.72	9.53	0.13	1.14
U1455_C18F_Zr6	92	64.10	86.88	75.84	46.95	3.77	0.81	0.78	0.78	9.99	0.15	1.14
U1455_C18F_Zr7	92	43.33	580.60	558.64	93.47	7.07	0.73	0.69	0.69	3.13	0.05	1.14
U1455_C18F_Zr8**	92	49.52	198.09	177.03	89.65	0.56	0.76	0.72	0.72	0.69	0.02	1.14
U1453_A40F_Zr1	198	44.98	513.55	499.34	60.45	2.83	0.73	0.70	0.70	1.40	0.03	1.30
U1453_A40F_Zr2	198	44.97	354.57	339.06	66.01	20.63	0.73	0.70	0.70	14.75	0.25	1.30
U1453_A40F_Zr3	198	70.23	314.63	287.92	113.67	717.41	0.82	0.80	0.80	492.48	6.87	1.30
U1453_A40F_Zr4	198	56.95	648.70	632.50	68.93	25.75	0.79	0.76	0.76	9.39	0.13	1.30
U1453_A40F_Zr5	198	47.27	498.58	493.51	21.55	5.25	0.75	0.71	0.71	2.63	0.05	1.30
U1453_A40F_Zr6	198	49.01	1031.89	971.03	258.97	20.12	0.75	0.72	0.72	4.82	0.07	1.30
U1453_A40F_Zr7	198	55.91	416.64	388.34	120.43	17.10	0.78	0.75	0.75	9.76	0.14	1.30
U1453_A40F_Zr8	198	56.04	145.21	127.36	75.94	1.52	0.78	0.75	0.75	2.49	0.04	1.30
U1449_A37H_Zr1	208	78.95	232.65	213.94	79.61	7.18	0.84	0.82	0.82	6.81	0.10	1.60
U1449_A37H_Zr2**	208	60.95	499.36	448.32	217.15	3.09	0.80	0.77	0.77	1.44	0.02	1.60
U1449_A37H_Zr3**	208	56.79	276.57	261.26	65.13	1.64	0.79	0.75	0.75	1.41	0.03	1.60
U1449_A37H_Zr4	208	43.68	666.04	633.13	140.05	6.62	0.73	0.69	0.69	2.55	0.04	1.60

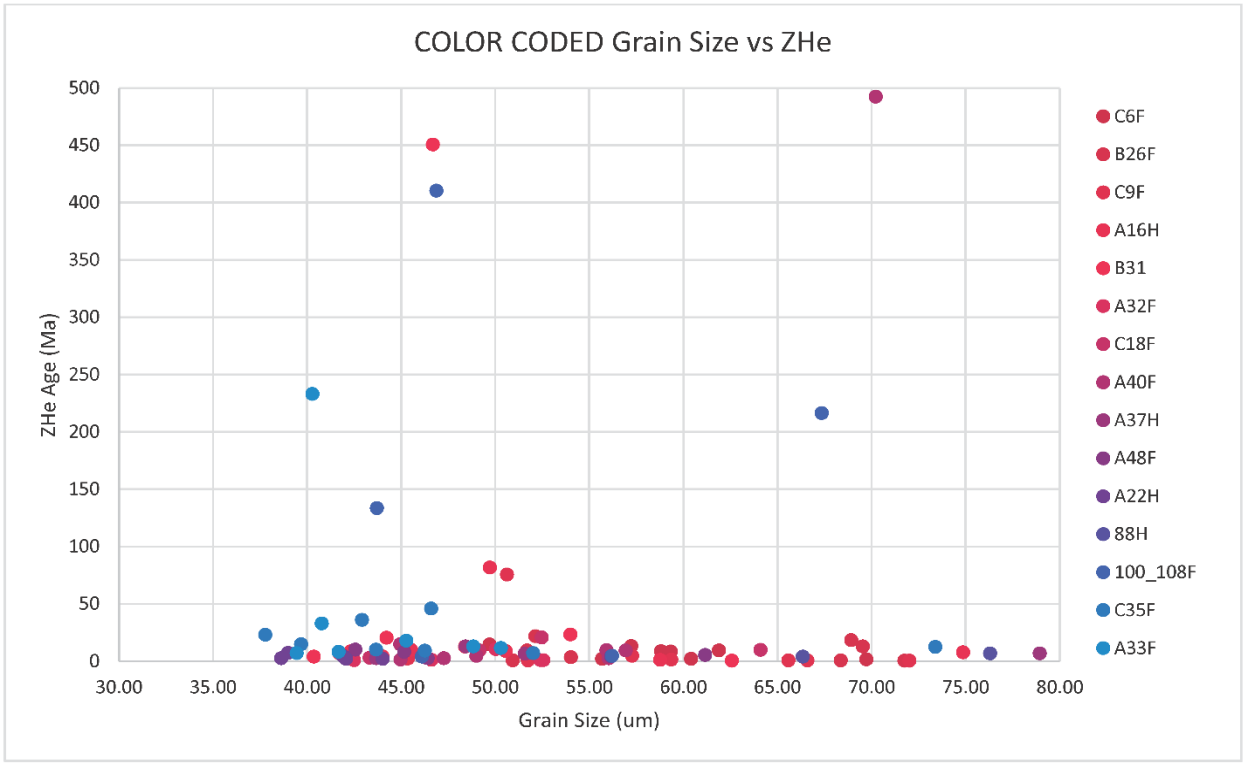
Table 1 (cont.)

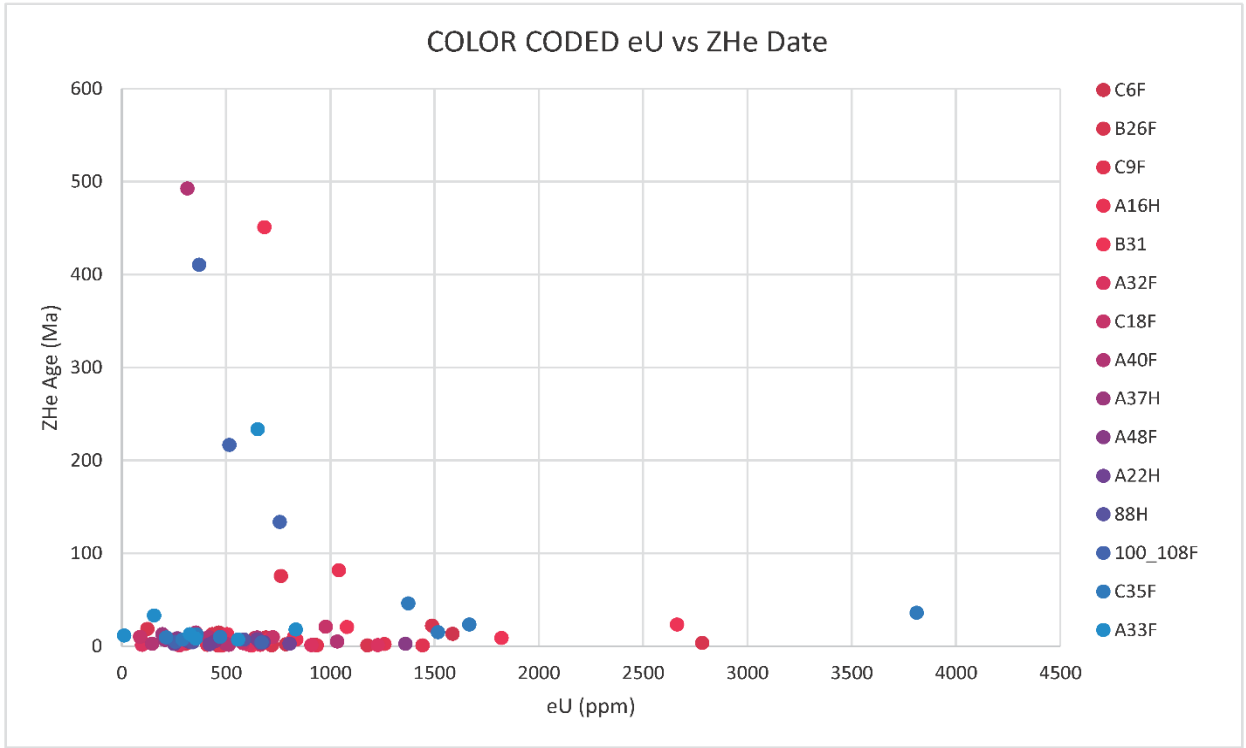
Sample Name	Depth (mbsf)	Rs (um)	eU (ppm)	U (ppm)	Th (ppm)	nmol 4He/g	Ft 238U	Ft 235U	Ft 232Th	Corrected Age (Ma)	1s ± age (Ma)	Depositional Age (Ma)
U1449_A37H_Zr5****	208	47.08	0.09	0.04	0.24	9.59	0.75	0.71	0.71	-2.1388E+12	14819.29	1.60
U1449_A37H_Zr6	208	51.59	206.64	194.69	50.88	5.69	0.77	0.73	0.73	6.70	0.11	1.60
U1449_A37H_Zr7**	208	54.41	204.57	193.37	47.67	1.19	0.78	0.75	0.75	1.40	0.04	1.60
U1449_A37H_Zr8	208	48.43	195.20	185.15	42.75	10.26	0.75	0.72	0.72	13.01	0.18	1.60
U1450_A48F_Zr1	230	61.16	445.28	390.71	232.19	10.17	0.80	0.77	0.77	5.32	0.07	1.80
U1450_A48F_Zr2**	230	52.31	323.63	296.03	117.47	1.75	0.77	0.74	0.74	1.31	0.04	1.80
U1450_A48F_Zr3	230	45.16	265.81	257.27	36.33	8.74	0.74	0.70	0.70	8.32	0.14	1.80
U1450_A48F_Zr4**	230	40.69	473.73	466.61	30.32	3.15	0.71	0.67	0.67	1.75	0.05	1.80
U1450_A48F_Zr5	230	42.57	332.21	316.20	68.12	13.08	0.72	0.68	0.68	10.18	0.15	1.80
U1450_A48F_Zr6**	230	68.11	565.20	539.81	108.03	3.72	0.82	0.79	0.79	1.50	0.02	1.80
U1450_A48F_Zr7	230	46.41	1360.09	1238.32	518.16	14.58	0.74	0.71	0.71	2.70	0.04	1.80
U1450_A48F_Zr8**	230	57.69	636.96	609.67	116.12	3.91	0.79	0.76	0.76	1.45	0.03	1.80
U1451_A22H_Zr1	115	44.02	420.60	416.94	15.57	3.46	0.73	0.69	0.69	2.10	0.04	1.90
U1451_A22H_Zr2	115	56.17	679.52	577.21	435.37	12.14	0.78	0.75	0.75	4.26	0.06	1.90
U1451_A22H_Zr3	115	42.07	250.70	217.76	140.17	2.05	0.72	0.68	0.68	2.13	0.05	1.90
U1451_A22H_Zr4**	115	48.49	174.03	161.06	55.15	1.12	0.75	0.72	0.72	1.59	0.04	1.90
U1451_A22H_Zr5****	115	39.72	0.08	0.09	-0.08	124.28	0.70	0.66	0.66	-2.2433E+187	533163.67	1.90
U1451_A22H_Zr6	115	38.63	804.54	794.82	41.35	7.73	0.69	0.65	0.65	2.57	0.04	1.90
U1451_A22H_Zr7	115	39.00	649.65	584.62	276.70	17.70	0.70	0.66	0.66	7.30	0.10	1.90
U1451_A22H_Zr8	115	41.89	319.51	293.92	108.90	6.08	0.72	0.68	0.68	4.96	0.10	1.90
U1450_88H_Zr1	425	66.35	338.36	325.17	56.11	5.99	0.82	0.79	0.79	4.04	0.06	3.25
U1450_88H_Zr2**	425	42.39	110286.14	102542.70	32950.81	3.51	0.72	0.68	0.68	0.01	0.00	3.25
U1450_88H_Zr4**	425	92.39	1337.06	1246.98	383.31	15.41	0.87	0.84	0.84	2.48	0.03	3.25
U1450_88H_Zr5	425	76.31	586.14	546.34	169.37	18.22	0.84	0.81	0.81	6.90	0.09	3.25
U1450_88H_Zr7**	425	59.40	241.99	224.05	76.37	2.76	0.79	0.76	0.76	2.67	0.04	3.25
U1450_88H_Zr8**	425	66.84	218.03	204.56	57.33	2.91	0.82	0.79	0.79	3.04	0.05	3.25
U1450_100_108F_Zr1	475	56.20	257.07	230.82	111.71	5.04	0.78	0.75	0.75	4.66	0.07	3.89
U1450_100_108F_Zr2	475	67.36	516.15	455.28	258.98	499.71	0.82	0.79	0.79	216.61	2.78	3.89
U1450_100_108F_Zr3	475	46.11	669.55	629.13	172.01	10.67	0.74	0.70	0.70	4.01	0.06	3.89
U1450_100_108F_Zr4	475	43.71	757.87	682.74	319.71	398.54	0.73	0.69	0.69	133.54	1.86	3.89
U1450_100_108F_Zr5	475	46.87	370.13	331.63	163.86	627.60	0.74	0.71	0.71	410.38	5.52	3.89
U1455_C35F_Zr1	140	52.03	290.31	275.13	64.60	8.45	0.77	0.73	0.73	7.06	0.10	6.00
U1455_C35F_Zr2	140	39.68	1515.24	1495.72	83.07	85.38	0.70	0.66	0.66	14.92	0.22	6.00

Table 1 (cont.)

Sample Name	Depth (mbsf)	Rs (um)	eU (ppm)	U (ppm)	Th (ppm)	nmol 4He/g	Ft 238U	Ft 235U	Ft 232Th	Corrected Age (Ma)	1s ± age (Ma)	Depositional Age (Ma)
U1455_C35F_Zr3	140	37.78	1666.57	1587.66	335.79	142.98	0.69	0.65	0.65	23.20	0.31	6.00
U1455_C35F_Zr4	140	42.92	3811.13	3743.29	288.70	533.94	0.72	0.68	0.68	35.98	0.51	6.00
U1455_C35F_Zr5	140	73.40	358.55	332.01	112.94	20.21	0.83	0.81	0.81	12.60	0.16	6.00
U1455_C35F_Zr6	140	46.27	211.82	201.04	45.86	7.83	0.74	0.70	0.70	9.29	0.16	6.00
U1455_C35F_Zr7	140	46.60	1374.13	1311.97	264.52	252.43	0.74	0.71	0.71	45.90	0.63	6.00
U1455_C35F_Zr8	140	43.67	471.54	428.52	183.05	18.41	0.73	0.69	0.69	10.02	0.15	6.00
U1451_A33F_Zr1	210	41.68	355.17	343.66	48.95	11.14	0.72	0.68	0.68	8.17	0.13	6.20
U1451_A33F_Zr2*	210	48.85	326.04	295.57	129.66	17.11	0.75	0.72	0.72	12.98	0.18	6.20
U1451_A33F_Zr3	210	39.45	557.01	495.14	263.30	14.52	0.70	0.66	0.66	6.96	0.10	6.20
U1451_A33F_Zr4**	210	42.37	641.54	587.24	231.05	14.64	0.72	0.68	0.68	5.92	0.09	6.20
U1451_A33F_Zr5	210	50.30	10.71	10.41	1.24	0.50	0.76	0.73	0.73	11.46	0.83	6.20
U1451_A33F_Zr6	210	40.78	154.99	126.34	121.92	19.32	0.71	0.67	0.67	32.89	0.49	6.20
U1451_A33F_Zr7	210	45.28	833.66	789.03	189.90	59.32	0.74	0.70	0.70	18.00	0.23	6.20
U1451_A33F_Zr8	210	40.28	651.01	578.58	308.17	585.21	0.71	0.67	0.67	233.34	2.95	6.20
labFCT2	-----	49.64	317.62	281.93	151.86	36.48	0.76	0.72	0.72	28.25	0.37	-----
FCT_Zr3	-----	85.17	248.16	222.88	107.54	31.54	0.85	0.83	0.83	27.63	0.33	-----
labFCT3	-----	66.52	275.89	247.96	118.85	31.55	0.82	0.79	0.79	26.07	0.35	-----
FCT_Zr4	-----	63.71	504.87	425.03	339.71	63.46	0.81	0.78	0.78	28.97	0.35	-----
FCT_Zr5	-----	98.82	154.19	138.10	68.48	21.02	0.87	0.85	0.85	28.97	0.38	-----
FCT_Zr6	-----	69.47	228.09	197.09	131.93	27.47	0.82	0.80	0.80	27.22	0.34	-----
FCT-Zr7	-----	45.76	398.73	353.94	190.60	45.54	0.74	0.70	0.70	28.83	0.38	-----
FCT_Zr8	-----	66.71	258.17	229.88	120.37	30.50	0.82	0.79	0.79	26.92	0.34	-----
FCT_Zr9	-----	108.83	237.14	210.57	113.10	31.01	0.88	0.87	0.87	27.43	0.36	-----
FCT10	-----	92.71	260.74	227.53	141.33	34.18	0.87	0.85	0.85	28.12	0.35	-----
labFCT10	-----	39.11	453.61	400.53	225.87	50.79	0.70	0.70	0.66	29.87	0.36	-----
FCT_Zr11	-----	76.42	261.68	232.73	123.18	32.11	0.84	0.81	0.81	27.20	0.35	-----
FCT12	-----	64.86	229.22	199.89	124.82	28.15	0.81	0.81	0.78	28.13	0.33	-----
FCT13	-----	79.94	230.43	199.25	132.69	29.18	0.85	0.85	0.82	27.83	0.31	-----
FCT14	-----	46.35	360.78	323.99	156.53	47.15	0.74	0.74	0.70	32.76	0.85	-----
FCT15	-----	68.25	241.18	211.97	124.28	27.87	0.82	0.82	0.79	26.18	0.36	-----

Appendix B2: Bengal Fan single Zircon (U-Th)/He Results: Plots





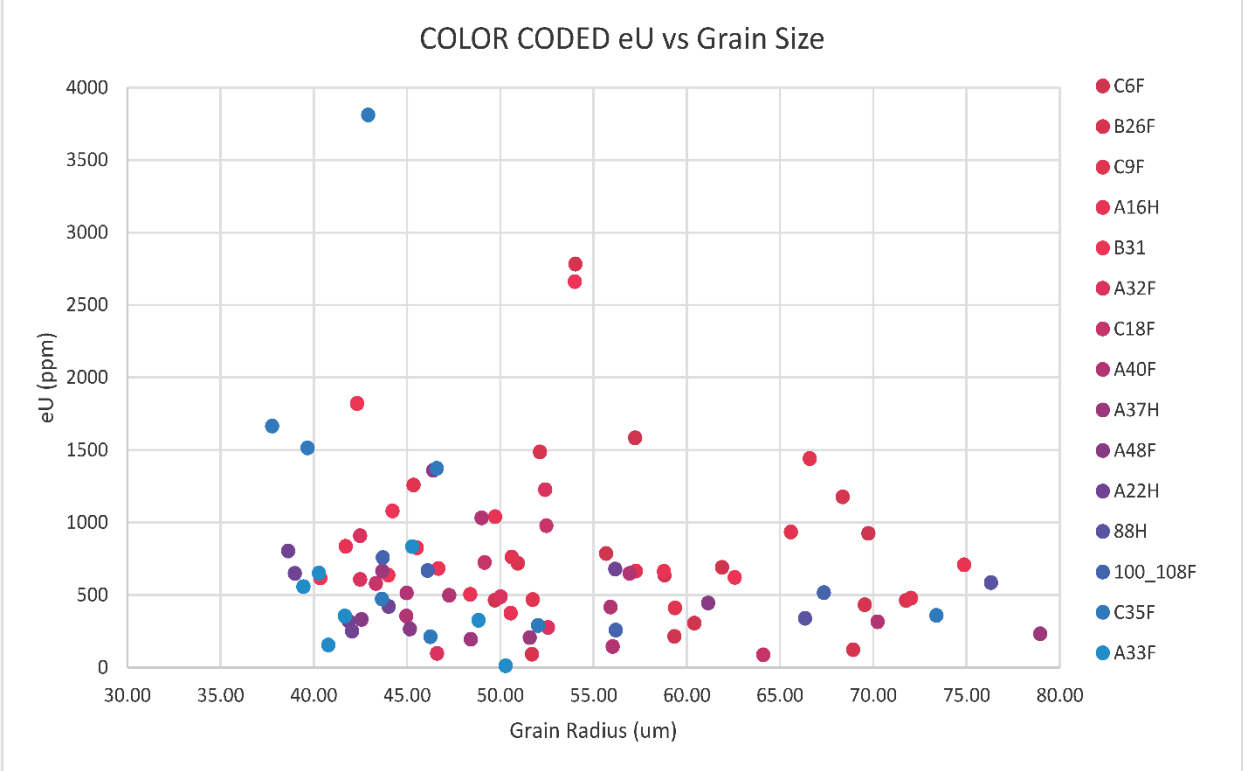


Figure B1: Zircon (U-Th)/He data plots from all single ZHe Bengal Fan samples 6.20 – 0.22 Ma deposition. ZHe dates are plotted against grain radii (Rs) and eU concentrations (ppm) along with Rs and eU plotted against one another to determine potential correlations in age distributions. Samples are color coded based on younging stratigraphic age (blue = older, red = younger).

Appendix B3: Bengal Fan Zircon He-Pb Results: Table 2

*ZHe age above U-Pb age **ZHe age below depositional age ***Empty packet ****negative ZHe age, Ft $^{147}Sm = 1$

Sample Name	Depth (mbsf)	Rs (um)	eU (ppm)	U (ppm)	Th (ppm)	nmol 4He/g (morph)	Ft 238U	Ft 235U	Ft 232Th	U-Pb Age (Ma)	U-Pb Age error	Corrected ZHe Age (Ma)	1s ± age (Ma)	Depositional Age (Ma)
B6F_010_DD1	40.5	27.29	206.38	126.62	339.39	2.42	0.59	0.59	0.53	8.36	0.76	3.83	0.33	0.13
B6F_1530_DD1	40.5	31.95	1082.87	1064.87	76.60	5.89	0.64	0.64	0.59	27.72	0.31	1.58	0.05	0.13
B6F_1530_DD2***	40.5	30.20	2.28	1.49	3.38	0.00	0.62	0.62	0.57	22.93	0.70	0.50	7.88	0.13
B6F_1530_DD3	40.5	65.36	1368.44	1361.42	29.86	35.62	0.81	0.81	0.78	23.21	0.18	5.95	0.08	0.13
B6F_1530_DD5	40.5	28.17	2421.39	2281.83	593.86	140.24	0.60	0.60	0.54	26.40	0.28	18.08	0.24	0.13
B6F_4560_DD1	40.5	78.83	640.39	617.83	95.98	3.47	0.84	0.84	0.82	47.13	0.54	1.20	0.02	0.13
B6F_4560_DD2	40.5	28.84	1761.24	1735.39	109.98	1.59	0.60	0.60	0.55	51.28	0.81	0.28	0.03	0.13
B6F_4560_DD3***	40.5	28.83	171.56	160.45	47.29	0.32	0.60	0.60	0.55	48.08	0.78	0.57	0.26	0.13
B6F_4560_DD4	40.5	30.57	1155.02	1116.71	163.00	4.20	0.62	0.62	0.57	49.49	0.39	1.08	0.03	0.13
B6F_4560_DD5	40.5	58.88	533.19	451.17	349.01	39.91	0.79	0.79	0.76	45.82	0.82	17.58	0.20	0.13
B12F_1530_DD1	65	53.74	3889.88	3810.57	337.50	21.95	0.77	0.77	0.74	25.88	0.31	1.35	0.02	0.22
B12F_4560_DD1	65	41.88	47.01	41.16	24.89	1.47	0.72	0.72	0.68	49.22	0.87	8.16	0.44	0.22
B12F_4560_DD2	65	40.81	443.81	390.37	227.40	6.75	0.71	0.71	0.67	54.25	0.76	4.00	0.06	0.22
B12F_4560_DD3	65	24.34	1675.01	1537.65	584.54	48.01	0.54	0.54	0.49	51.79	0.52	9.86	0.12	0.22
B12F_4560_DD4	65	39.90	1481.99	1130.67	1495.00	281.78	0.70	0.70	0.66	52.37	0.43	50.56	0.53	0.22
B12F_4560_DD5	65	36.57	619.29	523.08	409.41	72.99	0.68	0.68	0.64	48.94	3.92	32.40	0.37	0.22
B26F_010_DD1	130	34.84	1206.10	1102.87	439.26	8.01	0.67	0.67	0.62	4.96	0.13	1.86	0.04	0.33
B26F_1530_DD1*	130	29.03	76.48	58.60	76.10	24.19	0.61	0.61	0.56	19.00	0.91	97.71	1.94	0.33
B26F_4560_DD1	130	39.74	213.62	187.16	112.59	2.37	0.70	0.70	0.66	45.94	0.35	2.95	0.11	0.33
B26F_4560_DD5	130	29.64	592.34	543.35	208.48	10.23	0.61	0.61	0.56	53.72	1.52	5.25	0.12	0.33
A32F_010_DD1*	154	32.42	239.04	217.10	93.35	38.23	0.64	0.64	0.60	4.06	0.08	46.26	0.65	0.72
A32F_1530_DD1	154	36.05	1522.23	1399.50	522.24	28.81	0.68	0.68	0.63	19.21	0.65	5.23	0.08	0.72
A32F_1530_DD2	154	32.78	1031.92	988.06	186.62	36.22	0.65	0.65	0.60	20.92	0.73	10.10	0.14	0.72
A32F_1530_DD3	154	30.03	805.90	779.77	111.19	54.27	0.62	0.62	0.57	21.63	0.30	20.23	0.29	0.72
A32F_1530_DD4	154	47.45	367.28	363.36	16.70	35.71	0.75	0.75	0.71	26.12	0.80	24.12	0.31	0.72
A32F_1530_DD5***	154	38.81	12.99	12.61	1.62	0.08	0.70	0.70	0.65	27.71	0.34	1.64	0.74	0.72
A32F_4560_DD3*	154	30.90	452.48	385.42	285.32	648.39	0.63	0.63	0.58	58.95	0.69	413.19	4.94	0.72
A32F_4560_DD4	154	30.61	70.83	57.49	56.77	4.49	0.62	0.62	0.58	60.72	0.81	19.08	0.78	0.72
C18F_010_DD1*	92	33.57	308.54	266.28	179.84	2.16	0.65	0.65	0.61	0.05	0.00	2.01	0.12	1.14
C18F_010_DD2*	92	38.39	311.04	246.82	273.27	648.99	0.69	0.69	0.65	1.55	0.10	540.15	6.13	1.14
C18F_010_DD3*	92	33.44	237.54	212.98	104.50	6.86	0.65	0.65	0.61	1.23	0.12	8.26	0.23	1.14
C18F_1530_DD1	92	38.71	1365.24	1249.79	491.29	7.23	0.70	0.70	0.65	17.57	0.79	1.42	0.03	1.14
C18F_1530_DD2	92	39.80	571.11	569.60	6.41	4.84	0.70	0.70	0.66	18.65	0.71	2.24	0.04	1.14

Table 2 (cont.)

Sample Name	Depth (mbsf)	Rs (um)	eU (ppm)	U (ppm)	Th (ppm)	nmol 4He/g (morph)	Ft 238U	Ft 235U	Ft 232Th	U-Pb Age (Ma)	U-Pb Age error	Corrected ZHe Age (Ma)	1s ± age (Ma)	Depositional Age (Ma)
C18F_1530_DD3	92	43.03	380.07	301.11	336.02	2.39	0.72	0.72	0.68	21.06	0.27	1.63	0.04	1.14
C18F_1530_DD4*	92	27.61	535.65	408.80	539.81	662.48	0.59	0.59	0.54	24.97	0.30	384.83	4.77	1.14
C18F_4560_DD1**	92	46.64	364.50	327.19	158.74	1.31	0.74	0.74	0.71	48.71	0.41	0.90	0.03	1.14
C18F_4560_DD2***	92	60.42	0.30	0.30	0.00	-0.01	0.80	0.80	0.77	49.99	0.32	-9.87	5.47	1.14
C18F_4560_DD3	92	40.76	158.79	127.72	132.24	1.16	0.71	0.71	0.67	56.81	0.36	1.92	0.10	1.14
C18F_4560_DD4*	92	35.44	544.83	497.37	201.97	167.11	0.67	0.67	0.63	57.05	0.44	84.75	1.13	1.14
C18F_4560_DD5	92	38.14	547.33	537.90	40.12	36.55	0.69	0.69	0.65	53.46	0.38	17.92	0.23	1.14
A40F_010_DD1	198	49.03	1902.93	1885.92	72.39	11.20	0.75	0.75	0.72	9.78	0.31	1.45	0.02	1.30
A37H-1530_DD1	208	29.71	1107.12	1001.20	450.75	48.34	0.61	0.61	0.56	25.57	0.30	13.26	0.18	1.60
A37H-1530_DD2	208	28.59	632.50	557.52	319.03	28.44	0.60	0.60	0.55	29.49	0.52	13.99	0.24	1.60
A37H-1530_DD3	208	30.49	356.44	355.53	3.90	10.20	0.62	0.62	0.57	24.31	1.89	8.52	0.24	1.60
A37H-1530_DD5	208	25.72	1225.75	1220.51	22.31	57.21	0.56	0.56	0.51	21.46	0.22	15.35	0.27	1.60
A37H_4560_DD2	208	31.73	154.27	140.45	58.81	1.17	0.64	0.64	0.59	51.93	2.42	2.22	0.21	1.60
A37H_4560_DD3	208	35.45	110.19	94.66	66.08	3.15	0.67	0.67	0.63	53.24	4.91	7.97	0.24	1.60
A37H_4560_DD5	208	31.24	630.94	554.55	325.08	34.14	0.63	0.63	0.58	47.47	0.78	16.03	0.28	1.60
A48F_010_DD1	230	28.24	496.61	489.19	31.59	3.23	0.60	0.60	0.55	5.13	0.39	2.03	0.15	1.80
DDFCT_1	-----	118.55	250.97	223.18	118.24	32.19	0.89	0.89	0.88	-----	-----	26.60	0.32	-----
DDFCT_2	-----	48.94	610.39	551.25	251.63	71.17	0.75	0.75	0.72	-----	-----	28.74	0.34	-----
DDFCT_3	-----	55.30	506.20	451.56	232.53	61.34	0.78	0.78	0.75	-----	-----	28.85	0.38	-----
DDFCT_4	-----	53.03	440.67	390.59	213.09	47.29	0.77	0.77	0.74	-----	-----	25.86	0.32	-----
DDFCT_5	-----	45.26	527.73	474.75	225.48	59.58	0.74	0.74	0.70	-----	-----	28.54	0.39	-----
DDFCT_6	-----	63.98	448.90	394.63	230.93	50.23	0.81	0.81	0.78	-----	-----	25.72	0.31	-----
DDFCT_7	-----	61.91	468.64	416.27	222.86	50.58	0.80	0.80	0.77	-----	-----	24.99	0.30	-----
DDFCT_8	-----	41.80	500.51	450.38	213.33	61.70	0.72	0.72	0.68	-----	-----	32.03	0.38	-----

APPENDIX C

MODEL CONSTRAINTS AND JUSTIFICATION

Appendix C1: Kernel Density Estimate (KDE) and Probability Density Plot (PDP) Parameters

All KDEs with the exception of reconstructed sources in Figure 4 of Chapter 3 were constructed via the DetritalPy software package (Sharman et al., 2018). We utilize a bandwidth of 1 Ma for three reasons: 1) bandwidths of ~10 Ma or higher are best suited for large n datasets that cover a wide temporal range (such as U-Pb age data). 2) The 1 Ma bandwidth allows for smoothing of younger age peaks present in nearly all Bengal Fan and compiled Himalayan-Tibetan ZHe age populations, while simultaneously allowing for less prominent but geologically important age populations to be graphically noticeable. 3) ZHe data generally falls below 50 Ma for this region, and thus larger bandwidths would result in oversmoothing of key age populations. Plots were normalized to one another to avoid biasing of data with larger n sampling.

Age bins (color coding) of KDE curves and pie charts are based off the following age ranges, where color is filled between any two numbers (example: red coloration occurs between 0 – 1.8 Ma):

agebins = [0, int(1.8), int(5.3), 23, 66, 252, 541]

agebinsc = ['red','gold','lightgreen','powderblue','purple','darkgrey']

KDEs for reconstructed sources were created within the DZnmf software (Saylor et al., 2019). A bandwidth of 1 Ma was specified to maintain consistency with DetritalPy KDEs. Colorations of curves were chosen arbitrarily for distinction against comparable plots.

All He-Pb data was plotted using the DeritalPy software package. PDPs were utilized in place of KDEs to best visualize samples with very low n values (≤ 2 grains).

APPENDIX D

LOW-TEMPERATURE THERMOCHRONOLOGY COMPILATION: ZHE DATA

Appendix D1: Compiled ZHe data availability

All ZHe data used to characterize age signals for lithotectonic units and river drainages can be located and exported via the THermO master database spreadsheet, accessible via export options in the main table interface: https://tinyurl.com/TeST-Thermo-Database. Please see Chapter 2 of this thesis work for detailed examples of the user interface.